Re-Use and Volume Reduction of Scabbled Contaminated Concrete Arising from Nuclear Decommissioning

Toby James Alasdair Lord

Submitted in accordance with the requirements for the degree of

Doctor of Philosophy

UNIVERSITY OF LEEDS

School of Chemical & Process Engineering

December 2018

The candidate confirms that the work submitted is his/her own, except where work which has formed part of jointly authored publications has been included. The contribution of the candidate and the other authors to this work has been explicitly indicated below. The candidate confirms that appropriate credit has been given within the thesis where reference has been made to the work of others.

Acknowledgements

Firstly, I would like to thank my supervisor, Professor Leon Black, for his continuous support of my PhD study and research, and my development as a researcher, having faith in my abilities even when I didn't. There are many other academics in both the civil materials and nuclear groups without which this work wouldn't have been possible, and thanks and gratitude must go to them also.

To all the technical staff who have helped throughout the project; Pete, Steve, Les, Lucy, Becky, Ryan, Marv, Rob, Ben, Susanne, Adrian and many others. Without your help and support this research would not have been possible. Students and colleagues past and present, who have generously shared their knowledge and expertise, deserve much appreciation. In particular Dr. James Goode for helping and advising with LIBS work, for no personal benefit, and Dr. Josh Hawthorne, for providing so much knowledge, expertise and patience at the beginning of this journey.

There are a number of colleagues who I've had the pleasure of knowing, travelling and sharing an office with throughout the four years, all of whom have provided knowledge, laughter and support. Ian, Tom, Paul, Mike, Mo, Abdul, Joe, Alex, Matt, Jamie, Al, Laura, Yefeng, and especially Wes. In particular I would like to thank the wonderful and brilliant Dr Charlotte Parrington and Dr Jess Shiels - we came through this journey together, dragging each other through tough times and enjoying the good times, through so much laughter and great experiences. You both owe me a toastie.

Without Amy this thesis would not exist, her support and belief in me throughout the entire process was nothing short of incredible, and I can't thank her enough. Lastly I would like to thank my family; Mum, Dad, Owy, Nana and Grandma, for always being there for me, never pressuring me to get a 'real job', and for the countless times you've listened to me bang on about nuclear power and concrete. I can't thank any of you enough.

Abstract

During decommissioning of nuclear sites, radioactively contaminated concrete is scabbled from the bulk, creating an intermediate level waste (ILW) stream, requiring encapsulation in a cementitious matrix prior to storage and eventual disposal. A co-disposal option was investigated, using the scabbled material as a cementitious replacement within encapsulation grouts, to immobilise other waste streams, removing the need for direct disposal and increasing the overall waste to container volume ratio. Encapsulation grouts have strict specifications on performance, and so the effect of the inclusion of scabblings on the grout was investigated.

In this study, four simulant scabblings were synthesised, using a CEM I and CEM II based concrete, before they were crushed and ground, with half of the ground material from each undergoing accelerated carbonation, as the depth of scabbling is in the same range as the depth of carbonation in aged concrete. The scabblings were then used to replace predetermined percentages of the binder content in encapsulation grout mixes, with the cement to slag ratio (OPC:BFS) maintained at 1:3, and the effect on the hydration and engineering properties investigated.

The scabblings were found to affect the hydration of the grout above that of solely the filler effect, with the presence of remaining anhydrous material, and calcium hydroxide for slag activation, affecting the overall hydration. Mixes with 10% inclusion showed similar overall hydration and engineering properties to a reference grout, while beyond 10% inclusion these properties were significantly affected. The carbonated scabblings were found to affect the hydration and engineering performance differently to the non-carbonated, with the presence of calcium carbonate creating a ternary blended cement, and the resultant improvement in engineering properties was found. Overall, it was found that replacement of the binder with up to 10% recycled scabblings is possible, with the grout properties remaining within the specification limits. Replacement levels above 10% are not feasible.

Contents

List of Figures

List of Tables

Cement Formula

C=CaO	S=SiO_2	A=Al_2O_3	F=Fe_2O_3
M=MgO	K=K_2O	$\bar{S}$=SO_3	N=Na_2O
T=TiO_2	P=P_2O_5	H=H_2O	$\bar{C}$=CO_2

Cement Nomenclature

Phase	Mineral	Chemical Formula	Oxide Formula	Cement Nomenclature
Tricalcium Silicate	Alite	Ca_3SiO_5	$3CaO.SiO_2$	C_3S
Dicalcium Silicate	Belite	Ca_2SiO_4	$2CaO.SiO_2$	C_2S
Tricalcium Aluminate	Aluminate	$Ca_3Al_2O_6$	$3CaO.Al_2O_3$	C_3A
Tetracalcium Aluminoferrite	Ferrite	Ca_2AlFeO_5	$4CaO.Al_2O_3.Fe_2O_3$	C_4AF

Chapter 1

Introduction

1.1 Motivation

Within the UK, a growing aspect of the nuclear industry is decommissioning work, particularly at the old power generation sites of the Magnox fleet, and at Sellafield Site in Cumbria. During decommissioning, large volumes of contaminated materials are produced, of which a significant quantity are cement, concrete and rubble[1]. Nuclear reactor cores and their associated buildings, including containment vessels, plant rooms and shielding, walls contain large quantities of concrete, with some reactor core or shielding walls reaching up to 30m thickness.

The UK government is committed to geological disposal of nuclear waste, in a Geological Disposal Facility (GDF)[2], with interim storage of nuclear waste at Sellafield until such a disposal facility is operational. The high volume of concrete from nuclear sites, left untreated, would place a large strain on the capacity of any waste disposal facility. In an effort to reduce the overall volume of concrete waste, outer contaminated layers are scabbled from the bulk, such that it can be disposed of as exempt waste leaving only the contaminated scabbled material for disposal, classified in the UK as Intermediate Level Waste (ILW).

While scabbled contaminated concrete forms one Intermediate Level Waste stream, there are a number of other waste streams, including nuclear fuel cladding, pipework and solvent exchange residues. At present, the treatment method for these wastes is encapsulation

within a cementitious matrix prior to long term disposal[3], where the physical and chemical composition of the waste allows.

While scabbling of concrete helps reduce the total volume of concrete for which disposal is required, this project aims to investigate whether this volume can further be reduced, through re-use of the scabblings within the encapsulation grout formulation for ILW, a so called 'co-disposal' route, where the waste to container volume ratio is increased, and the overall waste volume decreased. Further to this volume reduction, the project aims to investigate whether the used of Laser-Induced Breakdown Spectroscopy (LIBS) can provide near-real time contamination detection for concrete, in an effort to reduce the amount of uncontaminated concrete unnecessarily scabbled.

1.2 Background

1.2.1 Nuclear Waste in the UK

The materials used on nuclear sites are classified based on their radioactivity levels, regulated nationally by the Nuclear Decommissioning Authority (NDA), which in turn is safeguarded by the International Atomic Energy Agency[4]. Waste materials in the UK fall into the following categories; High Level Waste (HLW), Intermediate Level waste (ILW), Low Level Waste (LLW) and Very Low Level Waste (VLLW), based on the limits shown in table 1.1, while fig. 1.2.1 shows the percentage of each waste by volume.

Table 1.1: Activity levels for nuclear waste classification[5]

Waste Category	**Activity Limits**
Exempt Waste	$<$ 0.4Bq per g
Low Volume Very Low Level Waste	$<$ 400kBq per 0.1m3 or $<$ 40kBq per article (see note 1)
High Volume Very Low Level Waste	$<$ 4MBq per tonne (see note 2)
Low Level Waste	$<$ 4GBq per tonne α $<$ 12GBq per tonne $\beta\gamma$
Intermediate Level Waste	No activity limits, except for long lived α
High Level Waste	No activity limits

(note 1 - if C14 or H3 can be 10 times the limit)
(note 2 - if H3 can be 10 times limit)

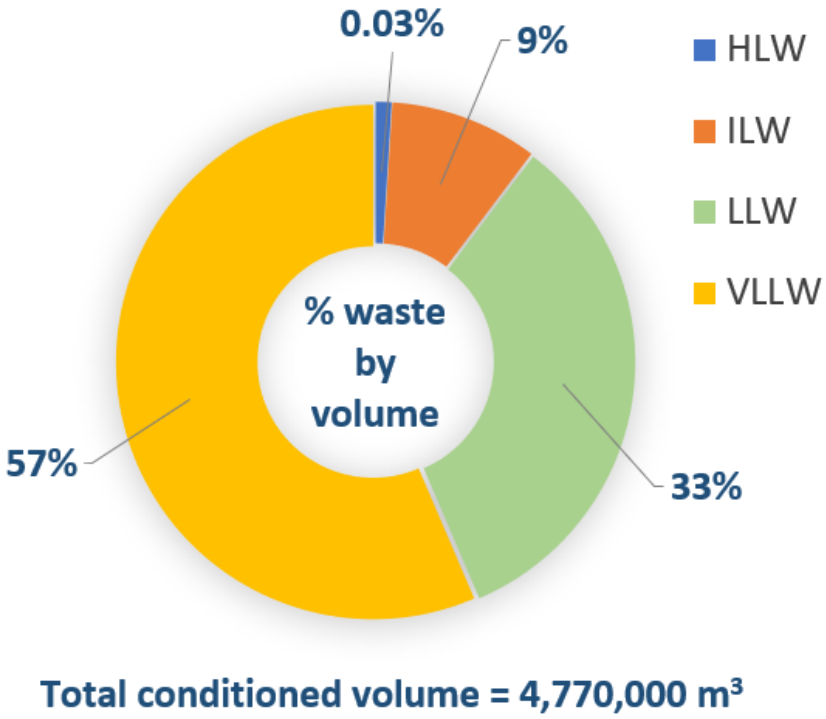

Figure 1.2.1: Percentage of UK nuclear waste by volume[6]

1.2.1.1 High Level Waste

High Level Waste, despite accounting for only 0.3% of nuclear waste by volume, accounts for 97% of waste by activity. Consisting of spent fuel, reprocessing products and highly contaminated materials, the high activity of HLW is heat-generating and so can't be encapsulated in cement based matrices. Instead, HLW is vitrified in specially designed glass systems, and is then stored in actively cooled intermediate storage prior to long term disposal. Both heat generation and criticality limit the size of each individual vitrified waste canister.

1.2.1.2 Intermediate Level Waste

Intermediate Level Waste is comprised of materials contaminated with radionuclides due to being in direct contact with, or close proximity to, nuclear fuel. It can also include waste effluent and materials from any reprocessing. This includes materials such as fuel cladding (left as undissolved material after fuel in rods has been dissolved in nitric acid for reprocessing, or sheared off the fuel rods prior to reprocessing), sludge and floc from storage

or reprocessing and other materials from the reactor core, such as shielding or containment vessels. As ILW is not a significant heat-generating waste, it is mostly encapsulated in a cement based matrix in 500l steel drums, before being placed in intermediate storage prior to eventual disposal.

1.2.1.3 Low Level Waste

Low Level Waste is by far the greatest volume of waste created by the UK nuclear industry, and includes most materials present on a nuclear site that aren't directly in contact with the reactor or the fuel. This includes a wide range of objects including building materials, plant equipment, safety clothing and paperwork. Despite having very low levels of activity, most of these materials aren't suitable for standard disposal without prior treatment, or at all. Many wastes, such as used protective clothing and papers, are compacted and stored as low level waste at the Drigg near surface repository[7]. Other waste, such as building materials, can be treated to remove any potentially hazardous materials, enabling the bulk material to be disposed of as standard waste.

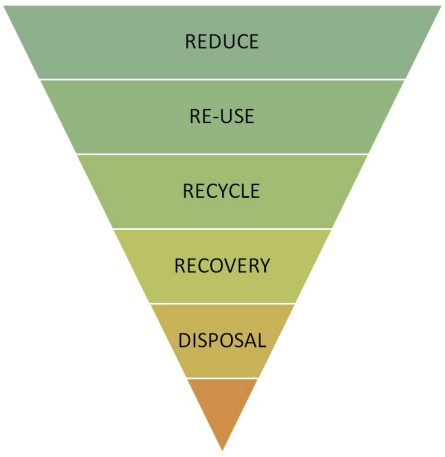

Figure 1.2.2: Waste Management Hierarchy[5]

1.2.2 ILW Encapsulation Grouts

ILW, within the UK, is encapsulated in high slag content encapsulation grouts. In order to ensure the long term performance, in geological disposal conditions of the grouts, they are required to adhere to stringent specifications, for both raw materials and engineering performance[8]. A brief list of the requirements are given below, while the chemistry and design of grouts is discussed in detail in section 2.5.

- ▷ Setting time must be within a 4 to 24 hour window such that 4h<setting time<24h.
- ▷ Cumulative heat of hydration must be less than 250 Joules per gram within the first 24 hours after casting.
- ▷ Bleed water must be less than 1% by weight.
- ▷ Flow must be above the pessimum level within the Colflow test[9].
- ▷ 3:1 Blast Furnace Slag (BFS) to Ordinary Portland Cement (OPC) mass ratio.

1.2.3 Geological Disposal Facility

Intermediate and high level wastes are currently kept in interim storage at Sellafield site awaiting long term disposal. Within the UK, government policy is for a long-term deep geological disposal facility[2], whereby conditioned ILW and HLW packages are placed in man-made underground vaults, before being backfilled and the facility eventually being shut off indefinitely, completely removing the radiation from human or environmental impact. The design, construction and management of a Geological Disposal Facility (GDF) is to be carried out by Radioactive Waste Management Ltd (RWM)[10].

HLW and ILW are packaged in specially designed containers, such that shielding and release barriers are always intact, and a conformity of waste package is maintained, so that design of a final facility will be eased. These packages come in a number of forms depending on the waste type and encapsulation method, but a pricing method has been agreed between site licence companies and the Nuclear Decommissioning Authority. While High Level Waste is calculated per tonne of uranium in the spent fuel, pricing equates to approximately £40,000 per m^3. For Intermediate Level Waste, pricing is set at £14,500 per m^3[11], while low level is set at £3,292 per m^3[12]. The high cost of ultimate disposal of this waste, as well as interim storage, means that substantial effort is put into reducing the overall waste volume through re-use and recycling, as part of the waste hierarchy[13], shown in fig. 1.2.2.

1.3 Research Proposal - Aims & Objectives

The aim of this project is to determine the suitability of simulated scabbled concrete for use within binary and ternary grout mixes, examining the effect that the inclusion of scabblings has on the engineering performance of the grout, and thus its suitability as an option for co-disposal, to reduce the overall volume of waste for disposal. The project can be split into the following aims.

1.3.1 Characterisation

Characterise the chemical and physical composition of simulated scabbled concrete

At this stage, little is known of the properties of the scabbled material, not just in terms of radionuclides present, but with respect to the composition, mineralogy and physical properties. Thus the first aim is to fully characterise scabbled concrete. This will be achieved through the following objectives;

1.3.1.1 Chemical Composition

Chemical composition will be analysed through thermo-gravimetric analysis (TGA) and X-ray diffraction (XRD). Both of these have been extensively used for chemical and phase analysis of cured cement pastes and concrete, and can be used to determine degree of hydration[14]. Scanning Electron Microscopy (SEM) will be used to examine the presence of any anhydrous material remaining in the original concrete, and determine the degree of hydration.

1.3.1.2 Degree of Carbonation

Degree of carbonation of the scabbled material is important, as it affects the chemical composition and thus its possible reactivity, particularly in combination with high blast-furnace slag (BFS) cements, where calcium carbonate ($CaCO_3$) can react with aluminates in the slag[15], see section 2.3.2. The depth of contamination of radionuclides is known to be in the order of several centimetres in aged concrete[16]. In aged concrete structures,

dependent on exposure, the depth of carbonation can also reach several centimetres[17]. Carbonation can be examined using TGA[18], and so as part of the chemical composition analysis, work will be carried out to determine the degree of carbonation of the sample.

1.3.1.3 Particle Analysis

Particle size analysis of the scabbled material will be carried out using laser diffraction. Other options for determining particle size distribution include sieve analysis, although this is more time consuming for both data gathering and analysis.

Particle shape analysis will also be carried out, as this could affect the behaviour of the particles in any future use, such as a replacement material in a new cementitious grout. Smaller and more angular particles are likely to increase the viscosity of any fluid they are part of, due to increased particle interactions, and so can affect the workability and fluidity of other grouts they are used in. This is a relatively simple and qualitative analysis, to be carried out using a desktop scanning electron microscope in (SEM) in secondary electron mode, as this will have sufficient resolution to examine individual particles within a wide distribution.

1.3.2 Cementitious Replacement

Investigation of the effect of any residual hydraulic behaviour, or other effect, of the scabbled concrete on the hydration and engineering properties of an encapsulation grout

As described in section 1.2.3, there is a pressing need to reduce the overall volume of nuclear waste in the UK, in order to reduce the pressure on the proposed deep geological disposal facility. Through re-use of scabbled contaminated concrete, a waste-stream could be eliminated, reducing total overall waste volume. Therefore the second aim is to examine the possibility of using scabbled material as an integral component within the cementitious matrix of an encapsulation grout for nuclear waste, as a method for co-disposal.

By re-using and recycling the material as a cementitious replacement material, utilised

in the disposal of other nuclear waste, the additional volume required for the disposal of scabbled waste would be very significantly reduced and kept to a minimum. This has been carried out in Japan as a method of increasing the waste fill ratio in containers for low level waste, primarily bulk concrete blocks[19].

Effect of scabbled replacement on properties of new grout will be examined, such that the grout will still conform to the stringent specifications of nuclear encapsulation grouts. Replacement of the fine binder content using synthesised scabblings will be carried out, at 0, 10, 20 and 40% replacement, and the properties of the grout mixes investigated and compared.

1.3.3 Ternary Replacement

Investigation of the ternary blended cement created by concrete carbonation

The depth of contamination in concrete has been shown to be similar to that of carbonation[16]. Concrete carbonation changes the microstructure, discussed further in chapter 2. As such, carbonated scabblings will be synthesised, and used as a replacement in encapsulation grout, as described above, this time in a ternary blended system. The effect on hydration and engineering performance of the grout will be investigated and compared to that of non-carbonated scabblings.

1.3.4 Volume Reduction of Scabbled Material

Development of methods for determination of contaminant depth in concrete to aid determination of scabbling depth

While other aims within the project focus on re-using the scabbled material, or reducing the overall volume of conditioned waste created when disposing of scabbled material, there is the possibility of reducing the volume of scabbled material produced on site. During decommissioning, the depth of contamination is occasionally taken from cores, but is primarily taken from surface samples only, and a conservative estimate used for the depth of scabbling required. There is therefore the possibility to reduce the volume of scabbling required by providing more accurate information on the depth of contamination.

Laser induced breakdown spectroscopy (LIBS) uses a high intensity pulsed laser to create a plasma plume on the surface of a material, the composition of which can then be analysed using spectroscopic detectors. It is therefore plausible that this method could be used to detect contamination within concrete, and when used in-line with a scabbling method could provide real-time data on the contamination levels within concrete. As LIBS is still a young technology with little use to date on concretes, there is the need for preliminary work to determine the feasibility of using this technology for contamination detection in concrete.

Part I

Literature and Experimental Methods

Chapter 2

Literature Review

This literature review will cover the background literature for this project. For a comprehensive overview of cement and concrete properties, refer to Properties of Concrete by Neville[20], or Cement Chemistry by Taylor[21].

2.1 Cement

Cement clinker is produced during the high temperature mixing of powdered clay and limestone, plus additions including quartz and iron, at temperatures in the range of 1400-1500°C[22]. Clinker leaves the kiln as small, roughly spherical particles with a size in the order of cm, and is then ground, together with gypsum, into the dark grey powder that we know as cement. Within cement clinker are four main minerals, first successfully described by Bogue in 1929[23];

- Tricalcium Silicate, $3CaO.SiO_2$ (C_3S in cement nomenclature), known as alite, comprising approximately 65%
- Dicalcium Silicate, $2CaO.SiO_2$ (C_2S in cement nomenclature), known as belite, comprising approximately 15%
- Tricalcium Aluminate, $3CaO.Al_2O_6$ (C_3A in cement nomenclature) known as aluminate, comprising approximately 7%
- Tetracalcium Aluminoferrite, $4CaO.Al_2O_3.Fe_2O_3$ (C_4AF in cement nomenclature) known as ferrite, comprising approximately 8%

As can be seen by the mineral names and formulae, the constitiuents of cement, due to the precursor materials, are primarily calcium, silicon, aluminium and smaller amounts of iron. Smaller quantities of other elements such as magnesium and sodium will also be present. Small amounts of gypsum are also added to clinker to regulate the setting properties of the concrete and as a grinding agent, as discussed in section section 2.1.1.3. Small amounts of limestone, up to 5% inclusion are allowable in CEM I cements[24], but not within the Portland cements used in nuclear encapsulation grouts within the UK.

2.1.1 Cement Hydration

Cement, in the presence of water, will undergo a series of irreversible hydration reactions and phase changes, resulting in a hardened paste.These reactions, with different and distinguishable time-frames, are illustrated in fig. 2.1.1, showing the heat flow against time of a typical cement during the early stages of hydration. The hydration process can be split into distinct regions, as discussed below.

2.1.1.1 Initial Mixing

Upon initial contact with water, gypsum and alkali sulphates in the cement dissolves in the water creating a sulphate rich alkaline solution. The first hydration reaction to occur is the fast (lasting in the range of several minutes) and strongly exothermic reaction of the aluminate phase reacting with the water to form an aluminate-rich gel. The sulphates that are now dissolved in the water react with the gel to form ettringite, which has long, rod like crystals. This reaction is denoted by stage I of fig. 2.1.1, with a high peak temperature but a short lived reaction. The reaction lasts only a limited amount of time due to the formation of a hydrated layer around the cement particles, forming a barrier between the general solution and the anhydrous material, significantly reducing the rate of reaction[21]. The chemical reaction occurring during stage I can be described and denoted as;

$$\text{aluminate} + \text{gypsum} + \text{water} \rightarrow \text{ettringite} + \text{heat}$$

$$C_3A + 3C\bar{S}H_2 + 26H \rightarrow C_6A\bar{S}_3H_{32} + \Delta heat \tag{2.1.1}$$

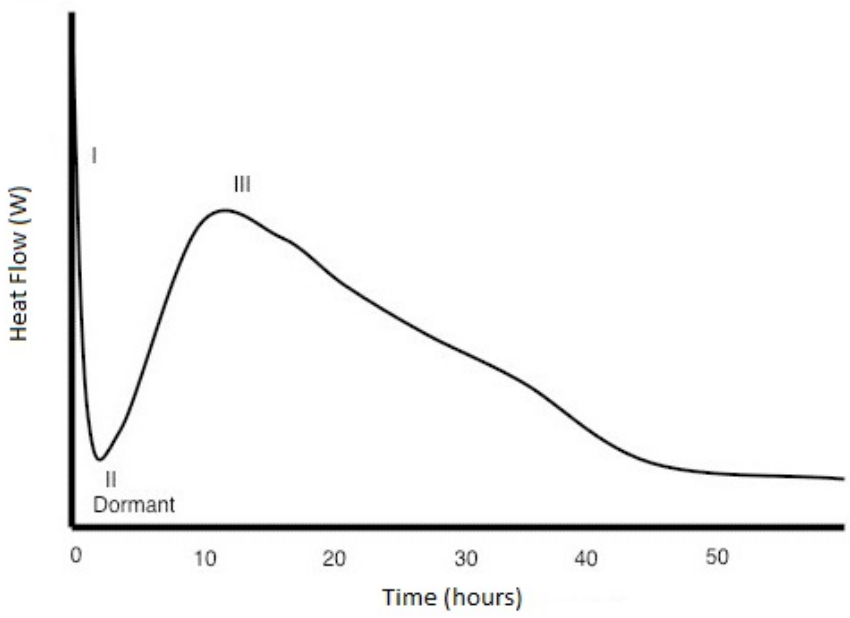

Figure 2.1.1: Typical heat evolution from cement hydration reaction during early stages of hydration[25]

2.1.1.2 Dormant/Induction Period

After the initial reaction, a dormant/induction period begins during which few reactions occur. The reasons behind the dormant period are still not completely understood, but it was thought that a 'protective' layer of a type of metastable calcium-silicate-hydrate forms around the anhydrous material preventing further reactions[21]. More recently however, this theory has been disputed, with studies, reviewed by Scrivener and Nonat[26], suggesting that despite great advances in imaging techniques, no protective layer has been observed. Instead, a dissolution theory has been proposed by Julliand *et al.*[27] whereby the dormant/induction period is brought about by a slowdown in the dissolution rate of C_3S from clinker grains due to super-undersaturation of the pore solution.

The end of the dormant period is brought about by the formation of calcium-silicate-hydrate (C-S-H) gel nuclei on the outside of the metastable layer, which differ in morphology and structure to the metastable hydrate. The C-S-H is more thermodynamically stable than the metastable layer, and so they begin to convert the inner layer into C-S-H gel, increasing the porosity of the layer around clinker grains. It is towards the end of the dormant period that cement begins to stiffen and is no longer workable, as further

hydration reactions occur reducing the free water available, and solidification begins.

2.1.1.3 Early Hydration Reactions

With the conversion of the metastable Calcium-Silicate-Hydrate into C-S-H gel, the porosity of the protective layer around the anhydrous cement particles increases, and so the solution can now access and react with the cement particles, and thus a number of hydration reactions begin to occur. The specific surface area of the cement or replacement material plays an important role in the rate and degree of hydration reactions occurring, with smaller particles providing an overall larger surface area for reactions to occur [28].

Denoted by stage III in fig. 2.1.1, the rapid increase in heat production is brought about by the hydration of the alite in the cement clinker, and this reaction usually occurs within the first 24 hours following initial mixing. During this reaction, the alite reacts to form C-S-H gel and CH, known as portlandite. The water content and calcium to silicon ratio (Ca/Si) within the C-S-H gel varies, and is dependent upon many factors including the exact composition of the cement clinker and the water to cement ratio within the cement matrix. The material structure at the end of stage III consists of larger cement clinker particles surrounded by hydration products, which have a very fine internal porosity which is filled with solution. At this stage between a third and a half of all cement clinker is hydrated. The hydration reaction of the alite phase is shown below;

$$\text{tricalcium silicate} + \text{water} \rightarrow \text{calcium silicate hydrate} + \text{portlandite} + \text{heat}$$

$$2C_3S + 6H \rightarrow C_3S_2H_3 + 3CH + \Delta H \tag{2.1.2}$$

2.1.1.4 Later Stage Hydration and Strength Evolution

At the end of stage III the majority of the C_3S has reacted and so heat generation significantly drops. This isn't the end of the hydration process however, and at this stage only around 30% of the total material strength has been reached. This is why during construction, even though the concrete may be set and hard and the formwork possibly removed, usually a time gap of 7 days is used before fresh concrete can be classed as being of a

suitable strength for further construction to occur that will induce loads on the structure.

Further reactions are occurring between the gel and capillary pore water and other phases in the cement. The depth of hydrated material is slowly increasing into the cement particles. The primary reactions occurring during this later stage are that of the belite. This is a slow reaction process but contributes high strength to the material, and it is this reaction among others that gives cements and concretes their unusual strength gain up to weeks, months and even years after initial mixing and casting. While there exist other phases within the cement, such as the aluminate and ferrite phases, the primary strength contributors are the alite and belite; alite is much more soluble than belite and so is the main contributor to early age strength, as discussed in section section 2.1.1.3, whereas belite is much less soluble and so has a much slower strength contribution.

The hydration reaction of the belite phase that contributes to the later age strength of the cement is shown below (it should be noted that although this is an exothermic reaction, the hydration process is at a low enough rate that heat dissipation outweighs heat production and there is no noticeable heat build-up at later ages);

$$\text{dicalcium silicate} + \text{water} \rightarrow \text{calcium silicate hydrate} + \text{lime} + \text{heat}$$

$$2C_2S + 4H \rightarrow C_3S_2H_3 + CH + \Delta heat \tag{2.1.3}$$

2.1.1.5 Chemical Shrinkage

During cement hydration, a number of phase changes occur, as described in section 2.1. These occur at different stages of hydration and result in a number of mineralogical changes. As a result of these changes, there is an absolute volume change within the cement matrix. In a pure sense, the shrinkage of hydrating cement paste can be calculated via chemical equations[29]. Although the number of different reactions occurring during cement hydration are numerous and thus can't be expressed as a single equation, the shrinkage due to each individual phase change can be calculated, as shown in fig. 2.1.2, from Zhang et al.[30], where V_CS is the chemical shrinkage. The phase changes and chemical shrinkage of the cement matrix result in an increased density and volume reduction of the material.

$$C_3S + 5.3H \rightarrow C_{1.7}SH_4 + 1.3CH$$

Molar weight (g/mole)	228	95.4	227.2	96.2
Specific gravity (g/cm^3)	3.15	1.0	2.12	2.24
Molar volume (cm^3/mole)	72.38	95.4	107.17	42.95

$$V_{CS} = \frac{V_s}{M} = \frac{(72.38 + 95.4) - (107.17 + 42.95)}{228} = 0.0775 \text{ (ml/g)}$$

Figure 2.1.2: Example chemical shrinkage calculation, from Zhang et al.[30], where V_CS is the chemical shrinkage

2.1.1.6 Mineralogy

Hydrated cement paste consists of a number of hydrous phases, of varying degrees of crystallinity. The exact mineralogy of a hydrated cement paste is strongly dependent on the presence and volume of each phase and dependent on the age of the paste and the raw materials used to produce it, and any minor constituents or impurities can have a significant impact on the assembled hydrates[20]. In a system based on Portland cement however, the major phases present within matrix of standard cement pastes can be classified as calcium-silicate-hydrate (C-S-H) gel, calcium hydroxide or portlandite ($Ca(OH)_2$), ettringite (AFt) and calcium aluminate hydrate (AFm) phases[21], described below.

2.1.1.6.1 C-S-H

Calcium-silicate-hydrate, or C-S-H, is the primary binding phase in Portland cement based systems[31]. The chemical composition of C-S-H varies between mixes, and even within sections of paste from the same mix, and so is referred to as C-S-H rather than CSH, as the ratio of constituents, particularly the calcium to silicon ratio (Ca/Si), varies significantly and affects the chemistry and micostructure of the C-S-H.

2.1.1.6.2 C-(A)-S-H

Calcium-aluminium-silicate-hydrate, or C-A-S-H, is an altered version of the C-S-H phase found in cements where partial replacement of portland cement has occurred, with the replacement SCM's (see section 2.2.2) having high aluminium content. The presence of the aluminium in the SCM's leads to partial replacement of the calcium within the C-S-H, leading to a lower Ca/Si ratio, and incorporation of aluminium into the C-S-H gel. The incorporation of aluminium from SCM's, in blended cements, leads to a change in morphology, with Richardson, and Richardson et al. reporting a fine, foil like morphology in hydrated slag[32,33].

2.1.2 Cement Microstructure

Cured concretes or mortars consist of a cement matrix surrounding the coarse and/or fine aggregate. The aggregates often consist of limestone for the coarse aggregate, although this can vary geographically, with other rock such as granite and quartzite being used, dependent on local availability and required properties. Sand is used for fine aggregate. The microstructure of these two materials doesn't change from pre- to post-casting. The microstructure of the cement matrix is complex however, and gradually evolves over the process of hydration. This hardened cement paste matrix can be broken down into two distinct phases, referred to as Outer Product (OP) and Inner Product (IP)[34].

2.1.2.1 Outer Product

Outer Product (OP) refers to the solid material that forms in place of the water in the initial fluid. Depending on the exact chemistry of the cement or other blended materials such as slag, the C-S-H gel forms in a fibrous or foil-like nature. It is an amorphous gel and thus non-crystalline, meaning no uniform chemical composition and no uniform shape[31].

2.1.2.2 Inner Product

Inner product refers to the phase changes that occur within the original outer edges of the anhydrous cement particles as a result of water ingress into the particles and subsequent

reactions. Over time the alite and belite minerals within the cement will hydrate and undergo a phase change, forming C-S-H within the original grains. Initially, the Inner Product (IP) C-S-H composition differs from that of the outer product. In more mature pastes however the composition and morphology of the IP and OP C-S-H phases becomes more similar[35]. The density and porosity of the IP also depends on the particle size of the original cement grains, with larger grains having a homogeneous, fine-scale and relatively dense C-S-H form, whereas smaller initial grains contain a less dense C-S-H with substantial porosity, surrounded by a zone of relatively denser C-S-H[31]

2.1.2.3 Interfacial-Transition Zone

The Interfacial-Transition-Zone (ITZ) is the area of cement matrix surrounding both the fine and coarse aggregate. It is the property of the ITZ and its bonding interaction between the cement matrix and the aggregate that gives concrete its inherent strength. The ITZ is usually weaker than bulk cement paste due to higher porosity and lower cement content.

2.1.2.4 Porosity

The porosity of a cement paste, and thus concrete when assuming that aggregates are non-porous, has two distinct types of porosity defined by the size and nature of the pores; capillary porosity and gel porosity[20].

As described in section 2.1.1.3, during hydration reaction the water filled area around the cement grains begins to be filled with hydration products forming a gel and binding the material together. As the reactions continue, the volume of water filled voids decreases as the solid volume increases. These water filled voids aren't entirely filled with solid products, and the residual voids at any stage of hydration are known as capillary pores[36]. The chemistry of the pore water within the capillary pores plays an important role in the further hydration and durability of the cement paste and concrete. Capillary pores are in the range of 0.1-10μm, visible in backscattered scanning electron microscopy (SEM) or transmission electron microscopy(TEM)[37].

Gel porosity is defined as the interstitial or interlayer pores within the C-S-H matrix itself, and are usually three orders of magnitude smaller than capillary pores[31], in the range of 0.5-10 nm. The nature of gel porosity is affected by the inclusion of pozzolans within the mix, changing the nature and morphology of the C-S-H formed, as discussed further in section 2.2.1.

2.1.2.5 Permeability

Permeability is governed by the interconnectivity of the pores within the cement paste, and the ability for fluids to move through the interconnected pores. While permeability can be affected by the porosity of the material, it isn't always directly related - two materials could have the same porosity with very different permeability. In soils for instance, while clays and sands have a similar overall volume of voids or pores, the permeability of the two materials is drastically different, with clays having much smaller and less interconnected pores, compared to the large and well connected pores of sand[38]. The permeability of a cement paste or concrete is often one of the leading factors for long term durability.

2.1.3 Workability

Workability of a cement or concrete is a measure of how easy the material is to work with in a physical sense prior to pouring or casting, and is in essence a measure of viscosity and flowability. A number of factors can affect the workability of a material, and a number of methods are available to alter the workability of a concrete or cement to suit the required application. The primary factors that control the workability are the water to cement ratio (w/c) of the mix, the size and shape of any cement and aggregates, and the presence of any additional additives.

In construction, a balance is often struck between the workability of the material, and the desired strength, as the material ratios for both can often differ greatly. For concrete fabrication and pouring, workability is usually controlled using w/c ratio within the mix. This therefore affects the solid to liquid ratio and enables a more fluid response of the concrete allowing easier pouring, with less vibration or additional work being required to

get the material into the desired spaces. Too high a water content however, can have an overall adverse effect on the finished properties of the concrete; too high a w/c (water to cement ratio) can leave an open pore network, reducing the durability of the cement matrix and reducing concrete strength.

Where a compromise isn't available due to limits on w/c ratio, the use of additives such as plasticisers can affect the workability of concrete, by reducing the water requirements of the fresh mix. Plasticisers and superplasticisers work by acting as dispersants within the fluid mix, by utilising binding and polarity properties to create repulsive forces within the fluid mix, dispersing the particles and reducing particle interactions, which cause friction and reduce flow. The use of plasticisers is common in the construction industry as they lower the water requirement of a concrete mix, reducing the w/c ratio and thus creating higher strength concretes.

2.2 Supplementary Cementitious Materials (SCM's) and Recycled Concrete

2.2.1 Pozzolans

The term Pozzolan refers to the town of Pozzuoli in northern Italy, dating back to around 100 B.C. This is due to the Roman use of hydraulic lime and soil to create a hydraulic binder, leading to the oft-cited idea that the Romans invented concrete. The incorporation of lightweight pumice stone into the hydraulic binder created a sort of light weight concrete, and was used on buildings such as the Pantheon[39].

In present day cement chemistry and manufacturing, Pozzolan refers to a broad range of natural and artificial materials, that although not hydraulic themselves, contain levels of reactive silica and alumina. In the presence of water, the silica and alumina will react with calcium hydroxide (portlandite, CH in cement chemistry) to produce compounds with cementitious properties. As the calcium hydroxide is a product of the later stage hydration of standard cement, the addition of Pozzolans within a standard cement will have no effect on early stage hydration and strength gain of a concrete aside from the filler

effect (see section 2.3.1.1, but instead will affect the long term strength of the material, as the reactions are ongoing and can continue for a number of years.

2.2.2 Supplementary Cementitious Materials (SCM's)

Latently hydraulic materials differ from pozzolans through their hydration reactions and the type of cementitious materials formed. Supplementary cementitious materials (SCM's), sometimes known as cement replacement materials include pozzolans and latently hydraulic materials, both natural and artificial, and are used to reduce the amount of cement required within a concrete. There are a number of advantages arising from the use of SCM's, both through positive changes to the material and a reduction in the quantity of cement required. As described further in section 2.2.3, cement manufacturing is responsible for high levels of carbon emissions, and so any reduction in the quantity of fresh cement required by the construction industry will have environmental benefits.

In terms of material properties, the use of SCM's can improve the long term strength and durability of a concrete, as the pozzolanic and latent hydraulic reactions will continue contributing to the strength for months or even years after initial mixing. Along with aiding in the strength evolution of the cement matrix, the addition of SCM's, through increased hydration reactions with soluble compounds held in the pore water, can decrease the capillary porosity of the bulk material, thus reducing the permeability and hence increasing durability.

The use of SCM's changes the microstructural nature of the C-S-H gel within the cement paste - the Ca/Si ratio is reduced and the strands of C-S-H form a more foil-like structure, as opposed to a more fibular nature within neat OPC pastes[31]. The structure of the C-S-H then acts to reduce the capillary pore sizes, and particularly affects the permeability of the cement paste. The reduction in porosity and in particular permeability of the cement paste can increase its durability and therefore any concrete created with a blended cement mix.

A secondary benefit arising from the inclusion of Pozzolans within a concrete mix, and

one that is utilised within nuclear waste encapsulation is the reduced heat of hydration occurring within the early stage reactions. As the total cement content is reduced, the amount of readily reactive material reduced and so the early stage reactions occur to a lesser extent, reducing total heat production. The overall reduction in heat evolution can reduce the chances of heat cracking within the bulk of the material, thus reducing the chance of later ingress of water or other compounds that can be detrimental to concrete durability. For nuclear uses, thermal cracking is detrimental for long term disposal plans as it could allow the ingress of groundwater into the bulk material, and thus creates the possible problem of leaching of radioactive material out of the encapsulated waste form.

The most commonly used SCM's in construction are ground granulated blast-furnace slag (GGBS or BFS) and pulverised fuel ash (PFA), although a number of other materials are growing in use, such as sugar-cane bagasse ash[40]. Figure 2.2.1, from Lothenbach et al[41]. shows the range of SCM's and resultant hydration products in terms of their CaO, SiO_2, and Al_2O_3 content. Within the nuclear sector, blast-furnace slag is the dominant waste material used in encapsulation grouts. These materials are of such wide use as they are common throughout the world, and are in effect waste materials, and so finding a secondary use for them has a double environmental impact, and also an economic impact[42].

2.2.2.1 Blast Furnace Slag

2.2.2.1.1 Production

The most common latently hydraulic material used in cement and concrete manufacturing is ground, granulated blast furnace slag (GGBS or BFS), and is used in high quantities in nuclear waste encapsulation grouts. Slag is a by-product from the manufacture of iron, when iron ore, coke and limestone are heated to around 1500°C. Molten iron is produced, with molten slag floating on top of the iron and comprising mostly silicates and alumina from the iron ore[43]. The molten slag is tapped off the top of the furnace and cooled rapidly using water or steam, creating granular glassy particles. These are then ground to create the powdered slag used as a cementitious replacement material.

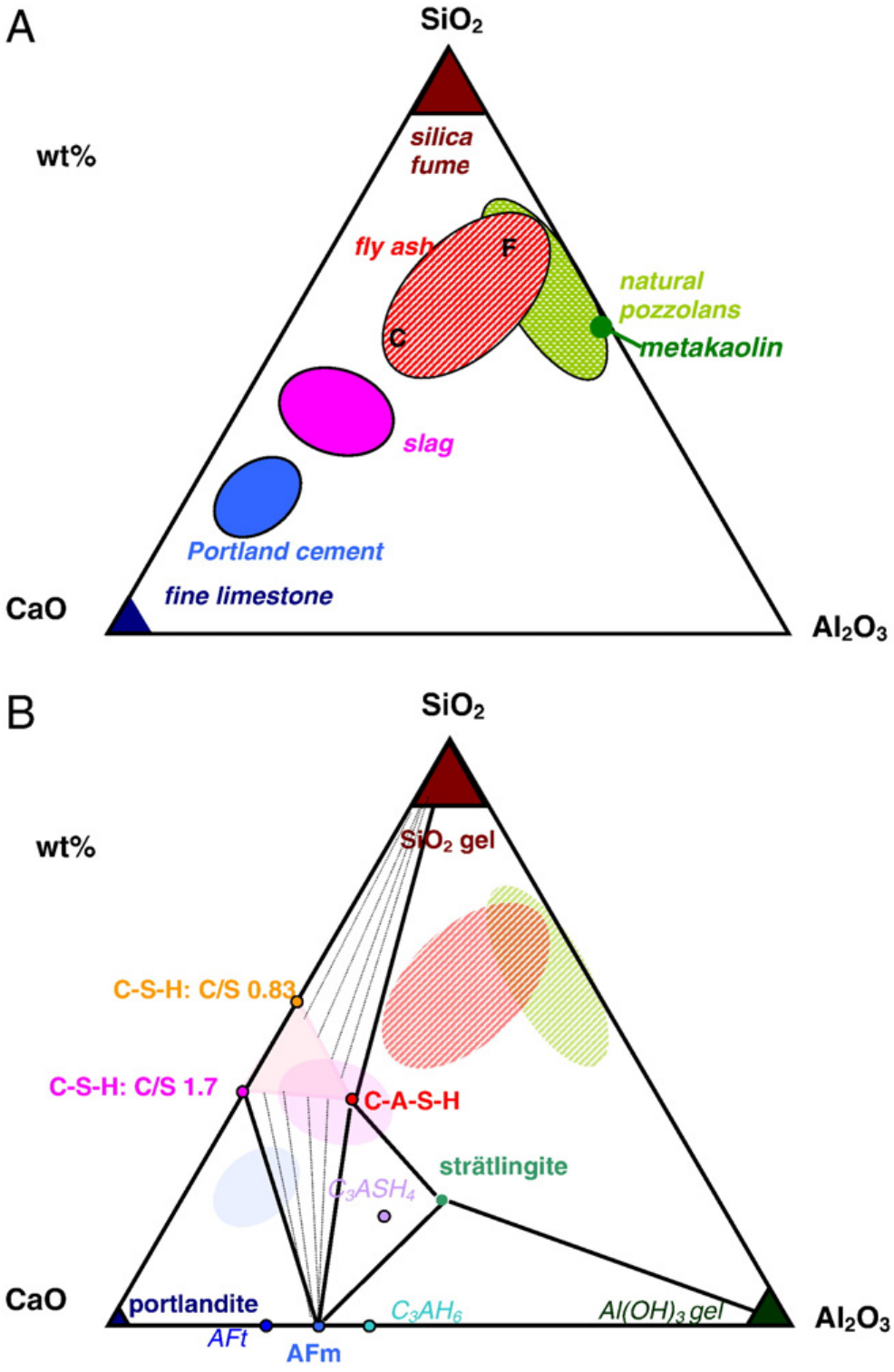

Figure 2.2.1: CaO, SiO_2, and Al_2O_3 ratios for A) supplementary cementitious materials, and B) their hydration products, from Lothenbach et al[41].

2.2.2.1.2 Hydration

When used within cement pastes, the presence of slag changes the hydration kinetics, with hydration products remaining similar to those within a neat OPC blend, but with the Ca/Si of the C-S-H reduced, and with some substitution of Al into the C-S-H, forming a calcium-alumino-silicate-hydrate or C-A-S-H[44,45]. Although slag is latently hydraulic, and therefore not technically a pozzolan, its reaction with water is so slow that it isn't feasible to use by itself as a cementitious material and needs a high alkali content to be activated. While this slow reaction leads to lower early age strength than a standard cement paste, slag blended systems at later ages have been found to have comparable or higher later age strengths, when used upto 55%[46]. When blended with a portland cement, the production of CH from the cement hydration acts to activate the slag hydration[33].

The alumina content of the slag reacts slower than that of the alite content in cement, and so these separate reactions can be shown using isothermal calorimetry, where the slower reaction of the aluminate results in a secondary peak after the first alite peak, shown in fig. 2.2.2, taken from the work of Whittaker et al[47], and denoted with by A. In their work, they describe how the large peak from the slag aluminate hydration is analagous to the small aluminate hump from OPC hydration, with the two inseparable through isothermal calorimetry, but that the difference in peak heaights is significant, with the vast majority coming from slag hydration. As these systems are normalised by their cement content, it can be seen that per gram of cement, the slag systems also have increased alite peaks. This increase has been attributed to the filler effect, as described in section 2.3.1.1[41,48]. The difference in onset time for the aluminate peak has been found to be due to slag composition[33].

2.2.2.2 Pulverised Fuel Ash

Following the combustion of coal within power plants, a combustion residue remains, removed from the flue gas stream by mechanical separators, electrostatic precipitators or bag filters[49]. The composition of the fuel-, or fly-ash, is dependent on the type of coal used, with anthracite or bituminous coal producing low-calcium fly-ash, and lignite or

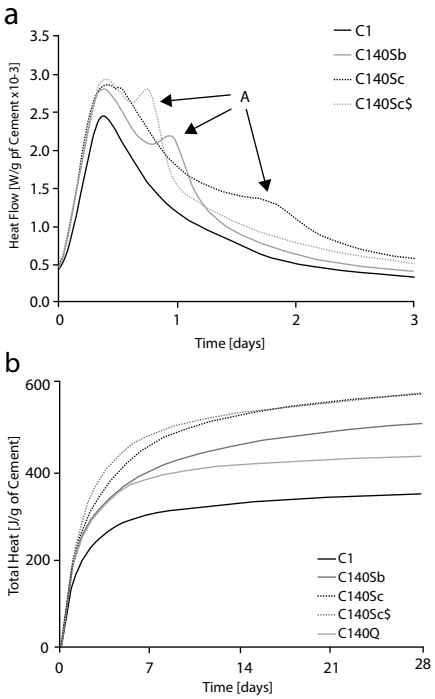

Figure 2.2.2: Isothermal calorimetry curves for the hydration of slag blended cement systems, showing a) heat flow, and b) total heat evolution, from Whittaker et al[47]. C1 represents an OPC paste, while other mixes contain blast furnace slags with different compositions and fineness

sub-bituminous coal producing high calcium fly-ash. The resultant recovered material is primarily a silicate glass modified with aluminium and iron, with CaO also present. By far the most common type of fly ash, and used in this project, is the low calcium, class EN450 fly ash, and so this will be focussed on.

Initially on mixing, OPC-PFA blended cements react as an standard OPC paste, due to the slow reaction of the PFA, although with a slightly higher portlandite content due to the filler effect[41]. As the paste matures, the pozzolanic reactions occur, and the portlandite within the system begins to be consumed[49]. The pozzolanic reactions are often said to occur only after ages of 28 days, while the exact time at which the full pozzolanic reaction begins to occur is debated, although it has been found that the pozzolanic reaction is strongly influenced by temperature[50], and this likely accounts for the range of onset times provided for pozzolanic reactions. It has been calculated that even moderate blending with fly-ash results in unstable portlandite and the production of additional C-S-H with a reduced Ca/Si ratio[41].

2.2.3 Recycled Concrete

As described in section 2.4, concrete is the most widely produced material in the world. With ever increasing pressure on the construction industry for environmental improvements and cost-cutting measures, the use of recycled concrete has risen sharply in the last couple of decades. Construction and demolition wastes in many countries make up large proportions of the total waste volume, and so efforts to reduce this amount have led to an increase in concrete recycling. In some countries where legislation and infrastructure is sufficient, such as The Netherlands, Belgium, Denmark and Japan, recycling rates of over 90% have been achieved[51].

2.2.3.1 Coarse Aggregate

Demolition waste materials and rubble are crushed and used as a replacement for the coarse aggregate fraction of fresh concrete with the new material widely known as recycled aggregate concrete (RAC). These materials include masonry structures, bricks, concrete, paving and even recycled bitumen aggregate from roads. Due to the differing qualities of some of the coarser aggregate replacement compared to natural aggregate, RAC is often used for non-structural concrete such as foundations or paving underlay. There is however a recent trend to use higher quality recycled aggregates for replacement in structural concrete, with standards for percentage amounts of contaminants[52].

Many studies have found that when washing is involved in the processing of recycled aggregate, its properties as a structural concrete aggregate are significantly improved. With washing and a proper screening process in place, the removal of impurities in building rubble such as paper and wood can be removed, as they often make up significant (in terms of affecting cement reactions) percentages of building rubble, up to 0.5%, enough to detrimentally affect structural concrete[53]. For recycled coarse aggregate, there are a number of factors that can affect performance;

- **Absorption**- The absorption of recycled concrete aggregate has been reported in the range of 3%[54] up to 7%[55], compared to that of natural aggregate in the range of 1% to 2.5%. The increased absorption of recycled aggregate has a detrimental effect on many properties of the concrete such as workability, creep, shrinkage and

elastic modulus. Although sometimes comparable, the compressive strength of RAC is usually lower, although some tests have found that early age compressive strength increases with increasing recycled aggregate usage[56]. This can be attributed to the increased absorption of the aggregate lowering the w/c ratio within the mix and thus increasing the hydration and therefore the compressive strength. Where in later age compressive strength RAC is lower than that of natural aggregate concrete, a lower w/c can be used to maintain comparable compressive strength but with a negative impact on the workability of the material. Due to this effect in the UK around 20% aggregate replacement can be achieved for structural concrete without the need for any additives such as water reducing agents[42].

- **Shrinkage**- When utilising primarily crushed concrete with little or no other contaminants, it has been found that structural concrete using recycled aggregate (RA) can achieve suitably similar compressive strength and elastic modulus properties compared to natural aggregate (NA) concrete[56], but that shrinkage is significantly higher. This is attributed to the much greater absorption of the recycled aggregate compared to the fresh natural aggregate, with Yong Ho et al[56]. reporting absorption in RCA to be 10 times that of natural aggregate. By the addition of a water reducing agent and slight alterations to the mix design, comparative compressive strength was gained. In an ideal situation concrete could be crushed and any of the existing natural coarse aggregate could be stripped from the matrix and recycled without any negative effects on the new concrete. It has been found however that when crushing concrete, significant amounts of cement mortar remain attached to the aggregate, leading to higher absorption causing lower compressive strength, durability, deformation and shrinkage properties compared to a natural aggregate concrete[57], when mix design isn't altered to account for the RCA.

- **Specific Gravity**- Recycled coarse aggregate also has a lower specific gravity than that of fresh aggregate. The presence of mortar coating the aggregate, and the high porosity of that mortar, is thought to affect the specific density. The specific gravity for recycled aggregate has been found to be in the range of 2.28[53] to 2.44 compared

to that of 2.67 for natural aggregate[58]. Due to the higher surface area available per volume of aggregate, a smaller coarse aggregate in the original concrete will result in larger proportions of attached mortar, and thus result in larger drops in specific gravity of the aggregate[59].

2.2.3.2 Fine Aggregate

Due to the relative volumes of material, the majority of recycled concrete research has focused on coarse aggregate replacement, with less work focussing on fine aggregate. Findings have shown, however, that the effect of recycled fine aggregate on mortar differs from the effect that recycled coarse aggregate has on concrete[53]. Whereas in recycled concrete using coarse aggregate the primary influence on compressive strength is the w/c ratio, with recycled fine aggregate mortars the percentage replacement of the aggregate is the primary factor affecting compressive strength. The decrease in strength due to aggregate replacement remains proportional at changing w/c ratios, as shown in fig. 2.2.3, with all three mortars following the same trend.

Within the nuclear industry in Japan, some work has been undertaken to examine the possibility of reusing contaminated concrete as fine aggregate for mortar in the disposal of their low level nuclear waste, where recycling of fine aggregate in these circumstances can prove economically beneficial and where compressive strength is a less important factor. A number of tests carried out compared a reference mortar to other mortars with varying w/c and sand/cement (S/C) ratios. It was found that mortars with higher S/C ratios outperformed those with lower ratios, and that recycled aggregate outperformed natural aggregate in terms of compressive strength[19]. This was attributed to the increased surface roughness of the recycled sand, much the same as rougher coarse aggregates increase the compressive strength of concrete.

2.2.3.3 Powder

Where research into recycling both fine and coarse aggregates have been driven by economic and environmental reasons, those drivers don't exist for fine aggregate, and so limited research has investigated the possibility of recycling very fine concrete powder.

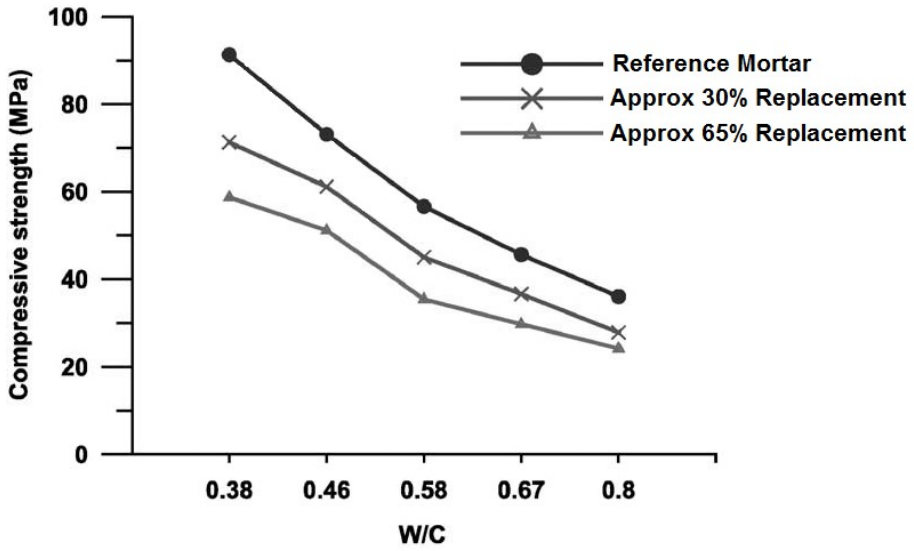

Figure 2.2.3: Compressive strength of mortars using varying percentages of recycled fines, from Chen et al.[53]

During the demolition and treatment of concrete to form recycled aggregates, there is a limited volume of powdered concrete produced, and the capture of this material is also difficult, and so the need for any processing of this material is non-existent. Thus the economic driver doesn't exist, and with such little of the material produced during concrete processing, the environmental benefits are outweighed by the difficulty and possible detrimental effects on new concrete, so little or no research has taken place.

While limited investigation has occurred investigating recycled concrete fines, a number of other fine powdered materials are used within concretes and cements in order to take advantage of aspects such as the filler effect (see section 2.3.1.1) or pozzolanic activity (see section 2.2.1) including materials such as pulverised fuel ash or ground granulated blast furnace slag. The chemical and physical advantages of using these materials are discussed further in other aspects of this report.

During research into reusing recycled fine aggregate as a solution to increasing the waste to disposal container volume ratio within the Japanese nuclear industry, a limited amount of recycled fine powder was used as a replacement material within some of the mixes and was found to increase the compressive strength of the mortar[19]. This was, however, linked to the increased absorption of the powder lowering the overall water to cement ratio in the mix, and thus increasing the overall strength. While this was assumed, it wasn't fully

investigated and it is possible that other causes of the strength increase may be possible, including the filler effect or some increased cementitious properties arising from the powder.

2.2.3.4 Two-Stage Mixing Approach

Developed in Hong Kong as part of their efforts to increase concrete recycling rates, the two-stage mixing approach (TSMA) aims to improve the properties of recycled aggregate for use in structural concrete. As discussed in section 2.2.3.1, recycled coarse aggregate has properties, such as higher absorption, that make it less suitable than natural aggregate for use in structural concrete. Two-stage mixing can often improve these qualities, or reduce the properties that have a detrimental effect on concrete strength and durability, as well as reduce the variability in strength of the recycled aggregate.

TSMA involves attempting to form a layer of cement slurry around the recycled aggregate, in order to fill in the cracks and voids on the surface that are due to the presence of attached mortar to the original aggregate. The concrete slurry will therefore reduce the porosity of the recycled material, which is the primary cause of the detrimental properties within recycled coarse aggregate. As well as reduced porosity, the addition of the cement slurry also improves the properties and thickens the interfacial transition zone (ITZ) allowing greater bonds between the cement matrix and the aggregate, increasing the overall strength of any recycled concrete[60].

It has been found that when using a TSMA the water sorptivity of the recycled concrete is reduced, with an almost 50% reduction when using entirely TSMA replacement aggregate as compared to recycled concrete using entirely untreated recycled aggregate[57]. As water sorptivity is related to direct water absorption of the concrete through capillary pore action, it can be shown that the TSMA decreases the absorption of the aggregate, improving its physical properties such that it is more comparable with natural aggregate. As part of the Hong Kong Housing Authority's work towards recycling demolition waste, it has been found that the two-stage mixing process can produce structural concrete using 20% recycled aggregate with comparable properties to that of concrete with fresh natural

aggregate[61].

2.3 Ternary Cements

2.3.1 Limestone-Portland Cements

Ground limestone has been used in cements as a filler in order to reduce costs, and in more recent times as a method for reducing CO_2 emissions related to cement manufacture. In Canada the addition of limestone filler was incorporated into construction standards in the 1980's (CSA 1983 - CAN3-A5-M83)[62]. Up to 5% limestone filler can be used within eurocode based CEM I cements, while eurocode CEM II/A-L can contain 6-20% limestone and CEMII/B-L can contain 21-35% ground limestone[63]. With the adoption of the precursor to EN197-1 in Europe in the early 1990's, there were over 25 countries that allowed up to 5% ground limestone filler in their Portland cement classes, while many allowed up to 35% in their Portland Composite cements[64]. Since then, more countries have adopted the inclusion of limestone filler into their cements. The prime constituent of limestone, calcium carbonate in its pure form, is known by the mineral names calcite, aragonite and vaterite, depending on the polymorph formed.

2.3.1.1 Filler Effect

As cement clinker reacts with water (hydrates), reaction products such as ettringite, calcium-silicate-hydrate (C-S-H) gel and portlandite are formed, at varying rates and at different ages of the cement. Pozzolans and latently hydraulic materials (see section 2.2.1), for instance, are only slowly reactive, with their reactions affecting the later age strength of concrete, from ages of around 14 days[41]. A number of factors affect the rate and amount of hydration, such as the water cement ratio (w/c), cement type and presence of any other additives.

It has been found that when using pozzolanic materials, such as pulverised fuel-ash (PFA), there is a significant increase in strength evolution at early stages, before the known pozzolanic effect is noticed and before phases within these materials have reacted. This has

been attributed to the filler effect, whereby the presence of additional surface area of anhydrous material allows for extra nucleation sites around which hydration reactions can occur[65,66]. At ages after around 7 hours the additional hydration can be noticed, and is accompanied by an increase in the quantities of bound water and portlandite, when compared to a reference mix with no anhydrous material. The additional reaction caused by the presence of these nucleation sites is known as the filler effect, and can be seen in fig. 2.3.1.

While the inclusion of inert material provides additional nucleation sites for hydration products, by replacing some of the cement or binder content with an inert or only slowly reactive material, the effective water to cement ratio (w/c) is increased, providing more water for hydration reactions to occur, thus increasing the early hydration reactions[67].

Berodier and Scrievener[68] found that the principal factor for the increased nucleation of C-S-H and the accelerated kinetics associated with the filler effect is the inter-particle distance, rather than the solely the provision of extra surfaces for nucleation sites.

2.3.1.2 Effects of Fineness and Particle Size Distribution

Initially limestone inclusion was thought to have little or no effect on cement hydration and concrete strength at replacement levels below 5%, besides that of its particle size affecting the nucleation sites available for the filler effect to occur[65,69]. Schmidt[70] found that for limestone replacements of 5-10% strength was normally not reduced, and finer grinding of the cement clinker and limestone was not required. Hawkins however, in a review of research conducted in many countries including Canada, the U.S. and the EU, found that for low limestone contents, finer grinding may be required to maintain the same strength[71]. The reduction in activity due to the inclusion of limestone requires offsetting by an increased fineness of cement. This increases the overall surface area of cement available for reactions to begin, increasing the reactivity and therefore the initial strength of the resultant cement or concrete. The findings of Schmidt can be linked to the hydration reactions described in section 2.3.1.3, with the expected strength reduction not found due to the accelerated hydration reactions.

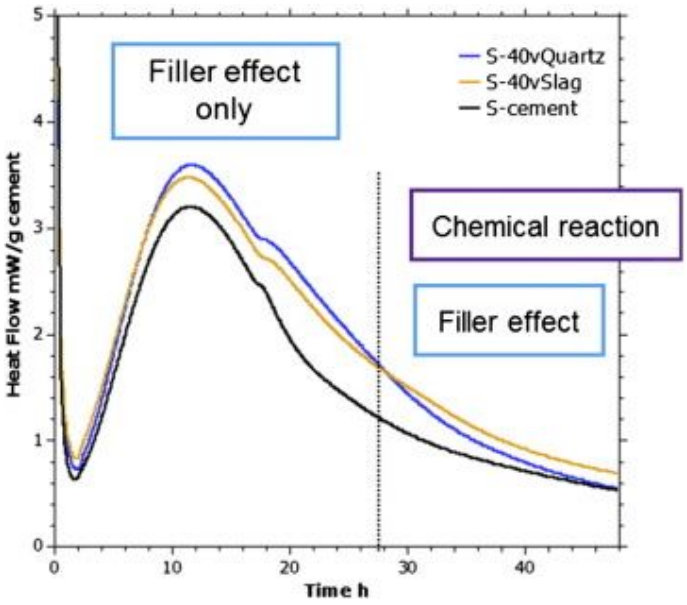

Figure 2.3.1: Filler effect in blended cements, from Berodier and Scrivener[66]

Schiller and Ellerbrock[69] found that the particle size distributions of constituents within ground mixed cements is greatly influenced by the resistance of other materials within the mix to being ground. Harder material becomes concentrated in the coarser fraction, while softer more easily ground material is concentrated in the finer fractions, as shown in fig. 2.3.2. Much of the early investigative work into Limestone-Portland cements was focussed on the physical properties of the two materials and achieving the correct fineness for the desired strength evolution[71]. Overall, it was found that finer grinding was required for higher replacement percentages to achieve the same overall strength classification[69], and that different grinding methods affect the fineness of the individual constituents[72].

2.3.1.3 Effects on Hydration

Klemm and Adams[73] studied the reaction of 5-15% of calcium carbonate and type II (moderate sulphate resistance) cement, at ages up to a year. They found that after 129 days 80 to 90% of the limestone (calcium carbonate) remains unreacted and acts primarily as an inert diluent. Their findings were supported by Sprung and Siebel[74]. At the same time however, a number of studies[75,76] show reactions occurring between the calcium carbonate ($CaCO_3$) and the tricalcium aluminate phase (known as aluminate or C_3A in cement chemistry, $3CaO.Al_2O_3$ in standard chemistry) during early age reactions, and an overall acceleration of the early hydration reactions. The type II cements used within Klemm and

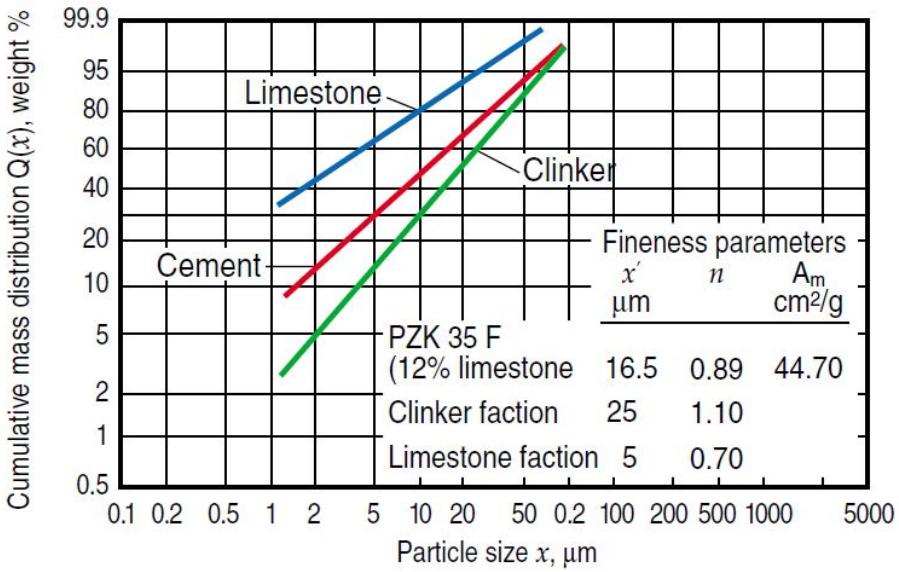

Figure 2.3.2: Cumulative mass distributions of a Portland limestone cement with a limestone content of 12% by mass, as well as of the two individual constituent materials after inter-grinding in an industrial ball mill, from Schiller and Ellerbrock[69].

Adams' work are sulphate resistant cements, and contain low aluminate (C_3A) content. The low aluminate content will have limited the formation of the carboaluminate phases found in other research[75–77], and so while limestone may stay unreacted in low aluminate cements, these results can't be claimed for all cement types, and in standard Portland cements limestone is a reactive inclusion.

The acceleration in early age hydration of cements with ground limestone filler was noted by a number of studies including by Ramachandran[78] and Pera et al.[79]. Figure 2.3.3, from Pera et al. shows the heat of hydration, from isothermal calorimetry experimentation, of the early age hydration reactions of a tricalcium silicate (alite) cement with and without calcium carbonate inclusion. From the data there is an obvious increase in the heat output at early ages up to 800 minutes, related to an increased rate of hydration. There is however no reference sample with an inert filler equivalent to the calcium carbonate inclusions used. The lack of any inert reference mix means that the increased hydration due only to chemical affects cannot be separated from those due to physical effects such as the filler effect[65], and so any quantification of results is invalid, particularly when trying to ascertain whether or not calcium carbonate is an inert filler.

While acting to increase the early age hydration, and therefore strength of cements, lime-

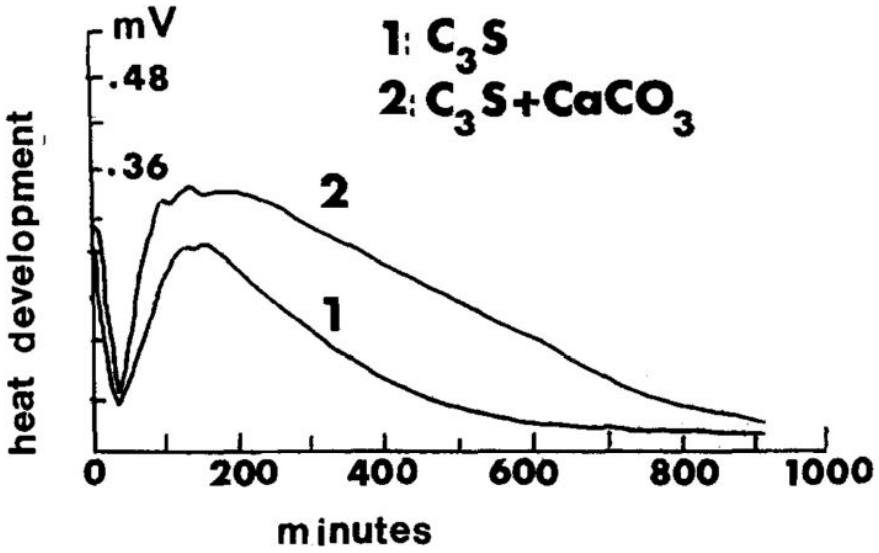

Figure 2.3.3: Isothermal calorimetry of early age hydration reactions for 1: tricalcium sulphate cement and 2: tricalcium silicate and calcium carbonate cement, from Péra et al.[79]

stone has been found to reduce the later age hydration, and therefore strength, of cements through the effect of dilution[80]. As limestone is used as a filler, the overall percentage of reactive cementitious materials is decreased, or diluted, and so at later ages the strength development is found to be below that of standard cements.

Lothenbach et al.[77], using both experimental and thermodynamic modelling results, found that limestone affects the hydrate assemblage of the hydrated cement. Supporting the earlier work of Stark[75] and Ingram[76], it was found that in the presence of limestone, calcium mono- and hemi-carboaluminate hydrate instead of calcium monosulphoaluminate hydrate was stable. Modelling showed that the stabilisation of calcium monocarboaluminate indirectly stabilised ettringite, increasing the total volume of the hydrate phase and decreasing porosity, due to the relatively low density of ettringite leading to a slightly larger volume per unit formula[81]. The effect of this interaction is limited however by the aluminate content within standard Portland cement clinker, but the reactions caused by the inclusion of limestone are more significant than earlier studies reviewed by Hawkins gave credit for[71]. Experimental results showed a lower than expected increase in porosity, possibly due to an overestimation in the amount of AFm phases in the calculations[77]. The volumes of hydration products calculated through the thermodynamic models are shown in fig. 2.3.4. The findings of Lothenbach et al. were further supported by the work of Matschei et al.[82]

who, using experimental and modelling results, found that much, if not all, of the calcite within limestone is reactive and alters the mineralogy of hydrated cement pastes.

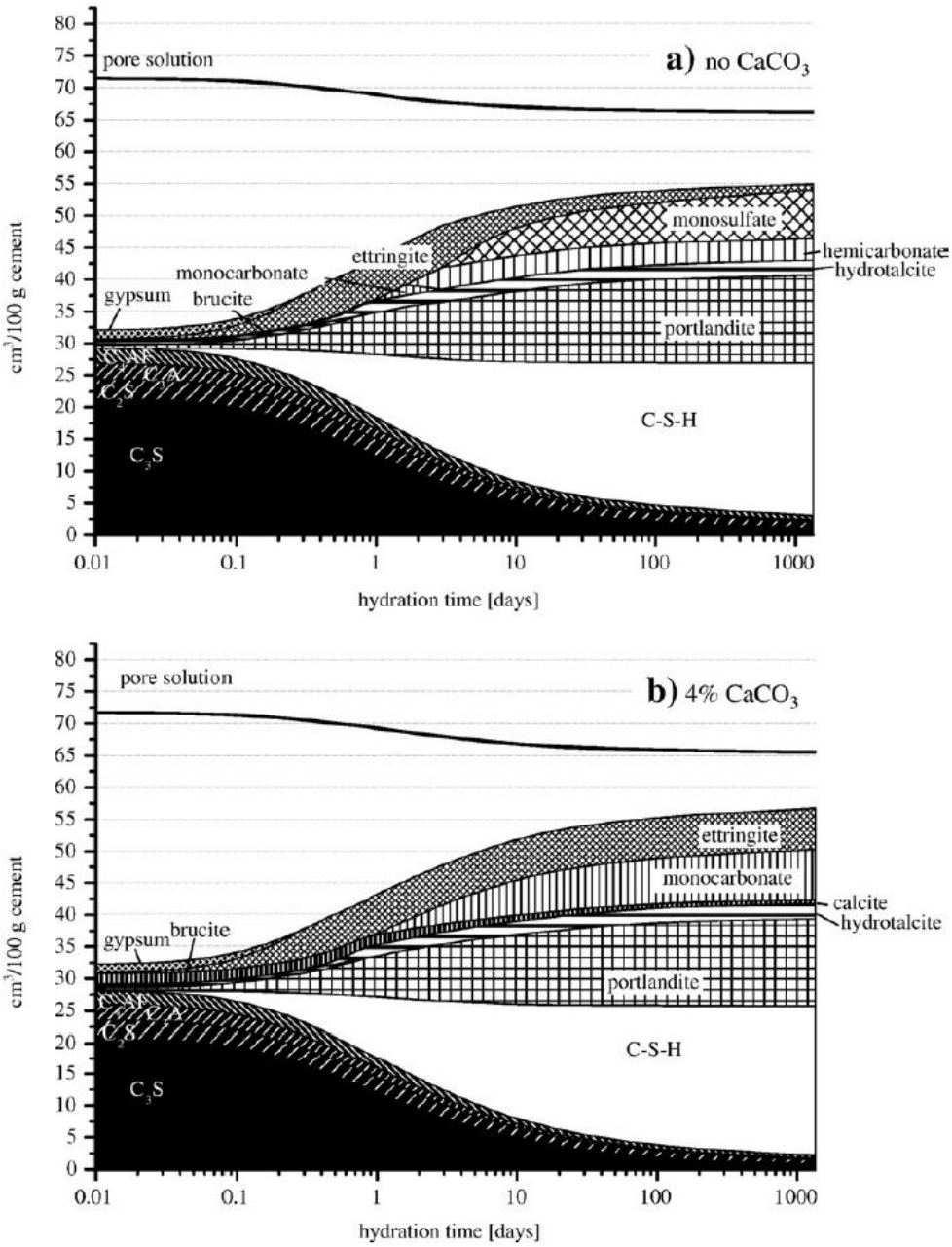

Figure 2.3.4: Modelled changes during the hydration of a) Portland cement with no limestone and b) Portland cement with 4 wt.% limestone addition, from Lothenbach et al. [77]

2.3.2 Ternary Cements

Unlike binary Limestone-Portland cements, ternary cements contain additional supplementary cementitious materials (SCM's). The addition of the two supplementary mate-

rials, as opposed to the more common single supplementary material lead to the term Ternary Cements. As nuclear encapsulation grouts contain high levels of slag, around 75%, this section will investigate primarily limestone-clinker-slag based ternary cements.

As discussed in section 2.3.1.3, the addition of limestone filler has been found to accelerate the early age hydration of cements, and therefore the early age strength [75,76,79], while reducing later age strength through the dilution effect [80]. The addition of pozzolans and supplementary cementitious materials, including pulverised fly-ash (PFA) and blast furnace slag (BFS), has long been known to increase the later age strength of cements in which they are used as a replacement material [21,41]. By combining these two effects in ternary cements, it is possible to significantly reduce the clinker content of a cement mix without reducing the overall strength [80].

2.3.2.1 Hydration of Ternary Cements with Slag

The overall chemical composition of slag varies with the impurities contained in the raw materials used during iron production [47], but is comprised predominantly of aluminate and silicate species, with additions of magnesia and lime species. When used in blended cement with Portland clinker, the slag reacts slower than the clinker, with earlier reactions required to provide the activation conditions under which slag will react [34]. Despite the slower reaction, slag produces analogous hydration products to that of standard cement, with the C-S-H having a lower Ca/Si ratio an increased Al/Si ratio [45].

As discussed in section 2.3.1.3, the inclusion of calcite (from limestone) in Portland clinker cement stabilises calcium mono- and hemi-carboaluminate hydrate instead of calcium monosulphoaluminate hydrate, stabilising the ettringite [77]. This process is limited by the low aluminate content of the clinker [82]. When limestone and slag are included in blended ternary cements, the higher alumina content of the slag means that the production of carbo-aluminates isn't limited by the clinker composition [81].

Adu-Amankwah et al. [83] have found that the inclusion of limestone in slag based ternary cements, as well as favouring the production of carbo-aluminates, increases the reactivity

of the slag within the system. In ternary cements with slag and limestone, the chemical shrinkage of the paste, which can be related to degree of hydration[84], increased with increasing limestone inclusion, shown in fig. 2.3.5. The C-S-H formed was found to have a lower Ca/Si ratio and higher alumina content than that formed during Portland cement hydration.

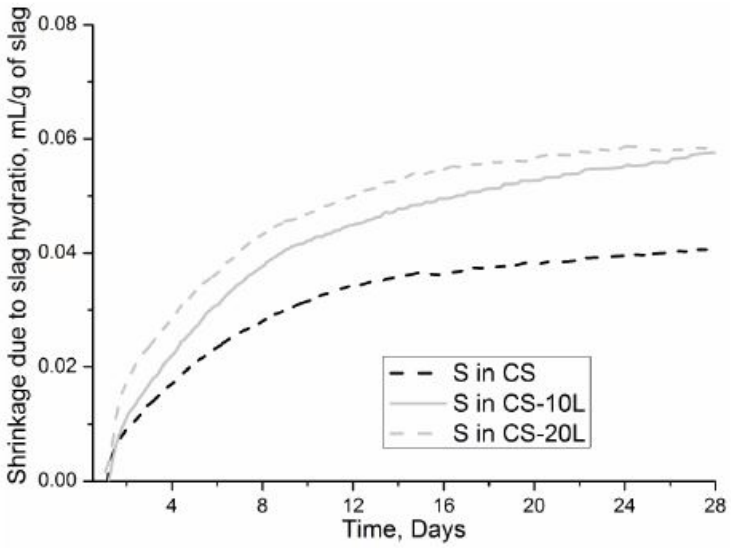

Figure 2.3.5: Chemical shrinkage of ternary cement pastes with different levels of limestone filler inclusion, from Adu-Amankwah et al.[83], normalised per g of slag. CS is with no limestone filler, where 10L and 20L represent 10 and 20% limestone filler, in the cement slag blend

2.3.2.2 Properties of Ternary Cements

When ground limestone is included within Portland clinker cements, there is an increase in early age strength, as discussed in section 2.3.1.3[78,79]. With limestone-slag ternary cements, the strength-increasing effect of the limestone addition is more pronounced than with limestone-portland clinker binary cements. Hoshino et al.[85] attributed this increase to the higher amount of calcium aluminate hydrates generated in the ternary cement system containing slag. The additional calcium aluminate hydrates fill pores as calcium carboaluminate, increasing the compressive strength.

Aside from the strength increases associated with the inclusion of limestone and slag in ternary cement blends, the mechanical properties of mortar and concrete can be improved through the use of ternary cements. Ghrici et al.[86] cast mortar prisms with ordinary

Portland cement replaced by upto 20% limestone filler and 30% natural pozzolan (quarried from Beni-Saf in Algeria). Compressive strengths were measured at 2, 7, 28 and 90 days, and strength was found to increase at both early and later-ages for both flexural and compressive strength. The strength increases at different ages are affected by the replacement material. For early age strength, 10% limestone inclusion and low natural pozzolan inclusion produced the higher results, whereas for later age strength, the highest values move towards higher pozzolan inclusion and lower limestone replacement. Durability of the mortar was also increased, with chloride ion ingress reduced in the ternary cement compared to both a binary cement with clinker and pozzolan and a simple clinker based cement. The durability increase is likely linked calcium aluminate hydrate filling the pores as described by Hoshino et al.[85], having a double effect of increase strength and durability.

2.4 Concrete

Concrete is the most produced material in the world, and second only in consumption to water, with an estimated 25 billion tonnes produced per year, equating to nearly 4 tonnes per person per annum, resulting in significantly more concrete being used around the world compared to all other construction materials combined[87], with around 5% of global CO^2 emissions coming from the cement industry[42].

Created by the combination of cement, aggregates and water, concrete is a versatile and durable building material, liquid when first mixed that solidifies within hours of mixing, eventually forming a solid material, with properties not dissimilar to those of stone or rock. Concrete's ability to be cast as a liquid and form into whichever shape an engineer requires has turned it into such a widely used building material. While the Romans are widely known to have used concrete, or concrete-like materials, the modern widespread use of concrete as a construction material dates back to the late 19th and early 20th century, with the first reinforced concrete bridge being the Alvord Lake Bridge in San Francisco built in 1889. It has since become the most widely used building material in the world, and the second most consumed material behind water.

As the aggregates used in concrete are largely unreactive, the bulk of the properties of concrete are governed by the cement paste, and the interaction of the paste with the aggregate. As such, only the properties of concrete relevant to this research will be discussed.

2.4.1 Concrete Carbonation

Atmospheric carbon dioxide will diffuse into bulk concrete, through gaseous diffusion into concrete pores, whereupon it will dissolve within the pore water, creating carbonic acid (H_2CO_3)[88]. The acid will then disassociate as HCO_3^- and CO_3^{2-} ions. Under these conditions, a number of physiochemical processes are reported to occur[89]. The importance of concrete carbonation is primarily related to the creation of carbonic acid and the associated drop in pore solution pH, with fully carbonated concrete having a pore solution pH of 8.3 compared to that of between 12.5-13.5 in bulk concrete[90]. In reinforced concrete, this drop in pH leads to instability in the passive layer protecting the reinforcing steel, such that it is then susceptible to corrosion and the durability of the overall reinforced concrete is compromised. For the scope of this project, the carbonation reactions that occur with the cement paste are of interest, and are discussed in further detail below. For a full guide to concrete carbonation, the review paper by Šavija and Luković[17] provides a thorough and up to date review of the present knowledge and challenges of concrete carbonation.

2.4.1.1 Carbonation of Portlandite

Calcium hydroxide (portlandite, CH) will react with carbonic acid to form calcium carbonate, of which two polymorphs are primarily formed; vaterite and calcite. The general formula for this reaction is shown in equations 2.4.1 and 2.4.2.

$$\text{carbon dioxide + water} \rightarrow \text{carbonic acid } CO_2 + H_2O \rightarrow H_2CO_3$$

$$\bar{C} + H \rightarrow \bar{C}H \tag{2.4.1}$$

$$\text{calcium hydroxide + carbonic acid} \rightarrow \text{calcium carbonate + water}$$

$$Ca(OH)_2 + H_2CO_3 \rightarrow CaCO_3 + 2H_2O$$

$$CH + \bar{C}H \rightarrow C\bar{C} + 2H \tag{2.4.2}$$

Groves et al.[91] investigated the carbonation of hardened C_3S paste. It was found that the carbonation of calcium hydroxide is initially fast, but the rate of reaction begins to slow down well before full carbonation of the CH has occurred. Through investigating the crystals using transmission electron microscopy (TEM), it was found that calcium carbonate microcrystals begin to form around the CH, with small pores. The slow down in the rate of reaction of the CH is attributed to a passive coating of calcium carbonate crystals around the calcium hydroxide. This slow down in carbonation rate, and protection of CH by dense calcium carbonate has been supported by further studies[17,92,93]. Galan et al. have found the dissolution rate of calcium through the protective layer to be 1-2 orders of magnitude below that of unprotected portlandite[94].

2.4.1.2 Carbonation of C-S-H

C-S-H has also been found to undergo carbonation, but with a slower reaction rate to that of portlandite[91]. Carbonation of C-S-H leads to decalcification of the phase, and full carbonation has been found to result in an amorphous silica gel and various polymorphs of calcium carbonate[95,96] (calcite, vaterite, and small quantities of aragonite). The general equation for C-S-H carbonation can be shown as in equation 2.4.3[17].

calcium-silicate-hydrate + carbon dioxide → silica + calcium carbonate + water

$$(CaO)_x(SiO_2)(H_2O) + xCO_2 \rightarrow xCaCO_3 + SiO_2(H_2O)t + (z\text{-}t)H_2O$$

$$C - S - H + \bar{C} \rightarrow C\bar{C} + C - S + H \tag{2.4.3}$$

As described in section 2.1.1.6, C-S-H composition can vary significantly, with a range of densities and Ca/Si ratio, within the same paste. The composition of C-S-H has been found to affect the carbonation process, with the C/S ratio shown to play a signifiacnt role in the carbonation mechanism[96,97] with inner product (IP) and outer product (OP)

C-S-H carbonating at different rates[98]. Ca from more fibrillar and less dense OP C-S-H will decalcify first, with Ca initially being lost from silica chains and defect sites, before full decalcification leads to a porous amorphous silica gel interspersed with micro vaterite or calcite crystals[98]. Inner product C-S-H has been shown to carbonate slower than OP C-S-H, with a number of different studies, using TEM , X-ray photoelectron spectroscopy and NMR results all showing some remaining IP C-S-H after long carbon exposure[91,98,99], or showing remaining C-S-H after carbonation of a synthetic version[96].

2.4.1.3 Carbonation of Blended Cements

Within blended cements, the phase assemblage and morphology differs from that of a CEM I OPC paste, where the use of SCM's and the subsequent alteration of the hydration kinetics changes the amount and type each phase. The reduction in cement content, and the pozzolanic reaction when PFA is used, leads to a reduced portlandite (CH) content, while the C-S-H produced has a reduced Ca/Si ratio[32].

The performance of blended cements under carbonation is dependent upon a number of factors[100]. The reduced portlandite content and porosity and permeability (see section 2.2.2) can make blended cements less susceptible to carbonation, yet also the reduced portlandite content can be detrimental for maintaining pH levels and thus passivity of reinforcement steel in concrete.

The reduced Ca/Si ratio present in C-A-S-H gel (see section 2.1.1.6) makes it increasingly susceptible to carbonation, and subsequent conversion to calcium carbonate and silica gel. Sevelsted and Skibsted found that decomposition rate of C-S-H and C-A-S-H decreases with increasing Ca/Si ratio[101], removed from the interlayer and defect sites until a Ca/Si of 0.67 is reached. From here, calcium is consumed from the principal layers, resulting in an amorphous silica gel. The reduced Ca/Si ratio of C-A-S-H therefore makes it more susceptible to carbonation that that of higher Ca/Si C-S-H.

2.4.1.4 Factors Affecting Carbonation

As previously mentioned, carbonation of concrete is driven by diffusion of CO_2 through the cement matrix, before dissolution within pore water whereupon carbonation reactions with cement phases will occur. Many environmental factors affect the rate and type of carbonation that take place, which are also of importance for accelerated carbonation testing.

2.4.1.4.1 Concentration

CO_2 concetration within the atmosphere is mostly constant, at 0.04%, with small local variations or +/- 0.001% due to environmental factors[102]. At this concentration, natural carbonation is a slow process, with degradation taking many years to occur[20]. In laboratory testing, accelerated carbonation of cementitious materials can be carried out through storage at higher CO_2 concentrations. These accelerated tests have been carried out at concentrations up to 100%, while many countries have their own standardised tests also covering a wide range of concentrations. In the British and German standards, these concentrations are limited to 2 and 4%, while Italy and China use 50 and 100% CO_2 concentrations respectively[103].

A number of studies have been carried out to determine the effect these raised concentration have on the carbonation mechanism. It has been found that upto 3% concentration, the carbonation process is the same as that occurring in natural carbonation[92,104,105], while an identical or very similar process has also been reported upto 5%[89,103].

Beyond concentrations of 5%, the carbonation mechanism changes, and is no longer similar to that of natural carbonation. Cui et al. reported a CO_2 concentration of 10% as suitable for accelerated carbonation, but carried out no tests below this level, aside from natural carbonation, against which to compare[106]. Tests at higher CO_2 concentrations have been found to differ from that of natural carbonation, with different carbonate polymorphs formed[91,97,103], and so an upper limit of 4-5% has been proposed for accelerated carbonation testing to mimic natural carbonation[17].

2.4.1.4.2 Relative Humidity

Dissolution into water to form carbonic acid is vital for the carbonation process, and so a high enough relative humidity (RH) is required for the process to occur. CO_2 diffusion through gaseous pores is however orders of magnitude higher than that through water filled pores[107]. In conditions where relative humidity is too low, the lack of moisture prevents sufficient formation of carbonic acid. When RH is too high, the moisture will fill pores in the cement paste, and prevent diffusion of CO_2 gas through the bulk. It has been found that at RH's between 50-70%, carbonation rate is highest[17,92,103], while some have suggested that 57% is the RH at which carbonation is a maximum[105].

2.4.1.4.3 Concrete Properties

With carbonation ingress being a diffusion and dissolution driven process, the properties of the concrete or cement paste determine the ease with which CO_2 can move into the bulk. Limiting the porosity and permeability of the cement paste will limit the gas diffusion through the concrete[17]. Not only will porosity limit gas diffusion, it has been found to limit carbonation due to limiting calcium hydroxide crystal formation. Chaussadent et al. investigated the effect of w/c on the carbonation of cement pastes. At levels below 0.4 w/c, with low capillary porosty, calcium hydroxide formed smaller microcrystalls, with less permeable surrounding mass, reducing the effect of carbonation. Above 0.4 w/c it was found that increased amounts of CH form, with the Ca/Si ratio of the C-S-H dropping. The CH also formed larger crystals and was easier to carbonate[108]. This was however carried out on cement pastes, within concretes the w/c threshold may change due to water demand of the aggregates.

The use of supplementary cementitious materials, or cement replacement products also affects the carbonation of concrete, although the effect is very much dependent on the mix design. SCM's are known to consume CH during pozzolanic reactions[41,47,109], providing less reactive species for carbonation. BFS has however been shown to produce C-S-H with lower Ca/Si ratio, particularly when high alumina slag is used[47], resulting in a C-S-H more susceptible to carbonation[110], with the same found for PFA[111]. While the C-S-H itself is

more susceptible to carbonation, blended cements create C-S-H with lower interconnected porosity[48] and so the overall susceptibility to carbonation, while still being greater than that of OPC cements[110], isn't as high as solely the increase in C-S-H carbonation.

2.4.1.5 Carbonation Rate

During the natural carbonation process of structures, the RH naturally varies significantly, from low levels at 10% RH, upto 100% RH. Thus exposure conditions play a large role in the natural carbonation process for structures. As the carbonation process is governed by the diffusion of CO_2 through the structure, a relationship between the depth of carbonation front and time can be written.

$$x = K\sqrt{T}$$

where;

x = depth of carbonation front

K = carbonation coefficient

T = time

As carbonation is dependent on a number of factors, as discussed, the carbonation coefficient can vary significantly, but the overall depth is related to a root time law. As such, the surface layer of concrete can become carbonated within a few hours or days after casting, but even after many years the depth of the carbonation front will remain within the outer few centimetres of concrete[17]. In order to protect the reinforcing steel, building codes specify a set depth of concrete cover over the steel, to protect from detrimental processes such as carbonation, dependent on exposure class[112].

2.4.2 Concrete - Contamination and Decommissioning

Concrete is a porous and permeable material, into which contaminants can ingress and bind themselves in a number of ways to the concrete. In the vast majority of concrete used in infrastructure, the three main contaminants causing harm to structures are chlorides,

sulphates and carbon dioxide. When used on nuclear sites however, concrete can also become contaminated with either airborne or waterborne radionuclides. The relevant radionuclides include ^{60}Co, ^{63}Ni, ^{90}Sr, ^{137}Cs, ^{129}I, U, Pu, Am and other actinide elements[16]. Concrete exposed to a neutron flux can also become activated, particularly close to any reinforcing steel. The activity levels within the outer, exposed layers of concrete on nuclear sites can reach the levels of intermediate or low level waste, and so special handling, dismantling and disposal are necessary for a successful decommissioning outcome.

2.4.2.1 Radioactive Contamination

The contamination of concrete on nuclear facilities is dependent on the exposure of the concrete to sources of radionuclides or a neutron flux. Concrete and building rubble from nuclear power plants are likely to be dominated by ^{60}Co and ^{137}Cs, whereas fuel production and cycle facilities are dominated by U isotopes, mainly ^{234}U. Fuel reprocessing facilities and others that deal with unsealed spent fuel are dominated by a wide range of radioisotope contaminants from uranium, transuranics, fission products and activation products of concrete and reinforcing steel. The relevant radionuclides at these facilities include ^{235}U, ^{238}U, ^{239}Pu etc. plus ^{137}Cs, ^{90}Sr, ^{55}Fe, ^{60}Co, ^{63}Ni etc[113].

The depth of the radionuclides and their bonding to the concrete depends on their properties, with more soluble and mobile nuclides such as iodine penetrating relatively deep into the concrete, wheres more particulate and strongly sorbed nuclides such as plutonium are likely to be found on the surface[16]. Usual depths of penetration found on nuclear sites are in the range of several centimetres, with radioactivity at a depth of 8 inches (20.32cm) found to be around five orders of magnitude lower than at the surface during U.S. Department of Energy (DoE) experiments using ^{60}Co[113]. The work of Bath et al., shown in fig. 2.4.1, shows a root time relationship for depth of contamination, as with carbonation, and therefore a strong likelihood that scabbled concrete may also be carbonated.

Radioactive contamination within concrete is almost entirely contained within the cement paste, with the aggregate containing very little contamination. Tests on cores from nuclear power stations in the Netherlands have shown that following complete separation,

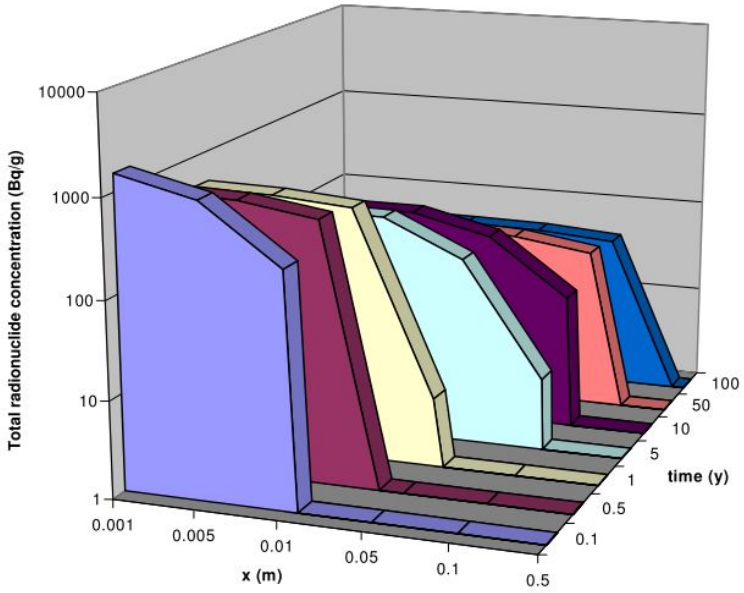

Figure 2.4.1: Radionuclide contamination depth in concrete (x) as a function of time (y), from Bath et al.[16]

the activity levels within the cement paste are around 10 times greater than within the aggregate[114]. The radionuclides are bound in two ways into the cement matrix; physically bound within the pore solution or chemically sorbed onto the large surface area of the cement gel phases[16].

The contamination of concrete in general, outside of the nuclear industry, is dominated by chloride contamination from seawater or de-icing salts. Chloride ions are particularly soluble and cause damage to concrete through the corrosion of reinforcing steel[20]. Other contamination can be in the form of sulphate attack and alkali-silica reactions[21].

2.4.2.2 Decommissioning

As part of the decommissioning process, and in line with the waste management hierarchy[3], efforts are made to reduce the overall volume of nuclear waste. For radioactively contaminated concrete this is primarily in the form of removing the outer contaminated layer from the bulk concrete, enabling the remaining bulk to be disposed of as exempt waste and requiring only the removed contaminated material to be disposed of as a controlled nuclear waste. Depending on the activity levels within the contaminated material, it will be classified as either low or intermediate level waste. There exist a number of

methods for removing the contamination from the bulk material, with some more technically mature and used more often than others[113].

2.4.2.2.1 Scabbling

Scabbling is the process of removing the outer contaminated part of the concrete through in-situ breakdown, through mechanical or other means. The material created is therefore primarily particulate in nature, depending on the method used, and contains a mixture of cement paste and aggregate. Scabbling is the most common form of decontamination of the concrete, with a number of methods employed using mechanical and physical means.

- **Mechanical** - Mechanical scabbling uses machinery to abrade the outer surfaces, essentially grinding away the contaminated concrete. The resultant material is particulate with a varying size distribution, primarily of particles less than one centimetre in diameter, often much finer. Mechanical scabbling has been carried out using diamond blade grinding[115], grit blasting and tungsten-carbide tipped pistons[113].
- **CO_2 and Cryogenic Blasting** - Through the use of highly pressured cryogenics, primarily liquid nitrogen and carbon dioxide, scabbling of concrete surfaces can be achieved. Grit blasting using frozen CO_2 crystals has been widely carried out, using similar mechanics to grit blasting, but with no secondary waste produced due to the evaporation of the crystals. High pressure liquid nitrogen blasting is a relatively new technology, with limited industrial use, but with good efficiency at removing up to 40mm of concrete in a single pass[116].
- **Thermal** - Unlike conventional scabbling using the pressure exerted through a secondary medium to pulverise and grind away the contaminated material, thermal treatments can be used to cause expansion and subsequent cracking and spalling of the outer layer of contaminated concrete. The two most common forms of thermal decontamination are laser[117] and microwave scabbling[113].
- **Water** - High pressure water removal has been widely used in the concrete repair and maintenance industry as an effective method for removal of broken and chloride contaminated cover, exposing reinforcement such that repairs can be carried out

and a fresh cover applied. This technology has been widely adapted for use in nuclear decommissioning as a method for removal of contaminated concrete[118]. The high pressure jet can be used to remove the radioactively contaminated outer layer, resulting in clean bulk material and a wet contaminated concrete waste stream. Some effluent capture and treatment is required for the water used to remove the material.

2.4.2.2.2 Removal

Where scabbling breaks off the contaminated concrete in small parts or as a particulate material, intact removal involves the separation of the contaminated layer from the bulk while maintaining large intact blocks or sheets of contaminated concrete. The choice between scabbling and intact removal can be dependent on the project circumstances and access. At Sellafield, diamond saw cutting of contaminated concrete for Windscale Pile 2 has taken place, with sheets of contaminated concrete produced[119].

2.4.2.2.3 Electrokinetic Removal

Electrokinetic removal is a novel technique that aims at reducing the radioactive concentration of the contaminated concrete below levels for certain waste thresholds, such that alternative and often simpler and more economic disposal options can be considered. Similar to methods for the removal of ions from chloride contaminated concrete, electrokinetic removal uses the charges on the radionuclide ions as a way of being able to draw them from the concrete into a liquid bath on the surface, using induced electric current and a cathode to draw out radionuclides from the cement matrix. Test have shown this technique to be particularly effective on removing caesium, but much less effective on cobalt due to its precipitation in the high pH of concrete[120]. When used with a pre-wash, removal rates of cobalt can be increased.

The use of electrokinetic removal techniques for radioactive concrete isn't high, particularly in the UK, with the complexity of the technique, its production of secondary waste and incomplete removal of radionuclides making it less preferable to more destructive techniques for contaminant removal.

2.5 Nuclear Encapsulation Grouts

Cementitious grouts are used as the main immobilisation technique for ILW in the UK, and throughout much of the rest of the world. While other encapsulation methods have been researched and investigated, and in some cases used for particular waste streams, by far the most common encapsulation method for non heat generating waste is within a cementitious grout matrix[121,122]. The wide knowledge base of cementitious materials, as well as the relatively low costs and simple deployment method make them a desirable encapsulation material, while proving shielding and providing sorption and reaction sites to further assist in the immobilisation of radionuclides[122].

A typical waste package is shown in fig. 2.5.1, where the conditioned waste has been exposed, showing the internal structure of the waste and grout interactions, and why a grout of specific properties is required to achieve full and affective encapsulation. A number of wide ranging reports by Glasser[123], and Glasser et al.[124] provides in depth detail about many of the issues, both beneficial and detrimental, posed by the used of cementitious systems for nuclear waste encapsulation, and form a large basis of the understanding of the chemistry of nuclear encapsulation grouts and conditioned waste.

Figure 2.5.1: Section of conditioned ILW canister

2.5.1 Properties

Unlike cementitious materials used for standard civil engineering purposes such as concrete and mortar, where structural performance is the primary factor, encapsulation grouts require a different set of properties to reflect their purpose, with chemical properties becoming more important at longer ages[121]. The high aqueous pH maintained by Portland cement based cementitious systems, and the the buffering reserve in cement solids to maintain this high pH over long time periods, has been cited as the most important factor in the immobilisation of waste species, leading to their precipitation as either hydrous oxides or hydroxides[125]. With high replacement levels possibly leading to a reduction in pH, measurements were taken for the highest replacement levels to determine whether pH was still raised sufficiently.

2.5.1.1 Composition

The current UK grout mix uses a composite system of Portland cement and blast furnace slag to attain the required properties, in which material ratios can be slightly altered where required to maintain the desired properties.

A 1:3 OPC:BFS ratio is used, while recent changes to the supply of raw materials has lead to a blend of two blast furnace slags being used, in order to maintain rheological properties and water demand[126]. Within the blast furnace slag, are a finer slag similar to those used for construction purposes, and a coarser slag used to maintain properties. The coarse to fine ratio is 3:7.

The specific materials used in Sellafield encapsulation grouts are Ketton OPC, Port Talbot BFS (fine slag fraction) and Calumite (coarse slag fraction). More detailed information on each of the materials can be found in section 3.1.

2.5.1.2 Physical Properties

2.5.1.2.1 Workability

In a concrete mix, workability describes the ease with which it is transported, pumped, formed and worked with. The water to cement (w/c) or water to binder ratio affects the fluidity of the mix, and so governs the workability. Aggregate and powder particle size and shape can also play a role within the workability of a concrete.

With the need for full encapsulation of any waste within waste containers, the fluidity of encapsulation grouts must be such that it can readily flow into any gaps and crevices present in the waste, and so the fluidity of the grout is highly important. The standard grout fluidity test within the UK nuclear industry is a Colflow test[8,9], in which a quart (2 pints, or 1.13l) of grout is released from a tundish, to flow down a measuring channel 102mm in width and has a measuring length of 890mm. The distance along the channel that the grout freely flows is known as the 'flow', with a standard UK ILW encapsulation grout having a flow of 258-480mm.

2.5.1.2.2 Porosity and Permeability

Over the long time scale of nuclear waste encapsulation, the porosity and permeability of of encapsulation grout becomes increasingly important in the prevention of groundwater ingress and subsequent radionuclide leaching. Whilst there are no defined limits for permeability and porosity, both should be kept to a minimum.

2.5.1.3 Chemical Properties

2.5.1.3.1 Heat of Hydration

Heat of hydration is limited in order to minimise the production and evolution of thermal cracking during curing, which would provide pathways for groundwater to infiltrate the waste package during disposal, and allow the leaching of radionuclides out of the waste package[127]. With the 500 l intermediate level waste drums being relatively large for a

grout pour, the cumulative heat of hydration is limited to 250 J per gram of binder (cement and slag content).

2.5.1.3.2 Setting Time

A set within the first 24 hours is required so that sufficient strength for transportation of the waste packages is attained. Due to the industrial process of mixing, pumping, filling and sealing the waste packages however, it is also important that the mixes don't set early, and so a setting time of longer than 4 hours is specified to prevent any blocking of the system, and to ensure that full encapsulation can occur before the mix sets[122].

2.5.2 Grout-Waste Interactions

Cementitious systems for encapsulation aren't selected solely for their physical encapsulation properties and low costs. As well as being physically encapsulated in a cement matrix, where the solid barrier will minimise leaching, there are further chemical properties of encapsulation grouts that make them suitable encapsulation materials.

2.5.2.1 Radionuclide Solubility

It is known that with increasing pH levels, the solubility of a number of radionuclides is reduced[128]. At a pH of over 12, many of the radionuclides remain largely insoluble or as colloidal deposits, reducing the risk of radionuclide leaching into groundwater and release into the biosphere.

The high pH environment created by the use of Portland cement, even within blended cement, is therefore a suitable mechanism to provide a solid barrier to waste leaching, while also minimising radionuclide solubility. Within systems containing ordinary Portland cement, the pore solution pH is high, usually >12.5, while the buffering reserve caused by remaining cementitious solids maintains a high pH even over significantly long periods of time[123].

2.5.2.2 Radionuclide Sorption

Within hydrated, and hydrating, cement systems, a number of different phases are present, as discussed in section 2.1.1. A number of radionuclides are able to be sorped onto, or into these phases.

Depending on the relative concentration of the radionuclide species (concentration in waste vs concentration in cement phase), there exist a number of mechanisms for sorption[123]. At low concentrations, radionuclides are held in weak electrostatic bonds to the cement solids and phases.

At higher relative concentrations however, some species can be chemically bound to cement phases, especially C-S-H, with its high surface area and number of sorption sites. At higher concentrations still, some radionuclides can be bound through solid solution and substitution of atoms within cement phases. The Al in AFm for instance, can be substituted with Cr(III) and other trivalent ions, chemically binding them into the cement phase and preventing leaching[123], while it has already been shown that C-S-H can incorporate minor and trace elements[44], which could include radionuclides. The increased alumina content in nuclear encapsulation grouts, and therefore the higher proportion of AFm phases, is beneficial to the sorption and encapsulation of radionuclides from radioactive waste[16].

Chapter 3

Materials and Methods

3.1 Materials

Within this project, and in line with current Intermediate Level Waste encapsulation grout formulations in the UK, a number of materials were used throughout. This section will describe the physical and chemical characteristics of these materials.

3.1.1 Ketton Ordinary Portland Cement

Within current UK standard ILW encapsulation grout, Ketton OPC is used as the cement phase. This cement differs from a standard CEM I cement as it contains no grinding aids or Minor Additional Constituents (MAC's) such as limestone, which is allowable within a standard CEM I cement at upto 5% inclusion. Due to the need for long term safe storage, the lack of MAC's or organic grinding aids reduces the risk of unexpected reactions with waste forms.

The Ketton OPC used within this study is of the same batch used within a previous study[126], with a chemical composition calculated through Bogue calculations based on the use of X-Ray Fluorescence (XRF), shown in section 3.1.3, and particle size distribution calculated through laser diffraction analysis (as described in section 3.2.3) and shown in fig. 3.1.1.

3.1.2 Port Talbot Blast Furnace Slag

Port Talbot steel works is an integrated steel production plant in Port Talbot, South Wales. Owned and operated by Tata Steel Europe[129], the plant produces blast furnace slag as a by product of steel production. For further information on the hydration of GGBS see section 2.2.2. The Port Talbot GGBS used within this project was provided by Hanson cement and its chemical composition was determined via XRF, as shown in section 3.1.3, while the PSD is shown in fig. 3.1.1.

3.1.3 Calumite

Calumite is a coarse, sand like blast furnace slag, with a particle size distribution similar to other raw materials in the glass manufacturing industry, for which it is primarily produced. Calumite is a trade name, owned by a subsidiary company of Hanson cement, operating under the same name as the material they produce.

In order to maintain the fluidity and heat of hydration required within nuclear encapsulation grouts, Calumite is used to replace some of the finer GGBS, and so is used within this research. A more detailed description of the use of Calumite within encapsulation grouts is given in section 2.5.1.1. The chemical composition and PSD of the Calumite used within this project is detailed in section 3.1.3 and fig. 3.1.1

Table 3.1: Material oxide composition as weight percent, determined by XRF

	Oxides										**d50 (um)**
Material	CaO	SiO_2	Al_2O_3	TiO_2	MnO	Fe_2O_3	MgO	K_2O	Na_2O	SO_3	
Ketton OPC	65.4	21.1	4.5	0.4	0.1	2.8	1.0	0.7	0.3	3.4	20.5
Port Talbot BFS	39.9	34.0	12.2	0.7	0.3	0.2	8.8	0.5	0.1	1.0	15.0
Calumite	40.5	36.0	11.8	0.9	0.4	0.36	7.9	0.6	0.3	0.6	470

3.2 Experimental Techniques

A number of experimental techniques are available to examine the behaviour of cements and concretes, as well as powders. A combination of these techniques are used in this project, with material characterisation involving a number of small scale tests examining

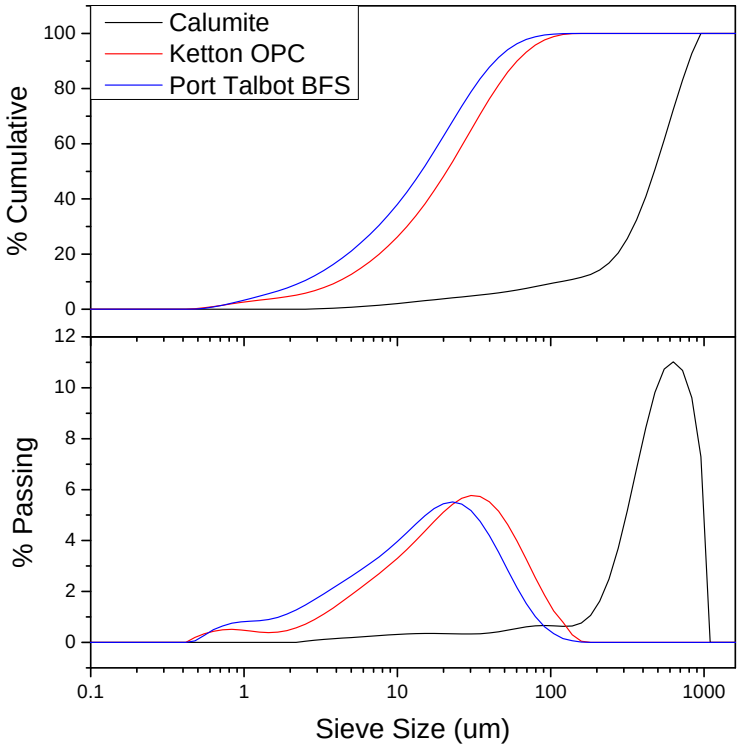

Figure 3.1.1: Particle Size Distribution for raw materials

individual materials or particles, while examining the engineering properties of the material uses larger scale techniques examining the new material as a whole. The techniques used throughout the project are described and explained below.

3.2.1 Isothermal Calorimetry

3.2.1.1 Background

Calorimetry is a measure of the heat transfer within a material associated with changes of state. Within cement science it is associated with the phase changes described within section 2.1 of this report. As many of the hydration reactions occurring during cement curing are exothermic, the degree of hydration can be related to the heat transfer to the surroundings.

A calorimeter consists of 2 primary aspects, the calorimeter block and data logging system. The calorimetry block has twin-channels, with vaults for both sample and reference ampoules. Attached to the calorimetry block is a thermometer and thermostat, where

the experiment temperature can be set. As the equipment is isothermal, this temperature is then maintained throughout the experiment, with the air surrounding all samples and references held constant. This then enables any temperature changes within the sample to be directly related to chemical reactions occurring. Any temperature changes within the reference ampoule due to temperature changes within the calorimeter are also known and so these background changes can be subtracted from the sample data increasing the reliability of the results. The reference ampoule should have a specific heat capacity as close to the reference ampoule as possible yet be inert, and so quartz is used at the same water to solids ratio as the sample.

3.2.1.2 Methodology

The equipment used during this research was a TamAir 8 channel Calorimeter. The manufacturer provided 20 ml disposable ampoules into which the samples were cast. 9 g samples (including water content) were mixed within the ampoules. Solids were measured out into each ampoule, and blended using a Vortex-Genie 2 mechanical shaker, on speed 6-8 for 30 s. Once calorimeter steady baseline conditions had been reached, the required water volume was added to each sample using mechanical pipettes, before all samples were mixed for 2 minutes using a the same mechanical shaker, on speed 7-8. The samples were then loaded into the calorimeter into one of the 8 available channels. Within each channel was then a sample and a reference vial, in which 9 g of solid material with similar heat transfer properties had been cast. Once the samples had been loaded, the experiment was started.

As the caps are removed from the measurement chambers to load the samples, the temperature within the calorimetry block is no longer constant, and so the data logging system carries out normalisation, waiting for constant temperature to be held throughout the block. This means that the initial strongly exothermic reaction of the aluminate into aluminate-gel is often missed, but the main heat of hydration peak is accurately measured and all the samples can be compared. The calorimeter block was held at 20 °C for the duration of all experiments in this project.

The use of a calorimeter block at constant temperature, and reference ampoules of the

same specific heat capacity also connected to thermocouples, removes the need for long term calibration, with the equipment able to automatically calibrate any fluctuations in baseline conditions, and remove these from the sample data.

3.2.2 Scanning Electron Microscopy

3.2.2.1 Background

The limits of light microscopy are governed by the wavelength of visible light - 0.4 µm - 0.7 µm. Visible light is therefore unable to distinguish anything below half that wavelength, and so light microscopy cannot be used in the sub-micron realm, with light microscopy typically being used in the x5-x1500 range. By using a focussed beam of high energy electrons, it is possible to investigate a sample to a much higher resolution, and gain information that light microscopy would be unable to provide.

When high energy electrons interact with a sample, the result of those interactions provides information about the surface texture and morphology, the crystalline structure and chemical composition, dependent on the type of detection used. By rastering the electron beam across a sample, it is possible to produce an image of the sample. Three types of electron-sample interaction can be detected;

- **Secondary electrons** are created when the primary electron beam interacts with atoms, and exciting the atoms such sufficient energy is provided to excite an electron from these atoms, and these secondary electrons can be detected to produce a topographic image of the sample.
- **Backscattered electrons (BSE)** are those that upon interaction with atoms on the sample surface are reflected back due to elastic scattering. The amount of backscattering that occurs is dependent on the electron density of the sample material, and so denser materials produce greater backscattering, appearing brighter on a grey-scale image produced from backscattered electrons.
- **Energy dispersive X-rays (EDX)** are a the result of the interaction between the electron beam and individual atoms, producing two types of X-rays; Bremsstrahlung, or breaking, X-rays and Characteristic X-rays. The X-rays produced by each element

have different energies, and the counts per second of the different energy X-rays produced by the electron beam at a particular point can be found, producing an elemental ratio of the sample. By using this technique as the electron beam is rastered over the image, elements can be mapped.

The different phases within a cement paste (section 2.1.1.6) have differing electron densities, which makes the use of BSE imaging using SEM an ideal method for analysing samples of different compositions and at different ages, in order to determine the degree of hydration, and the phase composition of the sample. Within a standard cement system, BSE imaging can often be enough to determine the presence of hydrous and anhydrous phases[130]. Within binary systems containing slag however, the electron density of anhydrous slag is very similar to that of portlandite, and so BSE imaging alone in insufficient to properly determine the phase assemblage and degree of hydration. As shown by the XRF data in section 3.1.2, GGBS has significantly higher MgO content than OPC and portlandite (CH). Thus by overlaying an Mg elemental map obtained through EDX analysis over the BSE image, it is possible to distinguish between anhydrous slag and portlandite, and thus determine the degree of hydration and phase assemblage[47,126].

Figure 3.2.1 shows a BSE image of a CEM I concrete hydrated for over 6 months, with the corresponding greyscale histogram. Different parts of the concrete have been identified through their greyscale density;

- **A** - fine aggregate, in this case builders sand, so primarily quartz, with a relative density in the region of 2.6-2.62 (2600-2660 kg/m^3)[131].
- **B** - anhydrous clinker, with different phases identifiable by their different densities. During clinker grinding dislocation occurs within grains, so individual clinker particles can contain crystals of different phases[132]. The brightest phases are that of ferrite. Although only a minor clinker phase, ferrite is slow to react and can remain in an anhydrous form in significant quantities[130]. Belite, also being slowly reactive (density 2.97[131]) and relatively dense, makes up the bulk of the remaining anhydrous clinker particles, with reaction products forming along the striations in the large central grain, as shown by Scrivener et al[130]. Unreacted aluminate and alite, as the two more reactive phases, are likely to be only present in very small quantities.

- **C** - inner product, formed within the original area of cement grains, and described in further detail in section 2.1.2.2.
- **D** - outer product, formed outside the original cement grains, and described further in section 2.1.2.1. The parts within the OP showing black are the capillary pores.

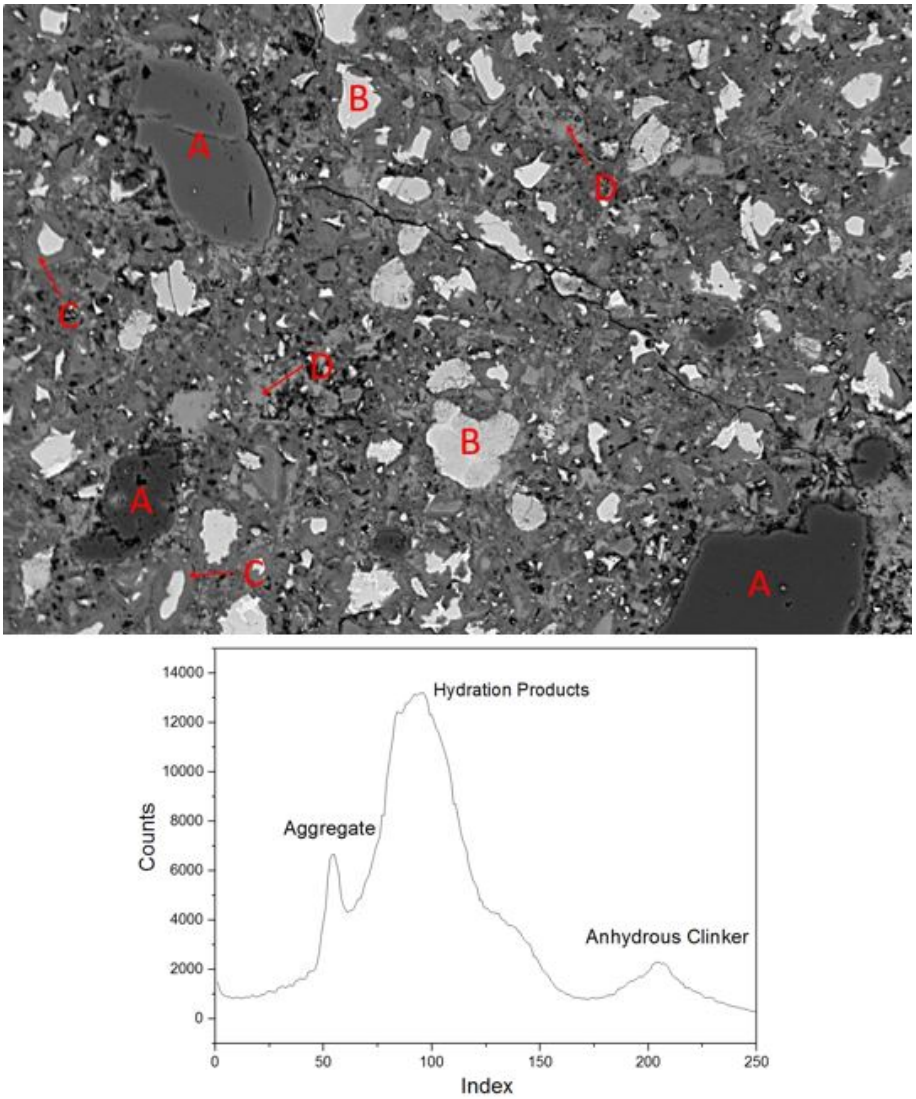

Figure 3.2.1: SEM BSE micrograph of a polished concrete sample showing main features, with associated greyscale histogram, where A is fine aggregate, B is anhydrous clinker, C is inner product, D is outer product

To further gain an insight into the ratios and amount of phases present, a histogram of greyscale values can be plotted, as shown in fig. 3.2.1, where clear peaks for aggregate, anhydrous clinker and hydration products can be seen. For hydration products however, there is significant overlap between inner product and outer product, with a number of

similar phases present in both, and it is not possible to differentiate between these phases on the basis of greyscale alone[130].

3.2.2.2 Methodology

Samples were taken from grout cubes following strength testing, the hydration was stopped (see section 3.2.10), and a flat surface was ground using silicon carbide paper. The samples were then resin impregnated using Struer's EpoFix epoxy. Following curing of the resin, samples were first ground with increasingly fine silicon carbide paper (600-2500 grit), to remove any resin above the flat surface of the sample, and then to remove any scratches. Following grinding, increasingly fine diamond paste was used to polish the sample ready for analysis, finishing with a 0.25 µm diamond paste. Prior to analysis, samples were splutter coated in carbon to prevent charging of the samples under an electron beam which results in a blurred image.

For particle shape analysis, a TM3030+ Hitachi Desktop Scanning Electron Microscope (SEM) was used to carry out the sample and particle small scale image analysis in this project. A pre-centred cartridge filament was used as an electron source, with a high sensitivity semiconductor 4 segment SE detector used. Powdered sample was applied to an adhesive carbon stub, before pressurised air was used to remove and sample that wasn't fully adhered, prior to sample loading within the chamber. The use of an adhesive stub created a more representative sample, preventing the finer material being easily removed by the air had a non-adhesive stub been used.

For determining degree of hydration of both concrete and grout samples, a Carl Zeiss EVO MA15 Scanning Electron Microscope was used. The capability of the device includes an Oxford Instruments AZtecEnergy EDX system with 80mm X-Max SDD detector - secondary and backscattered imaging, EDX elemental mapping and linescans plus CZ STEM detector.

Polished samples were then examined under back-scattered electron mode, at a working distance of 8.8-8.5mm, and 800x magnification, and 20.00 kV accelerated voltage. Mul-

tiple images were taken, at random positions, from each sample. ImageJ image analysis software was used for image processing and thresholding. Multiple images of cement paste, taken from random positions of the sample, but with the same brightness and contrast used, can be loaded into the software. Image processing using smoothing and sharpening can be carried out, until a grayscale histogram of the combined images, as seen in fig. 3.2.1. Each phase can be identified by a region in the grayscale, by calculating the anhydrous cement content, and comparing it to the cement volume fraction in the original mix design, the degree of hydration can be calculated. Section 4.2.2.3 shows the calculation required to calculate the degree of hydration from BSE imaging.

$$DoH\frac{cem}{SEM}(t) = 1 - \frac{V_{(t)cem}}{V_{(0)cem}} \tag{3.2.1}$$

where;

$DoH\frac{cem}{SEM}(t)$ is the degree of cement hydration, calculated through SEM imaging, at time t.

$V_{(t)cem}$ is the volume fraction of anhydrous cement at time t, from SEM imaging.

$V_{(0)cem}$ is the volume fraction of anhydrous cement at time 0, from mix design.

The volume fraction of anhydrous cement, at time 0, within the cement paste, is calculated using the water/cement ratio, and the density of cement, through the following equations.

$$V_{(0)cem} = \frac{Vol_{cem}}{Vol_{tot}} \tag{3.2.2}$$

$$Vol_{cem} = \frac{cementcontent}{density} \tag{3.2.3}$$

where;

cement content is in $\mathrm{kg\,m^{-3}}$, from the mix design

density is also is $\mathrm{kg\,m^{-3}}$, taken as 3,150 for Portland cement.

By using the water content from the mix design, and using a density of $1000\,\mathrm{kg\,m^{-3}}$, the

volume fraction of water can be calculated. By combining the two, to get a total volume, enables the volume fraction of anhydrous cement to be calculated as a percentage, to compare against that calculated at time t. The volume fraction of anhydrous cement at time t, within the cement paste, is calculated using the image processing software, and is given as a percentage averaged over a number of SEM images.

The same technique can also be carried out for determining the degree of hydration of supplementary cementitious materials, or cement replacement materials, by thresholding for anhydrous SCM's rather than cement, although this often requires further energy dispersive x-ray mapping to help distinguish between the SCM and hydration products.

3.2.3 Particle Size Distribution

3.2.3.1 Background

Particle Size Distribution can be calculated in a number of ways. Historically, a sieve stack would be used to determine the particle size distribution, with a known mass being poured through and the resultant mass at each sieve fraction recorded to produce a particle size distribution (PSD). This is a relatively time consuming method, and when a sample with a narrow PSD range is used, a sieve stack may not have sufficient discrete points in order to properly analyse the PSD. More modern techniques have been developed for particle size analysis, with laser diffraction the most common.

Particle size analysers, using laser diffraction through suspended solids, can calculate and analyse the particle sizes of the suspended solids. The degree of light scattering can be directly related to particle size, using the Mie theory of light scattering from small particles. When the particles, suspended in either a liquid or gas, pass in front of the laser, they produce a particular scattering based on their refractive index, and so software can then be used to automatically detect this fingerprint, and use it to calculate the size of the particles passing in front of the laser, and thus produce a particle size distribution. The limitation of this theory is when non-spherical particles are used, but it is deemed sufficient for use in comparing the PSD of the materials used within this project.

3.2.3.2 Methodology

Within this project, a Malvern Mastersizer 2000 was used for all particle size analysis. A solid powder was suspended in isopropanol (as using water with cementitious systems would cause reactions), with high frequency stirring, at 3000rpm, both mixing the suspension and driving it through the system. A 30 second background measurement time was used, and each sample was set to run for 10 measurements, each with a 10 second elapsed time. The average of the 10 runs was then used to compare particle size distributions.

The software used for measurement and analysis provides refractive indices for many materials and dispersants, including most of those used in this project. Blast furnace slag was not one of the materials for which a value was provided, with glass the closest material. As such, a refractive index was adopted from the literature[133]. The refractive indices used within the project are provided in table 3.2.

Table 3.2: Refractive indices, used during particle size analysis, for materials within used within this project

Material	**Refractive Index**
Water	1.34
Isopropanol	1.39
Cement	1.68
Quartz	1.544
Slag	1.62

3.2.4 Unconfined Compressive Strength Testing

In line with the BS 8500, cube compressive strength testing was carried out on 50mm grout cubes. This is a standardised industry test and can also be related to Eurocode 2. For this project, the machine used is a Tonipact 3000, operated using Servocon systems software. For the 50mm cubes, a low loading ramp rate of 0.77kN/sec was used for all tests.

50mm grout cubes were cast in plastic or steel moulds and cured under the ideal conditions (see section 4.1.1 for specific methodology) for the specified time period. Once cured to the required age, cubes were removed and placed on a pedestal beneath a loading plate.

The compressive load was applied to the opposite side of the cube in contact with the base, and is applied uniformly across the sample. As the load was applied via the movement of a plate onto the sample at a constant speed, a stress-strain plot until failure of the sample could be obtained. For this project however, a failure strength was the primary information required in order to compare replacement materials with a reference.

3.2.5 X-Ray Diffraction

3.2.5.1 Background

X-Ray Powder Diffraction, or XRD, is a crystallographic analytical technique, whereby the diffraction patterns produced from the interaction of an X-ray beam with a powdered sample can provide information on the crystal structure of the sample. By altering the incident angle of X-rays upon the sample, and recording the intensity of the diffracted beam, the electron density within the sample can be determined, from which the crystal structure, and hence the overall crystallographic nature of the sample, can be inferred.

William Henry Bragg, Cavendish Professor of Physics at the University of Leeds, and his son, William Lawrence Bragg, developed Bragg's law, which links the crystal structure to the reflection and diffraction of incident X-rays[134], for which they received the 1915 Nobel Prize in Physics. The technique has since been developed and improved, through both improved understanding and equipment.

With cement, and its hydration products, having a number of crystalline or semi-crystalline phases, XRD can be used as an analytical tool to help determine the phases present, and how they relate to the hydration of the cement[135][14]. Further micro X-ray analysis has been used to detect the elements incorporated into C-S-H gel and help determine the nature of C-S-H.[44]

3.2.5.2 Methodology

The equipment used to carry out the XRD analysis in this project is a Bruker D2 phaser desktop XRD. All samples were analysed over 2θ 5-70°, with a time step of 0.75. Data

capture, import and analysis was carried out using the Bruker DIFFRAC.EVA software. Samples were ground using a pestle and mortar, before being separated though a 50 µm fraction sieve, with the finer fraction being pressed into a sample holder and placed into the machine. Due to the differences in hardness between the cementitious matrix and larger calumite grain, the grinding and sieving process lead to slight concentration of cement matrix in the finer sieved material for analysis, this is constant for all samples, and provides a representative sample f the cement matrix.

3.2.6 Thermal Analysis

3.2.6.1 Background

Thermal analysis involves the heating of a sample at a constant rate, while measuring the mass of the sample so that any mass loss during heating can be known. Many of the phases within a cementitious matrix will decompose over a known temperature range, with papers by Bhatty[136] and Collier[137] providing a review of a wide range of literature and providing the typical temperature ranges over which phases will experience mass loss. The cause of the mass loss depends on the phase, with many phases experiencing dehydration, and calcium hydroxide undergoing dehydroxylation and calcium carbonate undergoing decarbonation[138].

Thermogravimetric Analysis (TGA) directly measures the mass of a sample as it is heated, producing a thermogravimetric curve. It is possible for phase changes to occur without mass loss however, and so Differential Scanning Calorimetry (DSC) uses a blank reference ampoule against which the sample temperature is compared as the furnace temperature increases. The heat flow into the sample is directly proportional to its specific heat[139], and so when compared against a blank reference can spot phase changes or reactions related through changes in specific heat, that wouldn't be detected through mass loss on solely TGA. By combining the two techniques in a TGA-DSC analysis, valuable information can be gained about the phases present within a sample.

Thermal analysis has been used to determine the degree of hydration of cement. Pane and

Hansen compared the results of thermal analysis to that of isothermal calorimetry [140], finding that loss of bound water determined using thermal analysis was directly proportional to the heat of hydration from isothermal calorimetry, and so can be used to determine degree of hydration. Through determining the mass loss from bound water, over the 50-550 °C, at which point all hydrated phases are considered to fully dehydrated, the continuing hydration of a system can be determined.

3.2.6.2 Methodology

The equipment used in this study is a Mettler-Toledo TGA-DSC, with 36 sample autosampler. Powdered samples were hydration stopped through quenching in isopropanol, at a ratio of 100:1 parts solvent to water within the sample, for 48 hours, before being dried in a desiccator, with silica gel to maintain a low relative humidity and reduce carbonation of the samples. Following hydration stopping, samples were ground using a pestle and mortar, until a consistently fine powder was achieved. Samples of between 10 - 20 mg were loaded into alumina crucibles which an autosampler then loaded into the furnace, and heated from 50 to 1000 °C at a ramp rate of 20 °C per minute. A nitrogen atmosphere was used for the heating, in order to prevent oxidation of any of the phases during heating. The nitrogen flow rate was 50 ml per minute. The sample mass was constantly measured, as was the temperature differential between the sample vial and a blank reference.

Certain phases within hydrated cement paste decompose within certain temperature ranges. Portlandite decomposes between 400 and 500 °C, while calcite (Calcium Carbonate) decomposes above 600 °C. Bound water content can be calculated in the difference in mass between 550 °C and the sample initial weight, after removal of all non bound water following solvent exchange. A thorough breakdown of the technique and calculations can be found in the book chapter 'Thermogravimetric Analysis' by Lothenbach, Durdzinski and De Weerdt [141].

The mass loss due to both calcite and portlandite, calculated via the tangent method, is then normalised to the sample mass at 800 °C, to work out a mass percentage. The weight loss due to each phase can be converted into the amount of each phase present, using the

molecular masses of the initial phase, and the breakdown products.

3.2.7 Gas Permeability

3.2.7.1 Background

The permeability of a concrete, mortar or grout is an important parameter affecting the durability of the material. The more permeable the material, the easier the pathways are for contaminants, whether they be carbon dioxide for carbonation, or chloride and sulphates for reinforcement corrosion. Within nuclear waste packages, the permeability will determine the rate of groundwater ingress in to the package, and subsequent radionuclide leaching. Also of importance is the rate of carbonation of the grout, as the reduction in pH associated with this will affect the radionuclide solubility also[16].

D'Arcy's law, which links gas flow rate to intrinsic permeability, can be expressed, for incompressible fluids such as water, as;

$$\nu = \frac{kA\Delta P}{\mu l} \tag{3.2.4}$$

where;

ν=flow rate (cm^3/s)

k=intrinsic permeability (m^2)

A=sample cross sectional area (cm^2)

ΔP=fluid pressure head (bar)

μ=fluid viscosity (Ns/m^2)

l=length of specimen (m)

When compressible fluids are used, such as gases, an extra term is required to account for the average pressure within the sample, and once rearranged for the intrinsic permeability, the equation can be displayed as[142];

$$k = \frac{2Q\rho_0 L\eta}{A(p^2 - p_a^2)} \tag{3.2.5}$$

where;

k = intrinsic permeability (m^2)

Q = fluid volume flow rate (m^3/s)

ρ_0 = pressure at which volume flow rate determined (N/m^2)

L = specimen length/thickness (m)

η = fluid dynamic viscosity ($N.s/m^2$)

A = specimen cross sectional area (m^2)

p = inlet pressure (N/m^2)

p_a = outlet pressure (N/m^2).

3.2.7.2 Methodology

Cylinders of 50mm ± 1mm diameter and 40mm ± 1mm length were cast in duplicate for each sample. Once hydrated to the required age (28 and 90 days) under ideal conditions, they were removed from those conditions and oven dried at 40 °C to remove all moisture from the sample, the full reasons of which are discussed in section 3.2.10. Once a steady mass was achieved, samples were stored in sealed containers with silica gel to prevent any moisture gain by maintaining a low relative humidity, also aiding in minimising carbonation. Figure 3.2.2 shows the sample masses, over time for the duplicate C1 and C2 28 days samples. The time taken for the sample to reach constant mass, and thus full free water removal, ranged from 60-90 days, with the higher replacement samples drying quicker, as they have a more open capillary pore network due to the reduced cementitious content.

Prior to testing, top and bottom surfaces were removed with silicon carbide paper, to expose the internal pore structure, before vernier callipers were used to determine the sample dimensions.

Prepared samples were then placed within a rubber sleeve, with only the top and bottom surfaces then exposed. This was placed within the Leeds cell, with a loading ring placed over the rubber sleeve, before the end cap was firmly tightened over the sample, such that any gas flow through the sample could then only flow uniaxially through the sample. Nitrogen was then forced through the sample under a known constant applied pressure (0.5 bar), with a bubble flow meter used to determine the time taken for a known volume of

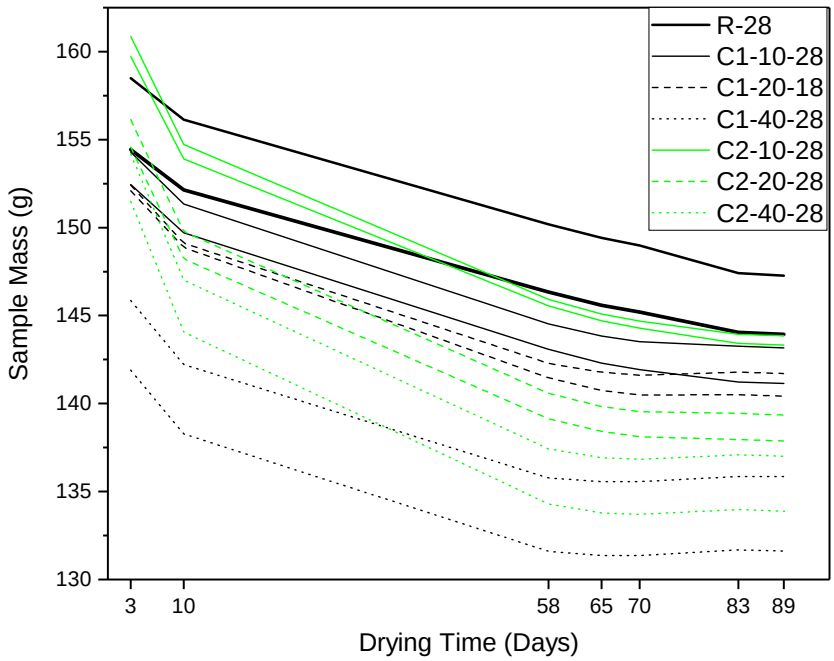

Figure 3.2.2: Sample mass versus time plot, for the oven drying of C1 and C2 28 day permeability and sorptivity samples

gas to flow through the sample (20cm flow within a 10mm pipette). With the volume flow rate calculated, the intrinsic permeability of each sample at 0.5 bar can be determined. The set up of the Leeds cell is described fully by Cabrera and Lynsdale[143], and is shown in fig. 3.2.3.

3.2.8 Sorptivity

3.2.8.1 Background

The sorptivity of a cementitious material is a measure of the tendency of the material to absorb and transfer water by capillary action[144]. As a measure of capillary action, it is related to the permeability of a porous material. In terms of waste encapsulation, it can be related to the intrusion of groundwater into the waste package, and so is a useful parameter for determining the durability of such encapsulation grouts.

The sorptivity of a porous material can be described using the following equation;

$$k = \frac{Q}{A\sqrt{t}} \tag{3.2.6}$$

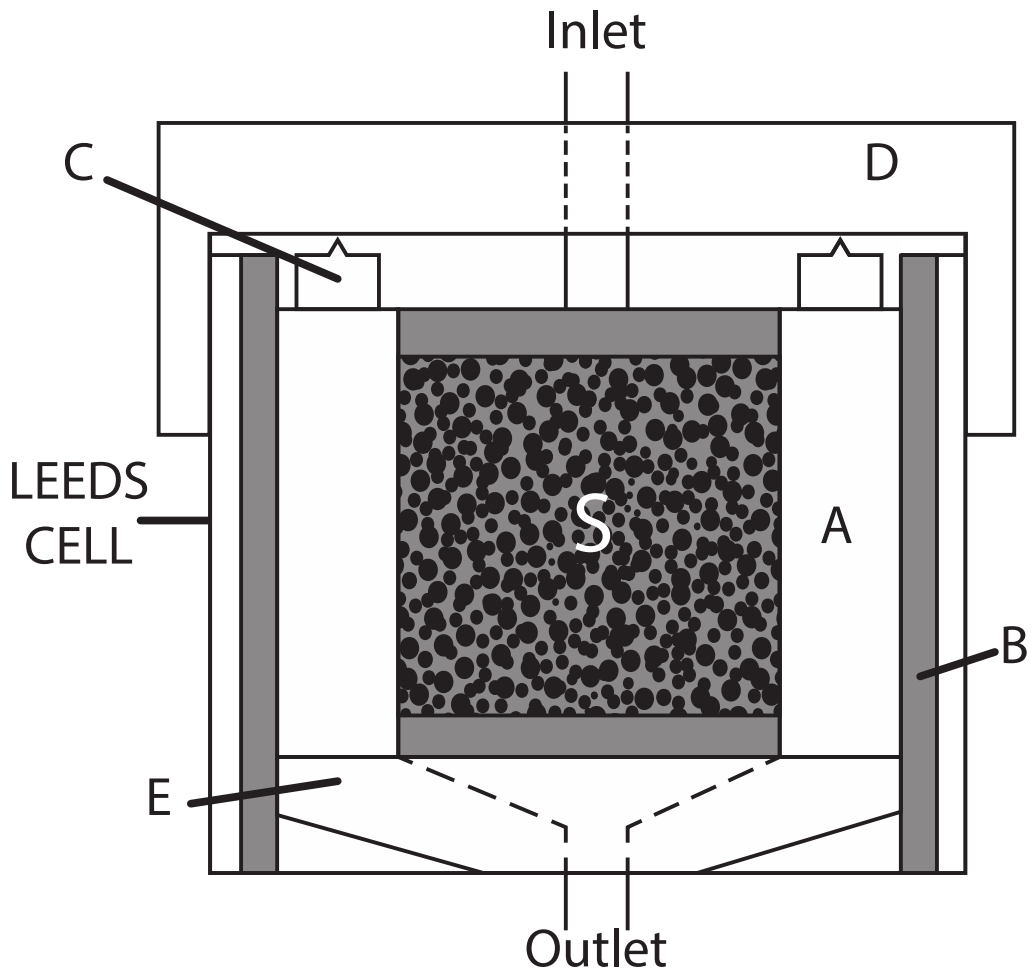

Figure 3.2.3: Set up of the Leeds Cell gas permeability apparatus, where; A) rubber sleeve B) plastic sleeve C) steel o-ring with rubber seal D) cell lid with gas inlet E) base cap with gas outlet S) sample

where;

k is sorptivity coefficient ($\frac{m^3}{m^2 s^{0.5}}$)

Q is the volume of water absorbed (m^3)

A is the specimen cross sectional area (m^2)

t is the time (s)

By measuring the value of Q at a number of different times, the data can be plotted, and the value of k determined from the slope of the linear fit.

3.2.8.2 Methodology

As with permeability testing, all moisture needs to be removed from the pore structure before a true value of sorptivity can be determined. Therefore, in order to reduce the number of samples for casting, once tested for gas permeability, the samples were tested for sorptivity.

Samples were placed on a raised mesh, in a trough of water with a water level maintained at 5mm above the base of the samples, in a similar method as used in many previous studies[126,145–147]. The vertical faces of each cylinder were covered with an impermeable petroleum jelly to ensure uniaxial flow. A schematic of the sorptivity set-up is shown in fig. 3.2.4.

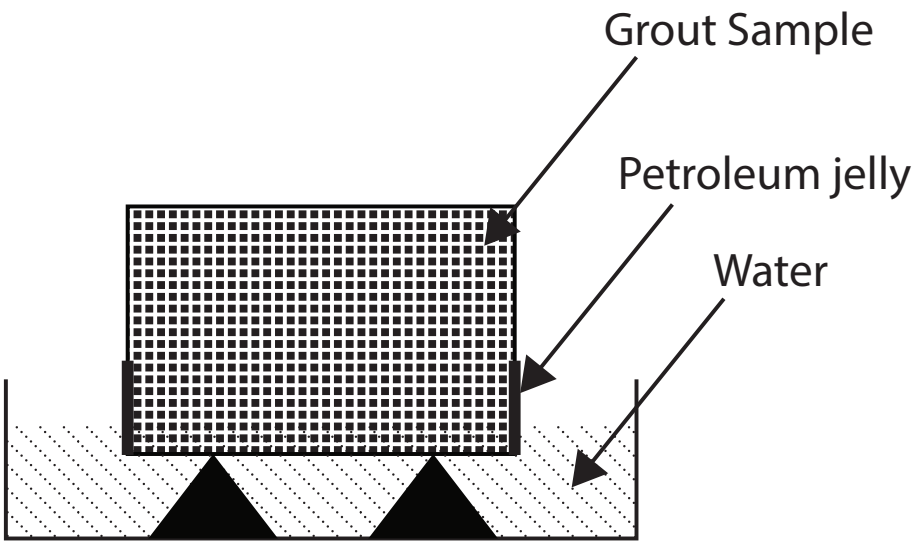

Figure 3.2.4: Schematic of the sorptivity test set-up

At specified time periods, the samples were removed from the water, any excess removed with a damp cloth, and weighed, so that the uptake of water can be calculated. The times used for testing, in order to provide a sufficient spread of data were 1, 4, 9, 16, 25, 36, 49 and 64 minutes. From this data, a value of k was determined from the gradient of the line of fit of the data points.

3.2.9 pH Testing

3.2.9.1 Background

The pH of the pore solution within a cementitious matrix is dependent on the materials used during casting, but in most systems containing ordinary portland cement is very high, in the range of 12-13.5, due to the number of alkali ions dissolving from the cement powder upon contact with water.

Blast furnace slag, as described in section 2.2.2, is latently hydraulic and reacts upon contact with water, but only very slowly. The reactivity of blast furnace slag can be activated in alkaline environments, and when used in binary or ternary systems with OPC, the high alkalinity works to activate the blast furnace slag. With nuclear encapsulation grouts having a high slag content, measuring the pH of the system during the early stages of hydration provides important information on the hydration progress and process.

3.2.9.2 Methodology

Cement paste samples, following the same mix design as the calorimetry runs, were cast in plastic vials. Single use pH probes, accurate to 2 decimal places, were then placed within the cement paste, with a small head of water above the sample to prevent drying out and to ensure the pH probes were completely surrounded. Although the water head diluted the pore solution, the pH scale is a log10 scale, and so any changes in pH were readily identified.

A Raspberry Pi computer was programmed to take images of the set up, shown in fig. 3.2.5, every 10 minutes during the first day of hydration. The values were then plotted over time to study the effect of the ground concrete on the early stages of hydration and the associated pH. While it has been noted that glass pH probes aren't the most suitable for use with cement, due to the solubility of the glass at high pH, the single use probes, and relatively short measurement time, made the reading reliable enough for investigating the changing pH within the systems. Due to the nature of the set up, it was not possible to seal the sample during testing, and so slight carbonation of the sample was possible, but consistent through all samples and so the results remain comparable.

Figure 3.2.5: Set up of the pH measurement

3.2.10 Hydration stopping

3.2.10.1 Background

For a number of the experimental and analytical techniques required to investigate and understand the properties of cementitious systems, such as those described in section 3.2.2, section 3.2.3, section 3.2.5, section 3.2.7 and section 3.2.8 it is necessary to dry the samples prior to analysis, to arrest hydration and make them suitable for testing, while maintaining the properties of the initial material at the required age. A number of hydration stopping techniques have been used in previous studies, such as solvent removal[148], freeze drying and oven drying. The impact of the drying technique on sample has been studied, with the overall consensus being that solvent removal is the most appropriate method for drying samples[149 150 151]. For that reason, solvent removal using isopropanol (IPA) was the chosen method to arrest hydration in this project, although larger samples for permeability and sorptivity testing had to be oven dried due to limitations in the solvent removal technique.

3.2.10.2 Methodology

Following strength testing of grout cubes (as described in section 3.2.4), thin sections of the broken cubes were collected for further analysis. These were taken from fractures planes within the cubes as opposed to from the surface to ensure they were representative of the internal matrix of an encapsulation grout. The sections taken were typically 10-20mm in length and breadth, and no more than 3mm in thickness, to ensure that isopropanol could penetrate through the sample and replace all the free water. The sections were placed in isopropanol at a ratio $> 100:1$ parts isopropanol:free water for more than three days. Following immersion, the samples were removed and placed in a dessicator under negative pressure, with the system being pumped with a slight 'leak' to provide air flow and increase the evaporation of the IPA for more than three days to remove all isopropanol from the sample, leaving a dry sample with the same microstructure as when it was initially strength tested. Although the samples were in cotact with air for this period and some carbonation was possible, this was minimised through keeping as high a vacuum as possible, in which the solid samples would have carbonated only very slowly.

For larger samples however, solvent removal is not a suitable technique for hydration stopping. The volumes of IPA required to replace the water in 50mm diameter by 35mm deep samples for sorptivity and permeability samples make the method impractical while the sample size would prevent full solvent replacement within the bulk of the sample. The only practical method for drying these larger samples is oven drying. Multiple studies have investigated the effect of oven drying on the microstructure of cement paste (aggregate remains unaffected at these temperatures) at temperatures upto 105°C. Many have reported at least partial dehydration of both C-S-H and ettringite at 105°C[151 152], while also reporting some disruption to microstructure at 60°C. For this reason, the large samples were oven dried at a temperature of 40°C +/- 2°C, in order to maintain as best as possible the original microstructure.

Part II

Waste Replacement Within Encapsulation Grouts

Chapter 4

Synthesis of Scabbled Material

4.1 Simulated Waste Concrete Methodology

In order to study the effects of scabbled material on the properties of encapsulation grouts, simulated scabbled concrete was created. Due to the contaminated nature of scabbled material arising from nuclear sites, removal of the material for use in research is prohibitively difficult and time consuming. As such, a simulant scabbled material was created for the purpose of this project.

4.1.1 Methodology

Due to being critical infrastructure installments, concrete on nuclear facilities is under high integrity demands, requiring high strength and performance concrete [153]. Many concrete elements are required to undertake a secondary shielding or containment role in addition to their structural purpose, and durability of these materials is of paramount importance as access for repair is often unavailable or expensive. As such, in order to produce relevant synthesised material, a high strength and performance concrete was cast, from which synthesised scabbled material could be created through crushing and grinding.

As the material removed during the scabbling process is the outer few centimetres exposed to air or water, there is a likelihood of carbonation occurring in this depth in aged concrete. The effect carbonated concrete has on the properties of an encapsulation grout is possibly different to that of uncarbonated concrete, and so half of the synthesised scabblings also

underwent accelerated carbonation. This resulted in four source materials, a CEM I carbonated and uncarbonated sample, and a CEM II carbonated and uncarbonated sample. The nature, name and colour with which the samples will be referred to throughout the project are given in table 4.1, with quartz also included.

Table 4.1: Naming convention for samples

Material	Reference	Colour
CEM I uncarbonated	C1	Black
CEM II uncarbonated	C2	Green
CEM I carbonated	T1	Red
CEM II carbonated	T2	Blue
Quartz	Q	Pink

4.1.1.1 Mix Design

A 50 MPa target 28 day characteristic strength was chosen as a reasonable target for legacy high performance concrete, with a CEM I and an CEM II 20% PFA used. 10mm quartzite coarse aggregate, and standard construction sand fine aggregate were used in both concretes, as well as a CEM I 52.5 cement. The mix designs used for both concretes are given in table 4.2. Following casting, samples were cured under ideal conditions of 20 ± 1 °C, and a relative humidity of >95% for 28 days, whereupon the concretes were removed from these conditions and cured to 180 days under laboratory ambient conditions.

Samples were tested after ageing for 180 days, and so the 28 day strength wasn't recorded. After 180 days however, the CEM I concrete had a mean compressive strength of 75.4 MPa, a standard deviation of 2.32 MPa, and a resultant characteristic strength (mean - 1.61 x standard deviation) of 71.65 MPa. For the CEM II concrete, the mean compressive strength was 88.175 MPa, with a standard deviation of 1.55 MPa, resulting in a characteristic strength of 85.67 MPa. Concrete is generally regarded to have achieved 90% of its strength by 28 days, which would have resulted in both concretes having achieved their target strength by 28 days. As the concretes were tested at 180 days, the increased strength of the CEM II concrete can be related to the inclusion of PFA in the CEM II concrete and the pozzolanic reaction.

Table 4.2: Mix designs for initial concretes

Material	CEM I	CEM II
Cement (kg/m^3)	643	558
PFA (kg/m^3)	0	140
Fine aggregate (kg/m^3)	531	523
Coarse Aggregate (kg/m^3)	886	872
Water (kg/m^3)	225	210

The coarse aggregate used was a crushed 10-20mm quartzite aggregate, while the fine aggregate was a 'micro' concrete, graded fine aggregate, with a particle size range from 400 µm up to 4 mm.

4.1.1.2 Grinding

Two types of grinding were investigated for use in this project; roller ball and disc milling. Ball milling uses small grinding balls inside a much larger vessel to crush and grind a sample through rolling the vessel. Disc milling uses a hardened steel 'puck' and 'ring' to crush and grind material against either each other or the hardened steel of the 'bowl' in which the sample and rings and puck are placed. The primary differences between the two methods are volume of sample that can be processed and the time required for grinding, with roller ball milling capable of processing much larger volumes of sample, but requiring a much longer grinding time.

For roller ball milling, 500g of sample (a total of 1/3 of the vessel volume) was placed, along with grinding balls (also filling 1/3 of the vessel) into the grinding vessel (with remaining 1/3 of volume being voids), sealed, and then rolled for 3 hours.

Disc milling was carried out using a Gyromill, with 150g of sample ground at a time, between a puck and two rings. Grinding times were varied from 30 seconds to 2 minutes, and the particle size distributions (PSD) investigated for different grinding times, as discussed in section 4.2.1.

On investigation and comparison of the grinding methods, it was found that roller ball milling wasn't appropriate for grinding the crushed concrete. After 3 hours grinding on a high speed setting, coarse aggregate fragments remained, as well as some of the fine aggregate, with the cement paste ground finely. For disc milling, even shorter grind times resulted in complete grinding of coarse an fine aggregate. As described in section 2.4.2.2, scabbling is a high energy grinding method for removing the outer concrete, and thus the lower impact and energies involved in roller mill grinding aren't appropriate for synthesising the scabbled material, and disc milling was chosen as the most appropriate grinding method.

Disc milling was carried out on both concretes, with 150g batches for 1 minute 30 seconds, in order to ensure a consistent grind to both concretes. The resultant fine powder, referred to as the filler, was used for accelerated carbonation, and for casting of cubes and cylinders for investigations into engineering properties. Only after accelerated carbonation and being cast, was a finer fraction separated, using a 50 micron sieve, for analytical work. This is referred to as the fine fraction.

4.1.1.3 Accelerated Carbonation

Following grinding of both concretes, half of the ground material from each was separated to be carbonated, over the entire particle size distribution. Accelerated carbonation of the ground concrete was carried out using an LEEC CO_2 incubator, with controlled temperature and carbon dioxide concentration. Ground material was placed in sample trays to a depth of 2 mm, with bed height being restricted to allow for maximum diffusion of CO_2 through the bed, and thus maximum rate of reaction. The trays were placed on shelves within the chamber, and CO_2 content was set at 4% and temperature controlled at 20 °C. As discussed in section 2.4.1, relative humidity (RH) is an important factor in the carbonation of concrete and should also be controlled. Sufficient RH is required to enable carbonation reactions to occur, and so the humidity of the chamber was kept above 50%. The powder was periodically mixed to maximise exposure to CO_2.

It has also been shown that above an RH of 70%, prehydration of cement can occur [154,155].

This prehydration could affect any remnant anhydrous material exposed during the grinding process, and so the RH was kept below 70%. In order to maintain a high enough RH for carbonation to occur, and yet low enough to prevent any pre-hydration of anhydrous material, saturated Sodium Bromide (NaBr) solution was used, maintaining the RH at 56-61% in the 20-25 °C range[156].

Throughout the accelerated carbonation period, the degree of carbonation was determined using thermal analysis. Samples from both the top and bottom trays were taken to ascertain whether there was any differences in carbonation rate at different positions within the chamber. Figure 4.1.1 shows the TGA plots for CEM I samples over the accelerated carbonation period. From this plot it is clear that after ages of around 9 days, little to no additional carbonation occurred, or the rate is slowed down very significantly, shown in the mass loss from around 600-800 °C, which remained constant from 9 up to 20 days. Between 0-9 days, the mass loss from portlandite decreases, while the mass loss from carbonate increases, showing the phase change from calcium hydroxide to calcium carbonate. After 9 days, and especially after 15, there is no discernible difference in these mass changes, suggesting full carbonation has occurred. Therefore, 15 days was considered the point of full carbonation, and so the ground material remained in the carbonation chamber for 20 days to ensure full carbonation, without unduly delaying the progress of the investigation.

4.2 Properties of Synthesised Waste

4.2.1 Particle Size

Particle size was determined using laser diffraction, as discussed in section 3.2.3. As seen in fig. 4.2.2, there is a bimodal particle size distribution. This is due to the difference in hardness between the aggregate and cement paste, with the aggregate (Mohs hardness $\sim$ 7) being concentrated in the coarser fraction, and the less hard cement paste (Mohs hardness typically 3-5) being concentrated within the finer fraction. From both fig. 4.2.1 and fig. 4.2.2, it can be seen that increased grinding time produces an increase in smaller fraction volume, while both decreasing the particle size, and volume, of the coarser fraction. Up to 1 minute and 30 seconds (1:30), this effect increases with grinding time, but past

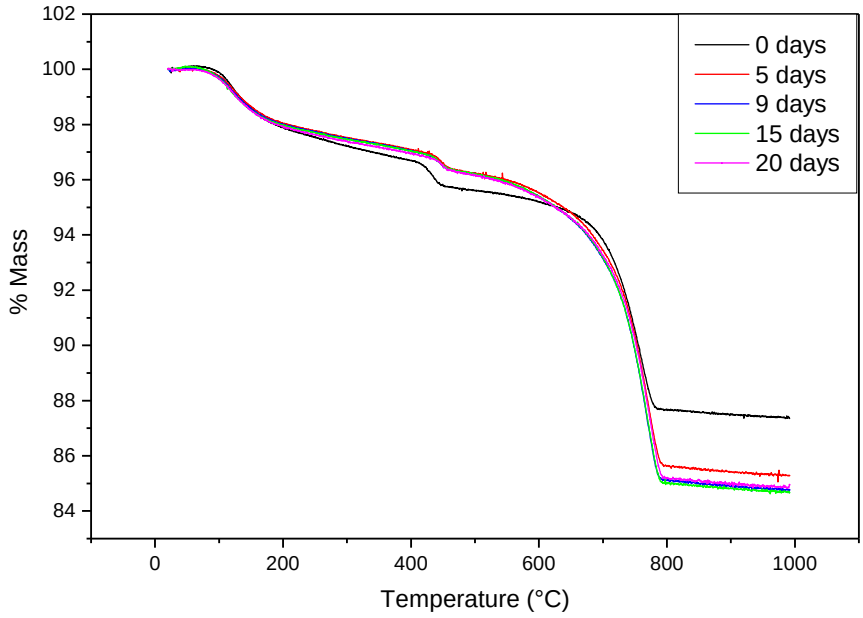

Figure 4.1.1: Thermogravimetric plot for accelerated carbonation of ground CEM I over time

this, the increased grinding is less effective and results in only a small decrease in particle size. To significantly decrease the particle size further would require a significant increase in grinding time, and so a 1:30 grind time was chosen as the most effective yet efficient. The resultant powder had a d5 of 2 µm, d50 of 13.5 µm, and a d90 of 160 µm.

Figure 4.2.3, repeated from chapter 3, shows the PSD of the three other raw materials used in the encapsulation grout. As can be seen, despite not having a bi-modal distribution like the ground concrete, the Ketton OPC and Port Talbot BFS have a similar overall particle size range and cumulative distribution, from $\sim$ 1-100 µm. This is significantly smaller than that of the calumite, which is largely used as an inert filler to maintain flow properties, which is why the calumite content is kept constant within all replacement mixes.

4.2.2 Particle Shape

Particle shape was analysed via scanning electron microscopy, using a Hitachi TM3030plus desktop electron microscope. Small amounts of powdered sample were placed on a carbon stub and pressurised air was used to remove the bulk of the sample, such that individual particles could be seen clearly. This was then placed within the sample chamber for analysis. The adhesive on the carbon stub helps ensure the full range of particle sizes remain on the stub following removal of the non-adhered particles with pressurised air. A number of images were taken, at a number of magnifications from different areas of the sample, to

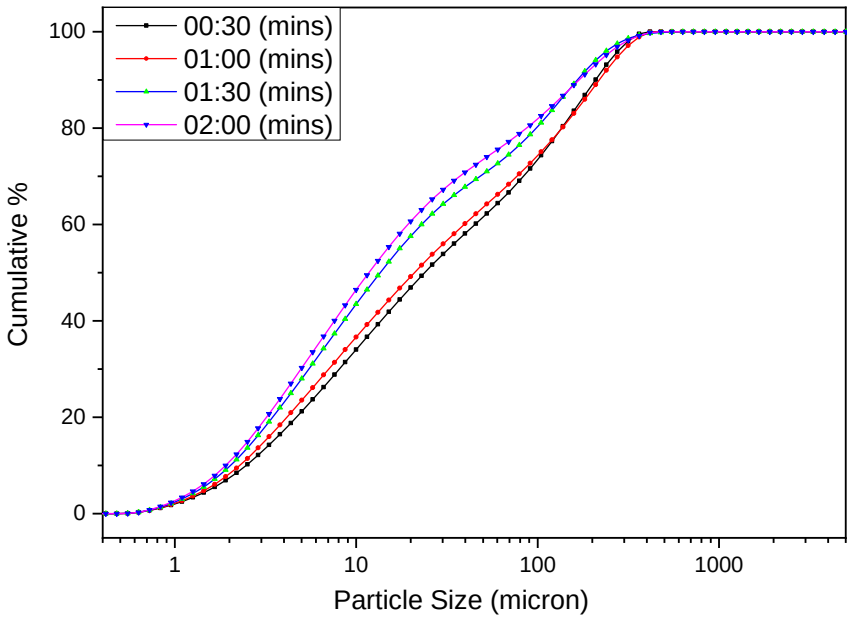

Figure 4.2.1: Cumulative particle size distribution of CEM I concrete resulting from different gryomill grind times

ensure a representative particle shape was observed.

Figure 4.2.4 and fig. 4.2.5 show the ground C1 and T1 powders at 500x magnification. In both images, larger, highly angular grains, with relatively smooth faces are visible. Combining these images with the particle size data, it is clear that these larger angular pieces are broken pieces of aggregate, where completely smooth faces showing internal fractures of aggregate, while some faces show a rougher surface, with attached cement paste. The smaller particles are less angular, and exhibit rougher surfaces, indicating that they are particles of cement paste. With a particle size in the region of 5-20 µm, these also fall within the finer peak of the particle size distribution shown in fig. 4.2.2.

In fig. 4.2.6 and fig. 4.2.7, both powders are shown at x2000 magnification. Again, some more angular particles can be seen, showing that atleast some of the aggregate is found within the finer fraction of the ground material, but the majority of the particles of this size are indicative of cement paste, which will fracture more readily than aggregate and concentrate in the smaller fraction.

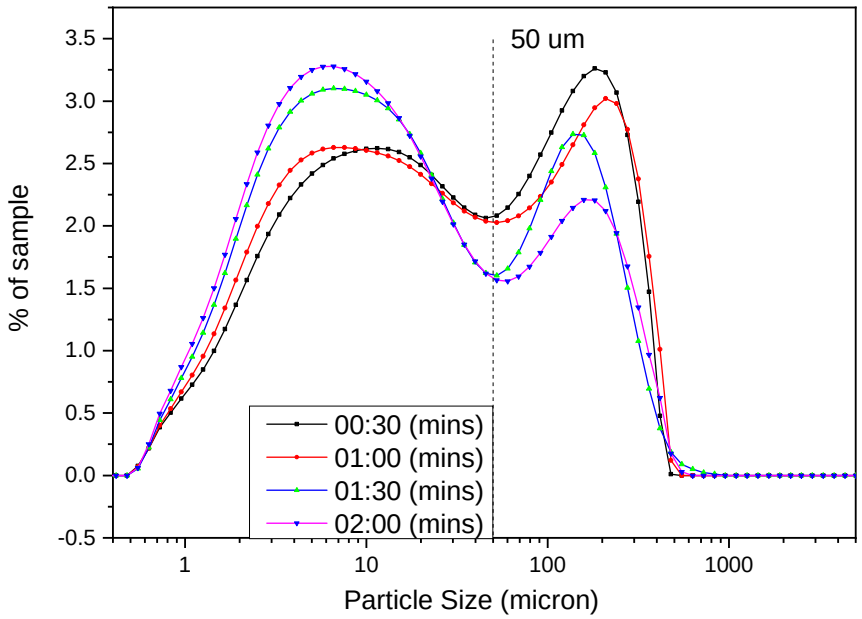

Figure 4.2.2: Particle size distribution of CEM I concrete resulting from different gryomill grind times

4.2.2.1 Separation of Fine Fraction for Analysis

As discussed in section 4.2.1, following grinding of the source concrete, a bimodal PSD is obtained, with aggregate concentrating in the coarser fraction, and cement paste concentrating in the finer fraction. As the aggregate is essentially inert quartz and quartzite, separation of the finer fraction for smaller scale analytical techniques was carried out in order to examine any latent reactivity from the cement paste. To separate the finer fraction, a 50 µm fraction sieve was used (separation occured after the entire powder fraction, including the particles above 50 µm, had been used to cast larger specimens. This meant that the cubes and cyclinders had a full representative sample of the ground concrete). The resultant PSD for each of the four reference powders can be seen in fig. 4.2.8, with all four showing a very close match for particle size distribution. The d5 and d50 of the analytical fraction are very similar to that of the full fraction, with both having a d5 of 2 µm, and the analytical d50 (9 µm, being close to that of the full fraction (13.5 µm). The d90 however shows that the coarser material, primarily consisting of the quartz from the aggregate in the concrete, has been largely removed in the analytical fraction, with the d90 (34 µm) being significantly lower than that of the full fraction (160 µm).

For larger scale testing samples, such as cubes for strength testing, and cylinders for per-

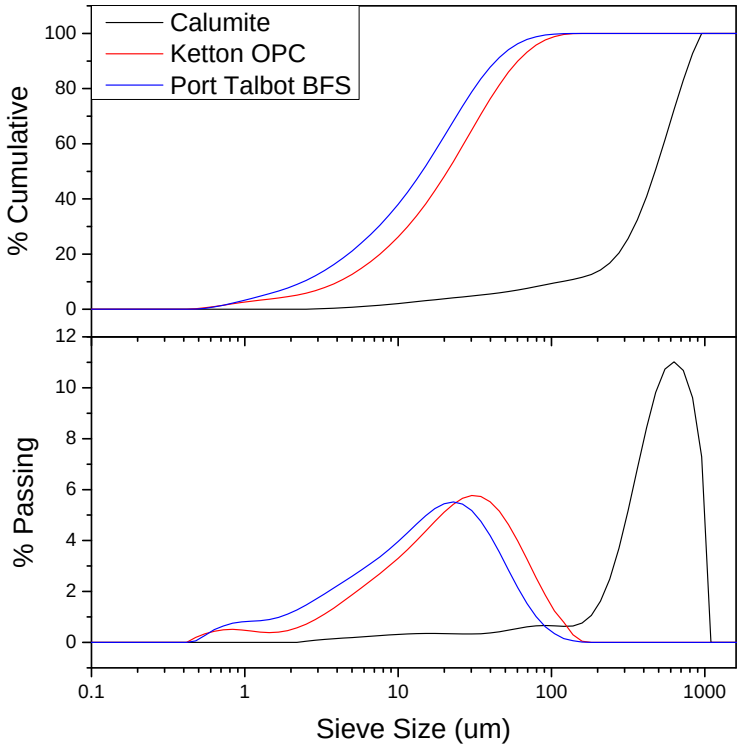

Figure 4.2.3: Particle Size Distribution for raw materials

meability and sorptivity testing, and the subsequent analysis of these samples, the entire powder fraction was used, to represent the complete re-use of scabbled material within an encapsulation grout and the effect its inclusion has on the engineering properties of the grout.

4.2.2.2 Mineralogy

The mineralogy of the synthesised concrete is important in understanding the impact it has on the properties of an encapsulation grout. Here, the mineralogy was studied through a range of techniques.

Figure 4.2.9 shows the thermogravimetric curves for the C1, C2, T1 and T2 analytical fractions. The analytical fractions have been examined, as opposed to the whole powder fraction, in order to amplify any mass changes, as quartzite and quartz experience very little mass loss during heating over the 0-1000 °C range[157]. The T1 and T2 fractions both show a significant increase in the volume of carbonate content to the C1 and C2 mixes, as well as a reduction in mass loss upto 400 °C, related to the reduction in C-S-H content

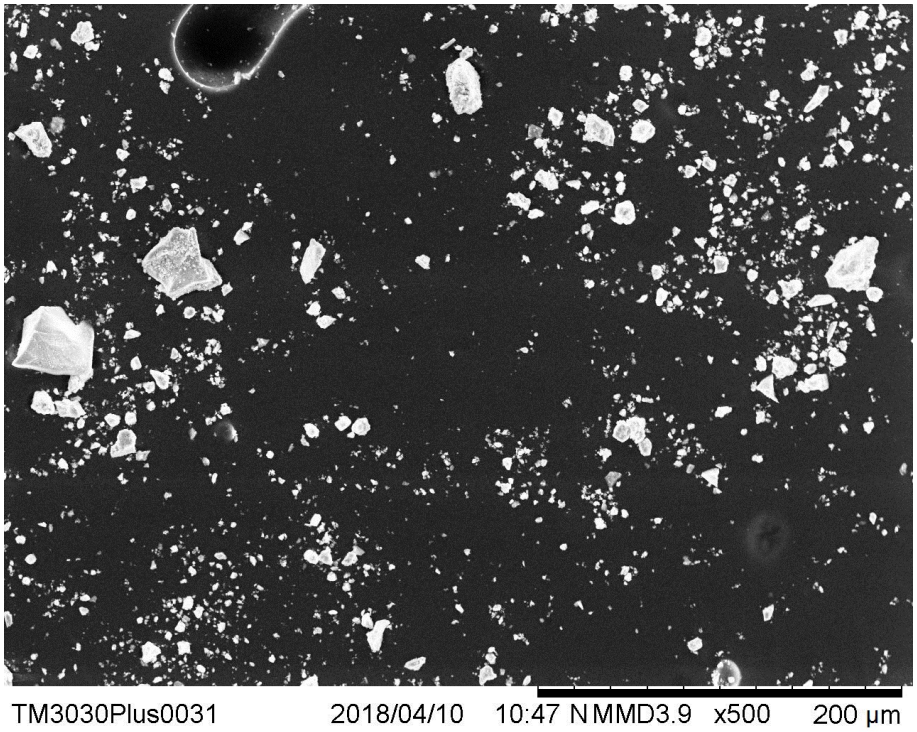

Figure 4.2.4: SEM image of C1 powder with 200 micron scale bar shown

following carbonation and the subsequent decalcification[91,96].

In fig. 4.2.10 the tangent method has been used to calculate the carbonate content of the C1 and T1 fractions. C1 was found to have 23.6% carbonate content (10.4% mass loss due to carbonate), while following accelerated carbonation, T1 had 44.5% carbonate content (19.6% mass loss due to carbonate), compared to their percentage masses at 800 °C, shown in fig. 4.2.10. The same method was used to determine the carbonate content in the C2 and T2 mixes, with C2 having 29.6%, and T2 having 40.7% carbonate content. As well as carbonate content, the portlandite content was also determined for each fraction. Table 4.3 shows the calculated carbonate and portlandite content for each fraction, determined via thermal analysis, as well as their percentage mass loss relative to the mass percentage at 800 °C, from which the percentage content of each were calculated.

Within the carbonated, T1 and T2 fractions, despite the significant reduction in carbonation rate experienced after approximately 15 days, there remains a small amount of CH. As described by Groves et al.[91], and a number of other studies[17,92,93], calcium carbonate will form around the calcium hydroxide crystals, forming a protective layer and prevent-

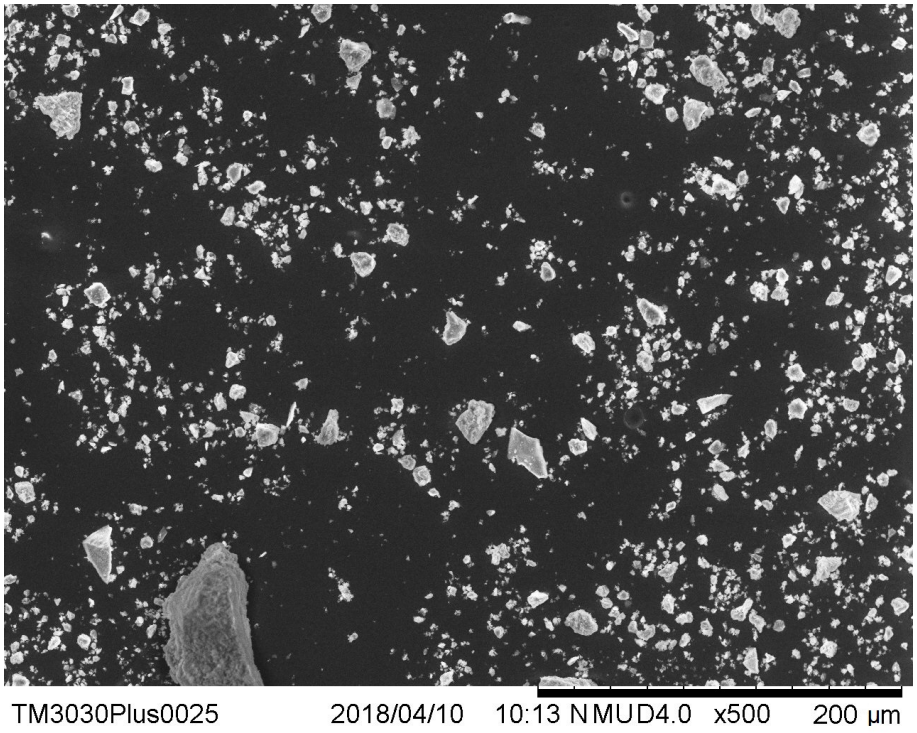

Figure 4.2.5: SEM image of T1 powder with 200 micron scale bar shown

Table 4.3: Carbonate and portlandite contents for each fraction, determined via thermal analysis

Fraction	Mass loss due to carbonate (% mass)	Calculated carbonate content (% mass)	Mass Loss due to portlandite (% mass)	Calculated portlandite content (% mass)
C1	10.4	23.6	1.40	5.8
C2	13.0	29.6	0.78	3.2
T1	19.6	44.5	1.05	4.3
T2	17.9	40.7	0.60	2.5

ing, or significantly reducing, the further carbonation of the CH crystals.

4.2.2.3 Degree of Hydration

To determine the degree of hydration, scanning electron microscopy (SEM), backscattered electron (BSE) imaging was used, as described in section 3.2.2. 25 images of the cement paste were captures, with no aggregate in each image. These were then processed, and the anhydrous clinker mapped using thresholding to separate out the phases of different densities. Using the imageJ software, the percentage of this anhydrous material can be found in each image, for a series of images. 24 images were used for this investigation, at a magnification of x800. Figure 4.2.11, shows one of the CEM I SEM images, with the

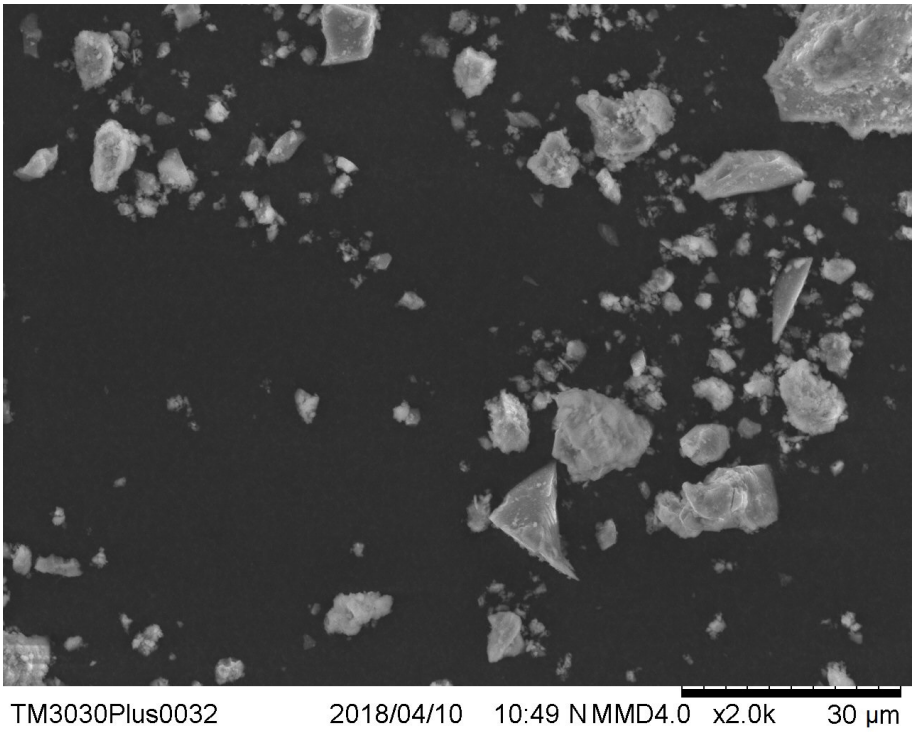

Figure 4.2.6: SEM image of C1 powder with 30 micron scale bar shown

greyscale threshold applied to pick out the anhydrous material, highlighted in red, and the corresponding percentage calculated using imageJ. There is significant variation in the percentage of anhydrous material present, showing why a large number of images must be analysed before the result can be considered representative of the sample.

In table 4.4, the anhydrous cement content calculated from each image is given, as well as the mean for the whole series. This mean has then been used to calculate the degree of hydration of the cement, using the full method described in section 3.2.2, with the calculations shown below.

$$V_{(0)cem} = \frac{\frac{643}{3.15}}{\frac{643}{3.15} + \frac{225}{1}} = 47.6\% \tag{4.2.1}$$

$$DoH\frac{cem}{SEM}(t) = 1 - \frac{V_{(t)cem}}{V_{(0)cem}} = 1 - \frac{13.94}{47.6} = 70.7\% \tag{4.2.2}$$

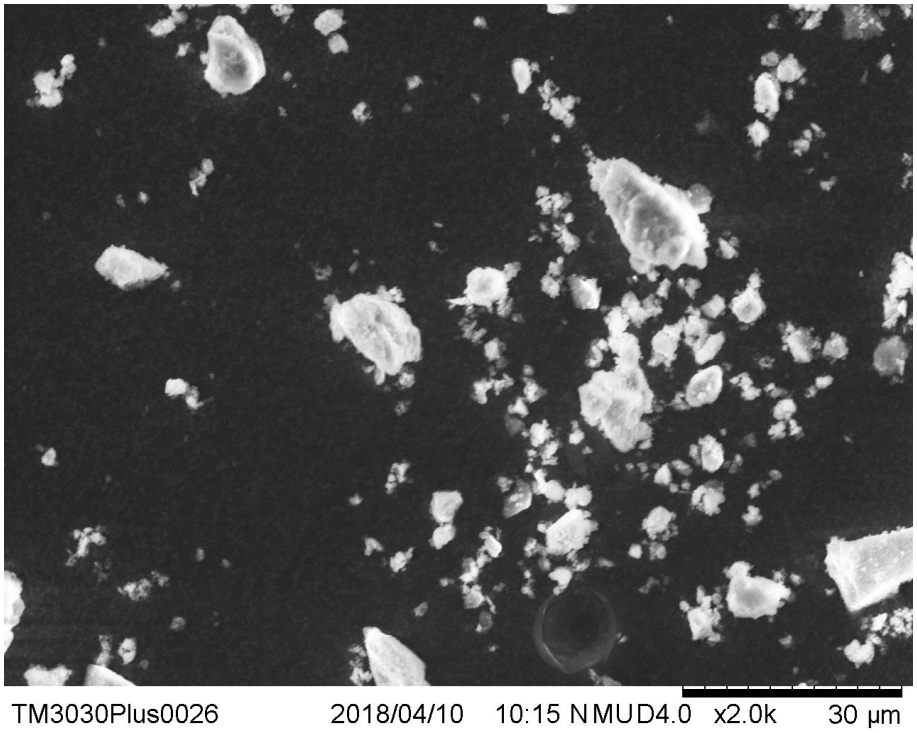

Figure 4.2.7: SEM image of T1 powder with 30 micron scale bar shown

Through BSE SEM imaging, the degree of hydration of the CEM I concrete has been calculated to be 70.7%. The standard deviation was 2.186%, producing a standard error of 0.44%. This value, for a high strength ideally cured concrete, corresponds well to those found by Idowu and Black[147] using the same method. Despite this being a high strength concrete, where a higher degree of hydration might be expected, the relatively low w/c, while helping to increase the compressive strength of the concrete through decreasing the spacing between cement particles, can limit the amount of free water remaining to cause full hydration, resulting in the roughly 30% of anhydrous material remaining in the mix.

The same image analysis process has been carried out for the CEM II concrete, using 28 BSE SEM images. Once again the mean has been taken from all 28 images, and used to calculate the DoH of the cement fraction. The standard deviation of the sample was 2.792%, leaving a standard error of 0.52%. Table 4.5 shows the percentage of anhydrous material in each image, which has then been used to calculate the degree of cement hydration. The volume fraction calculations are slightly complicated by the inclusion of PFA within the CEM II mix, shown in the following calculations, with the original equations, discussed further in section 3.2.2, shown for clarity. The density of PFA varies from par-

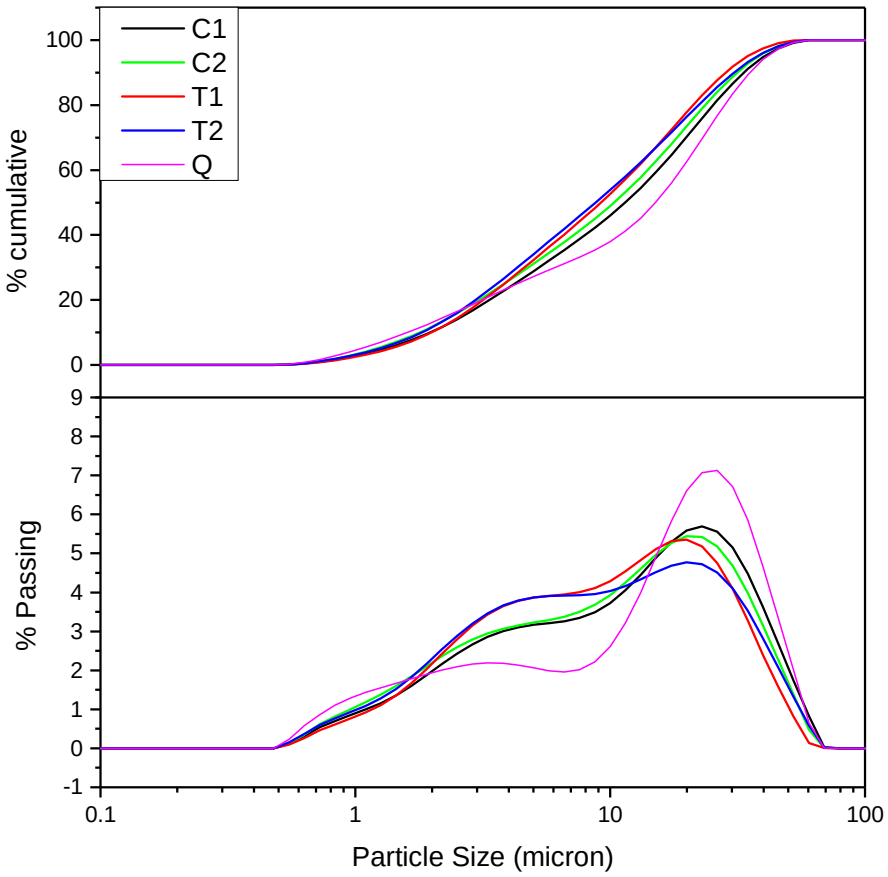

Figure 4.2.8: Cumulative PSD of fine fractions of simulated scabbled concretes after grinding, for analytical work

ticle to particle and depending on the raw material and production process[158], with a particle density range of 1.8-2.4. Thus an average particle density of 2.1 has been used for volume fraction calculations.

$$DoH\frac{cem}{SEM}(t) = 1 - \frac{V_{(t)cem}}{V_{(0)cem}} \tag{4.2.3}$$

where;

$DoH\frac{cem}{SEM}(t)$ is the degree of cement hydration, calculated through SEM imaging, at time t.

$V_{(t)cem}$ is the volume fraction of anhydrous cement at time t, from SEM imaging.

$V_{(0)cem}$ is the volume fraction of anhydrous cement at time 0, from mix design.

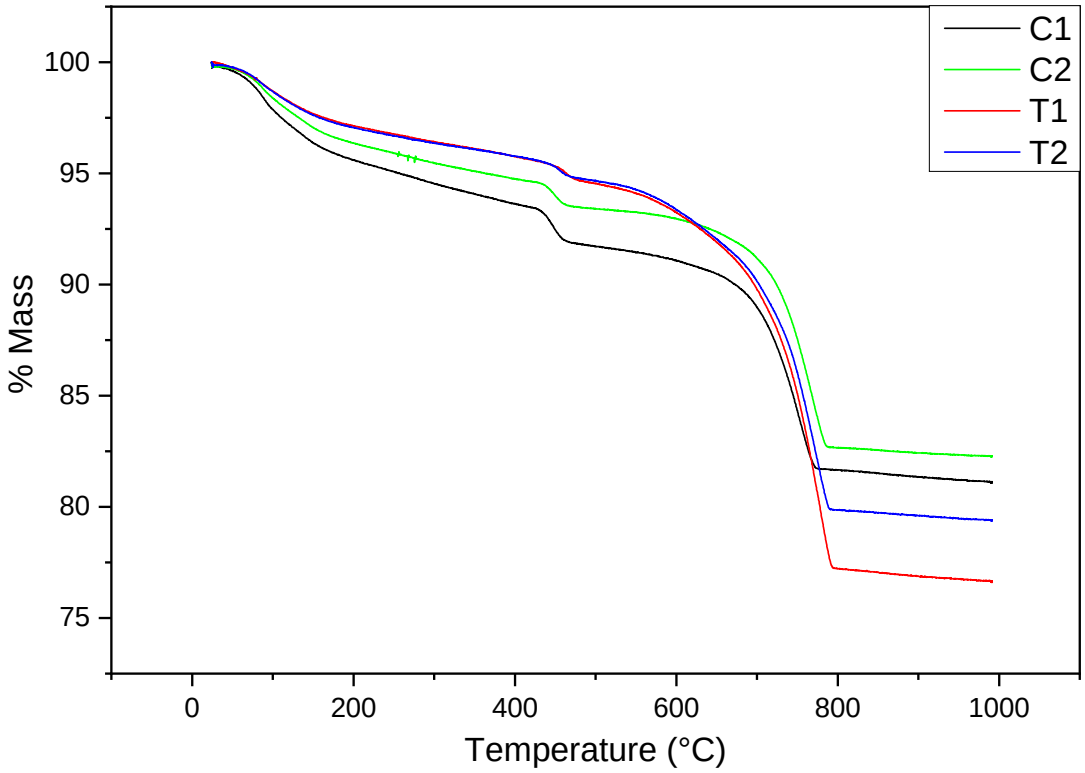

Figure 4.2.9: Thermal analysis for finer analytical fractions

The volume fraction of anhydrous cement, at time 0, within the cement paste, is calculated using the water/cement ratio, and the density of cement, through the following equations.

$$V_{(0)cem} = \frac{Vol_{cem}}{Vol_{tot}} \tag{4.2.4}$$

$$Vol_{cem} = \frac{cementcontent}{density} \tag{4.2.5}$$

where;

cement content is in $\mathrm{kg\,m^{-3}}$, from the mix design

density is also is $\mathrm{kg\,m^{-3}}$, taken as 3,150 for Portland cement.

$$V_{(0)cem} = \frac{\frac{558}{3.15}}{\frac{643}{3.15} + \frac{225}{1} + \frac{140}{2.1}} = 39.0\% \tag{4.2.6}$$

$$DoH\frac{cem}{SEM}(t) = 1 - \frac{V_{(t)cem}}{V_{(0)cem}} = 1 - \frac{10.77}{39.0} = 72.4\% \tag{4.2.7}$$

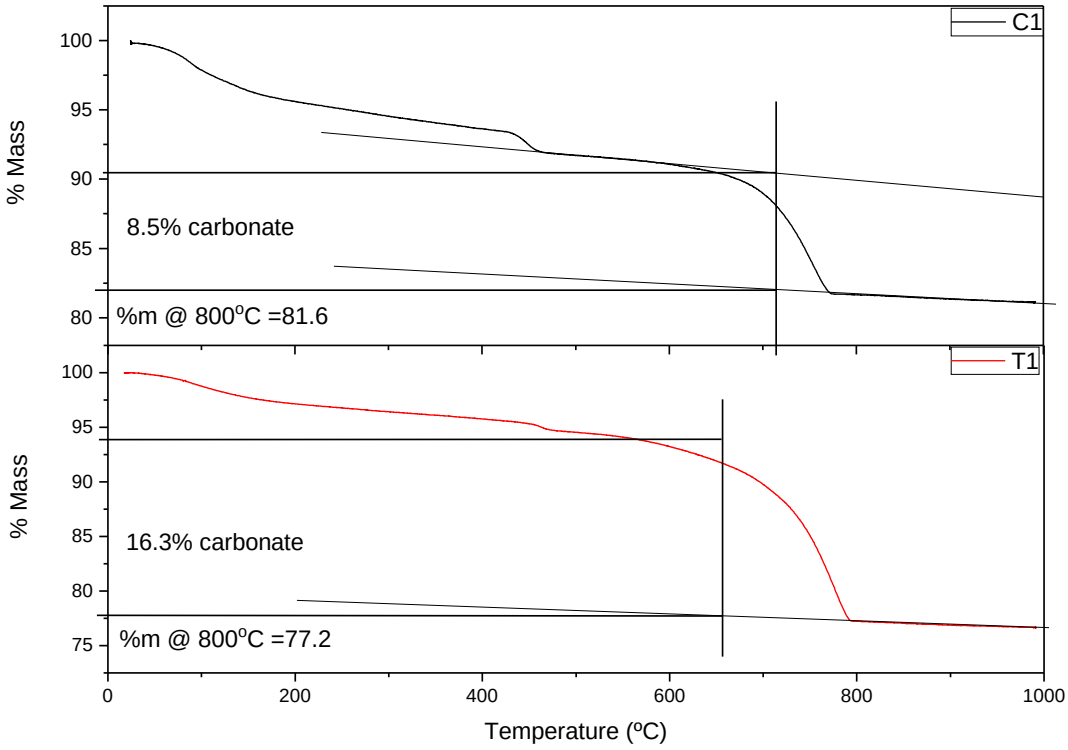

Figure 4.2.10: Mass loss due to carbonate composition, calculated from thermal analysis, for C1 and T1 fractions

Within the CEM II concrete, there are also glassy PFA particles. Liu et al.[159] showed that over a range of w/c ratios, and ages upto 180 days, only upto 35% of PFA is reacted. In fig. 4.2.12, a BSE image, with Ca, Si and Al EDX maps are shown, with a number of round PFA particles detectable in all images, showing incomplete hydration. While the degree of hydration hasn't been calculated, it is clear that anhydrous PFA remains in the CEM II concrete, and thus C2 and T2 fractions.

As the two concretes have then been ground, it is hypothesised that the grinding process has exposed some of this residual anhydrous material, and that when re-used as a filler or replacement material, the exposed anhydrous material will contribute to the overall hydration, rather than the ground material being an inert filler.

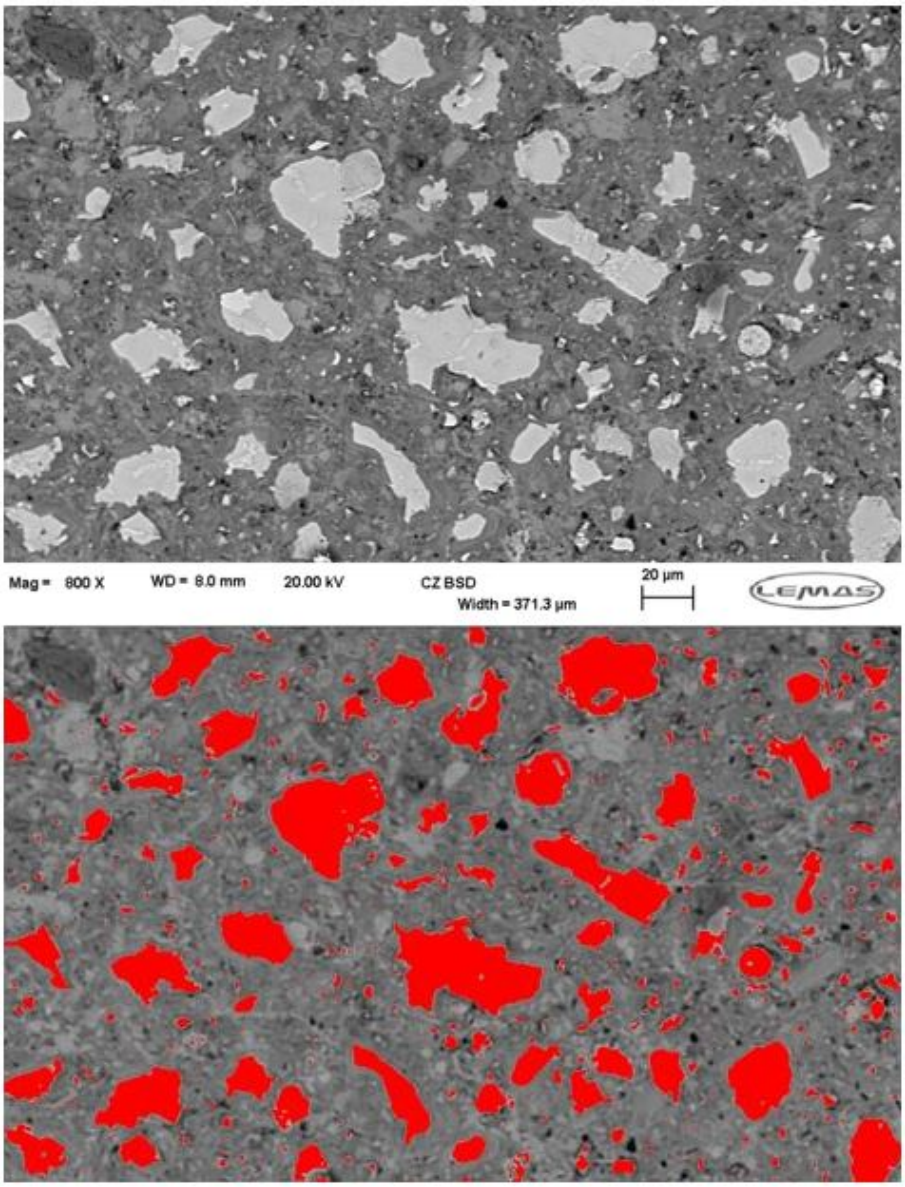

Figure 4.2.11: BSE image of CEM I (image 1) concrete, showing threshold, used to calculate remaining anhydrous material, after image processing, calculated at 18.419%

4.3 Conclusions

Grinding of the two original CEM I and CEM II concretes resulted in a fine powder with a bimodal particle size distribution, due to the differences in hardness between aggregate and cement paste. Half of the resultant powder, across the entire particle size distribution, from each concrete underwent accelerated carbonation, leaving four resultant synthesised materials; C1, C2, T1 and T2. In order to examine more closely the cement paste within the original concretes, a finer fraction from each of the C1, C2, T1 and T2 powders was also sieved for analytical work, with a 50 µm sieve being used to separate this fine fraction,

Table 4.4: Percent of anhydrous material in CEM I concrete from SEM imaging

Image (CEM I)	% anhydrous clinker	Image (CEM I)	% anhydrous
1	18.419	13	17.032
2	16.100	14	15.507
3	13.509	15	15.971
4	11.752	16	12.534
5	12.847	17	12.711
6	13.402	18	11.967
7	13.120	19	12.556
8	15.816	20	11.714
9	12.747	21	10.840
10	12.289	22	15.754
11	16.672	23	11.125
12	17.739	24	12.488
		average	13.942
		standard deviation	2.187

Table 4.5: Percent of anhydrous clinker in CEM II concrete from SEM imaging

Image (CEM I)	% anhydrous clinker	Image (CEM I)	% anhydrous
1	14.094	14	9.123
2	11.896	17	9.135
3	4.739	18	9.628
4	7.23	20	9.952
5	9.092	21	9.141
6	8.251	22	10.05
7	11.104	23	8.153
9	14.731	24	13.772
10	16.05	25	9.831
11	13.703	26	10.224
12	15.807	27	13.623
13	9.963	28	9.128
		average	10.7675
		standard deviation	2.792

leaving sufficient quantities of the entire PSD range to use as a cementitious replacement in further work.

The degree of hydration of the clinker within the initial concretes was calculated using SEM analysis, where backscattered electron image analysis was used to distinguish between the different phases, and remaining anhydrous clinker was present in both concretes, with the CEM I clinker being 70.7% hydrated, and the CEM II clinker being 72.4% hydrated. It is hypothesised that after the grinding process, some of this anhydrous material may be exposed, and contribute to the hydration process when used as filler.

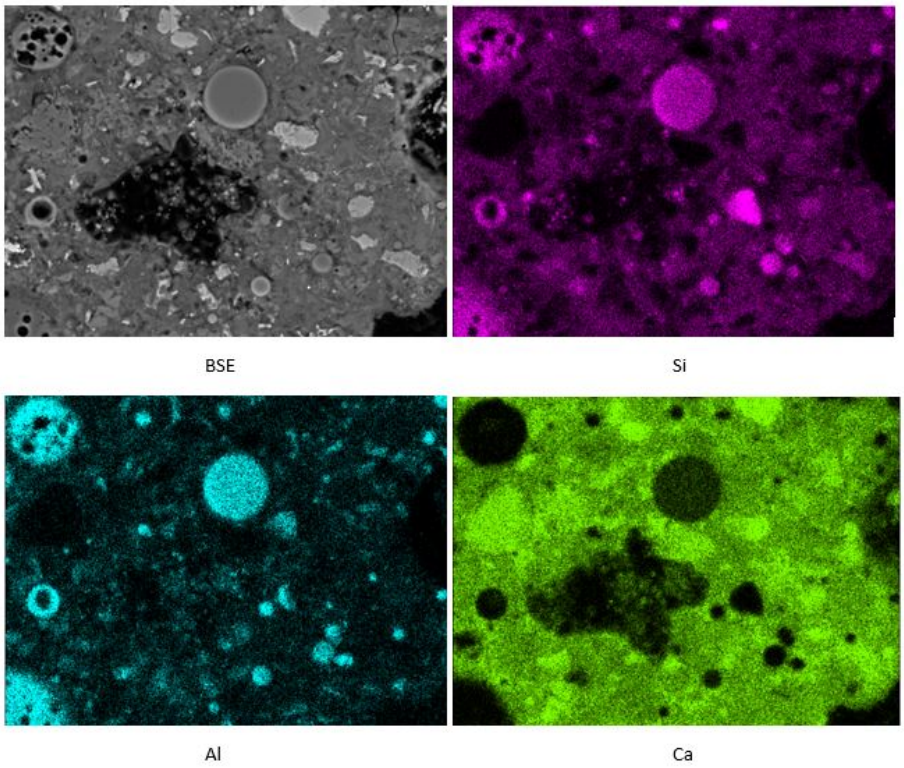

Figure 4.2.12: BSE and EDX maps of CEM II concrete, with Al, Si and Ca maps, showing anhydrous PFA remaining

Degree of carbonation of the synthesised scabblings was determined through thermal analysis. The tangent method was used to calculate the mass loss due to decarbonation of the calcium carbonate phase, and thermal decomposition of calcium hydroxide. It was found that C1 and C2 had carbonate contents of 23.6 % (10.4% mass loss due to carbonate) and 29.6% (13.0% mass loss due to carbonate), and CH contents of 5.8 and 3.2% (mass loss dur to portlandite of 1.40 and 0.78%) respectively, while following accelerated carbonation, T1 and T2 has carbonate contents of 44.5% and 40.7%, and CH contents of 4.3 and 2.5% respectively.

The increase in carbonate content following accelerated carbonation, seen in the T1 and T2 mixes, is higher than theoretically possible based on the reduction in mass of portlandite (CH), if only CH was carbonated. Therefore it is found that a significant portion of the increase in carbonate content is attributed to C–S-H carbonation, in the original CEM I concrete, and C-A-S-H carbonation in the CEM II based concrete. This is evidenced further in the earlier carbonation onset temperature from thermal analysis, with this attributable to C-S-H and C-A-S-H carbonation[160].

The C1 and C2 powders showed higher quantities of carbonate than may have been expected, due to the unprotected curing conditions of the cubes, and the storage conditions of the powder. With hindsight, these would have been aged and stored under a nitrogen atmosphere to prevent carbonation, although this wouldn't have represented the expected condition of aged concrete on site.

Chapter 5

Waste Replacement in Encapsulation Grouts

A number of studies have examined the use of recycled concrete from nuclear facilities as part of an encapsulation matrix for disposal of nuclear waste. These studies have focussed on the re-use of aggregate, either large or fine, and the effect this has on a mortar or concrete system[19,114,127]. As scabbling is a high energy process, the resultant material will contain a significant fine fraction, below that of a standard fine aggregate. The effect of such a fine fraction, when used as a cementitious replacement material, on the engineering performance of an encapsulation grout must be understood.

As discussed in section 2.5, there are a number of tightly controlled properties that a nuclear encapsulation grout must attain. By comparing all samples to a reference grout mixture containing no recycled material, these effects can be investigated and their causes identified.

Using the scabblings created in chapter 4, each resultant powder was used to replace a percentage of the binder in a grout mix. The two original concretes, a CEM I and CEM II, were ground to produce synthesised scabblings. These were subsequently referred to as C1, for the CEM I and C2 for the CEM II, and used a replacement filler in encapsulation grouts. Quartz was used as an inert filler, at the sample replacement levels, against which to compare results. To clarify the naming convention, these are shown in table 5.1.

Table 5.1: Naming convention for samples made with replacement filler

Material	Naming Convention	Colour
CEM I uncarbonated	C1	Black
CEM II uncarbonated	C2	Green
Quartz	Q	Pink

5.1 Replacement Methodology and Mix Designs

The synthesised scabblings were used as a cementitious replacement material, replacing both the cement and fine blast furnace slag in the encapsulation grout mix, such that the slag:cement ratio was maintained. A 0% replacement reference mix was used against which to compare result, and is referred to as R throughout. The replacement percentages used were 0 (R), 10, 20 and 40%. It was decided not to replace calumite, the coarser blast furnace slag, as this has been found to be a largely inert filler material[126], and is used to maintain the necessary flow characteristics of the mix. The water to binder (w/b) ratio within all the mixes was also kept constant, at 0.35. 6kg mix designs, for each replacement percentage, as well as the reference mix, are shown in table 5.2, where the replacement is either C1 or C2. Using the naming convention described above, a second number, either 10 20 or 40 is used to denote replacement percentage. Where a third number is included, this denotes the age of the sample, such that a C2-20-28 label, denotes a sample that uses ground CEM II concrete as a filler, at 20% replacement, and is cured/aged for 28 days.

Table 5.2: Design for 6kg Reference, C1 (ground CEM I concrete) and C2 (ground CEM II concrete) mixes of all replacement percentages, with all units being mass in kilograms

Material (kg)	**0% (R)**	**10%**	**20%**	**40%**
Ketton OPC	0.975	0.878	0.780	0.585
Port Talbot BFS	2.048	1.843	1.638	1.229
Replacement	0	0.302	0.605	1.209
Calumite	0.878	0.878	0.878	0.878
Water	2.10	2.10	2.10	2.10

The 6kg mixes were cast into 12, 50mm cubes, and 4, 50 d x 40mm h cylinders. The 12 cubes enable strength testing and characterisation to be carried out at ages of 1, 7, 28 and 90 days, with the cylinders being used for permeability and sorptivity testing at 28 and 90 days, with testing done in duplicate. By using testing days of this spread, the early age hydration and structural development of the grout could be investigated, using

1 and 7 day testing, probing the impact of the filler effect and dilution of the binder, while the longer term microstructural properties could be investigated using the 28 and 90 day samples, investigating any long term latent hydraulic properties.

Following casting and de-moulding, all samples were stored in a fog room under ideal conditions, with temperature maintained at 20 ± 1 °C, and a relative humidity of >95%. These conditions were chosen as the closest possible to replicating the conditions within an ILW drum, where the RH would be maintained at high levels.

Samples were strength tested in triplicate, and fragments of the cubes were taken for hydration stopping, prior to sample preparation and characterisation. For the smaller fragments where solvent exchange was a viable method for hydration stopping, this was carried out. The samples for sorptivity and permeability testing, where the volume of material meant solvent exchange wasn't a viable method for hydration stopping, were oven dried at 40 °C to constant mass, before being prepared and tested. Drying took between 60-80 days depending on the sample, shown in section 3.2.7. During drying, relative humidity was minimised in order to prevent carbonation as much as possible.

The mix designs for chemical shrinkage and calorimetry work differ slightly from the encapsulation grout mix designs used elsewhere in the project - calumite has been omitted in order to examine more closely the hydration related to inclusion of scabblings and a w/c of 0.4 has been used in order to match that of the reference ampoules. Within the analytical testing, quartz, also sieved below 50 µm has been used at the same replacement percentage, against which to compare results to the filler effect.

The 3:1 BFS to OPC ratio has been maintained, with the scabblings replacing both the BFS and OPC at the relevant percentage, to enable results to be used against comparative studies. Table 5.3 shows the mix designs for calorimetry testing, where 9 gram samples are required.

Table 5.3: Calorimetry mix design for each replacement percentage, with 9g mixes

Mix	**Ketton OPC (g)**	**Port Talbot BFS (g)**	**Replacement (g) (fine fraction)**	**Water**
0% (R)	1.61	4.82	0	2.57
10%	1.45	4.34	0.64	2.57
20%	1.29	3.86	1.29	2.57
40%	0.96	2.89	2.57	2.57

5.2 Effect on Hydration

A range of techniques were used to investigate and assess the effect of the synthesised scabbled material on the hydration of encapsulation grouts. Through the combination of a number of techniques, a more representative analysis of the hydration process could be attained.

5.2.0.1 Early Age Hydration

Within cementitious systems, the early hydration reactions occur over the first hours and days after mixing, with reactions then continuing at a slower rate for days and weeks. Isothermal calorimetry is a suitable method for investigating the early age hydration of cement systems[140]. Through separating the finer fraction of the synthesised scabblings, that which has passed through a 50 µm sieve, the cement paste fraction of the original concrete is concentrated, and the more inert aggregate partly removed. Any latent reactivity within the cement paste can therefore be investigated. The mix designs for calorimetry work are provided in a previous section, in table 5.3.

Figure 5.2.1 shows the heat flow from hydration reactions within the first day of hydration after mixing. Where quartz has been used as an inert filler, the aluminate peak still occurs at the same time as the reference mix, at 0.52 days, or 12 and a half hours. Those mixes using either C1 or C2 filler show accelerated hydration, with the slope of the initial alite hydration occurring at the same time, or even before that of the reference mix, and a significant acceleration of the aluminate peak from cement and slag hydration. Not only is the aluminate peak accelerated compared to the quartz mix, the total peak height, in both alite and aluminate hydration is increased.

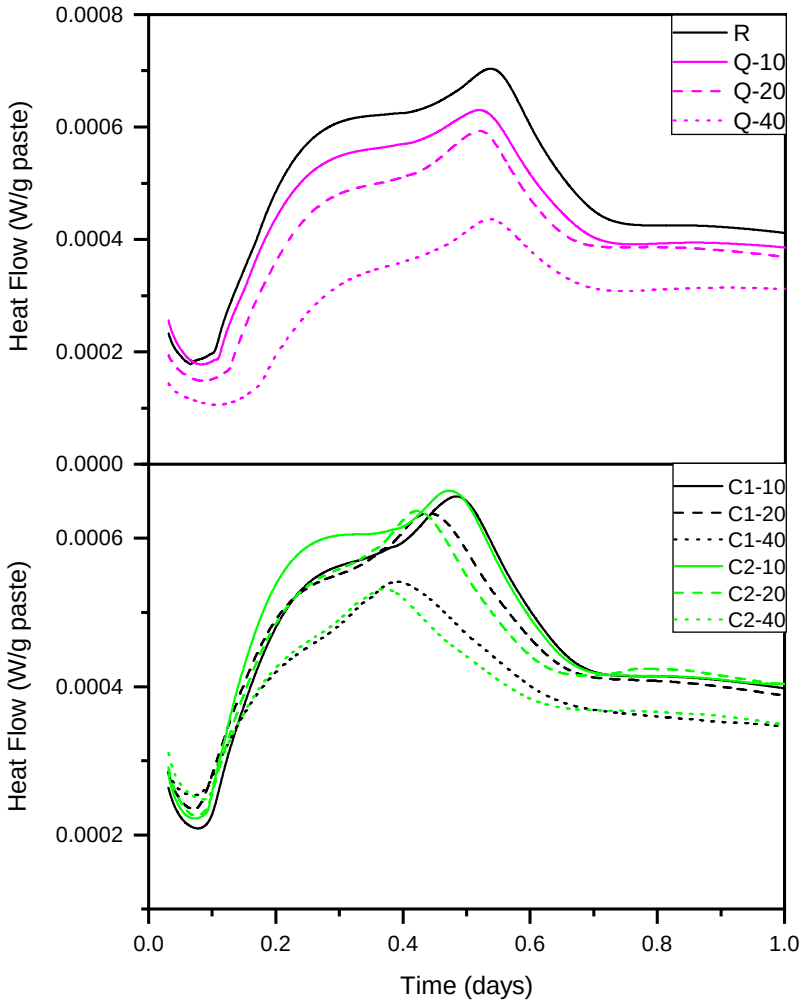

Figure 5.2.1: Heat flow from isothermal calorimetry for Reference (R), Quartz (Q) , C1, and C2 - 10, 20 and 40% mixes, within the first day of hydration, normalised per gram of paste

In order to further examine the filler effect and any contribution the synthesised scabblings may have on early age hydration, the heat flow has been normalised by gram of cement in the mix (constant cement/slag, so also equivalent to normalising by binder content). Figure 5.2.2 shows the normalised heat flow, within the first day of hydration, for the C1, C2 and Q mixes, with the reference included. Within the quartz mixes, the aluminate hydration peak is occurring at the same time as that of the reference mix, while the filler effect is small. Within the C1 and C2 mixes, the shift in aluminate peak by % inclusion is obvious, while the heat flow is increasing with replacement percentage, and significantly above that of quartz.

As well as using heat flow to measure hydration using isothermal calorimetry, cumulative

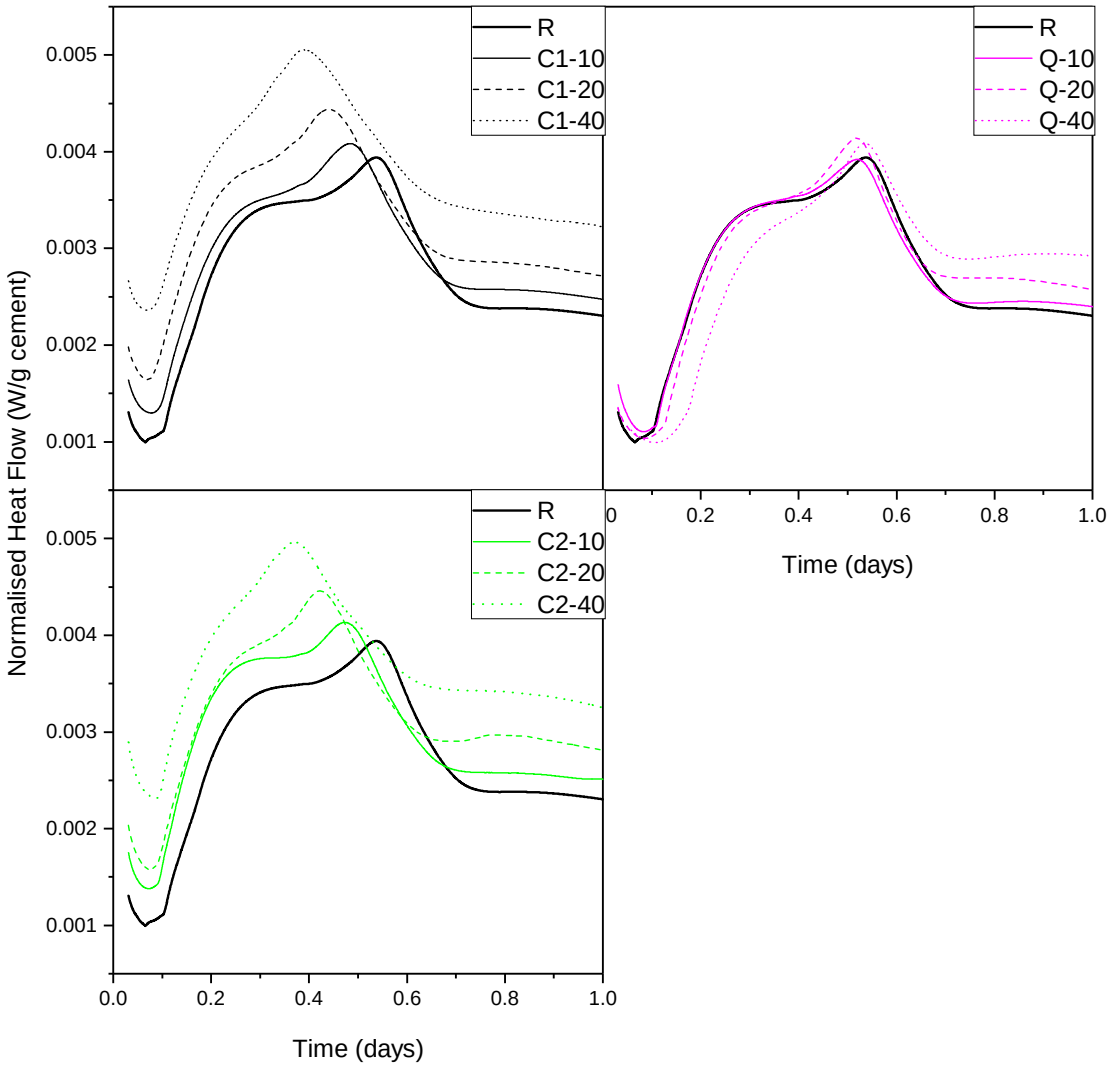

Figure 5.2.2: Heat flow from isothermal calorimetry for Reference (R), Quartz, (Q), C1, and C2 - 10, 20 and 40%, within the first day of hydration, normalised per gram of cement

heat can also be used to investigate the total reactions taking place. Figure 5.2.3 shows the cumulative heat of hydration, from each 9g sample, over the first 5 days of hydration, for the C1 and Q mixes. Straight from initial mixing, all C1 mixes show increased hydration to their quartz counterparts, showing hydration above and beyond that of the filler effect.

Figure 5.2.4 shows the normalised cumulative heat, when the quartz mixes are subtracted from that of the C1 mixes. This further shows increased hydration above and beyond that of the filler effect, with the difference in aluminate peak hydration clearly visible in each mix. After 3-4 days, the increase in cumulative heat begins to drop, as the quartz mixes begin to show a slight increase in overall heat generation compared to the C1 mixes.

When the C2 mixes were examined, the same trends were also observed.

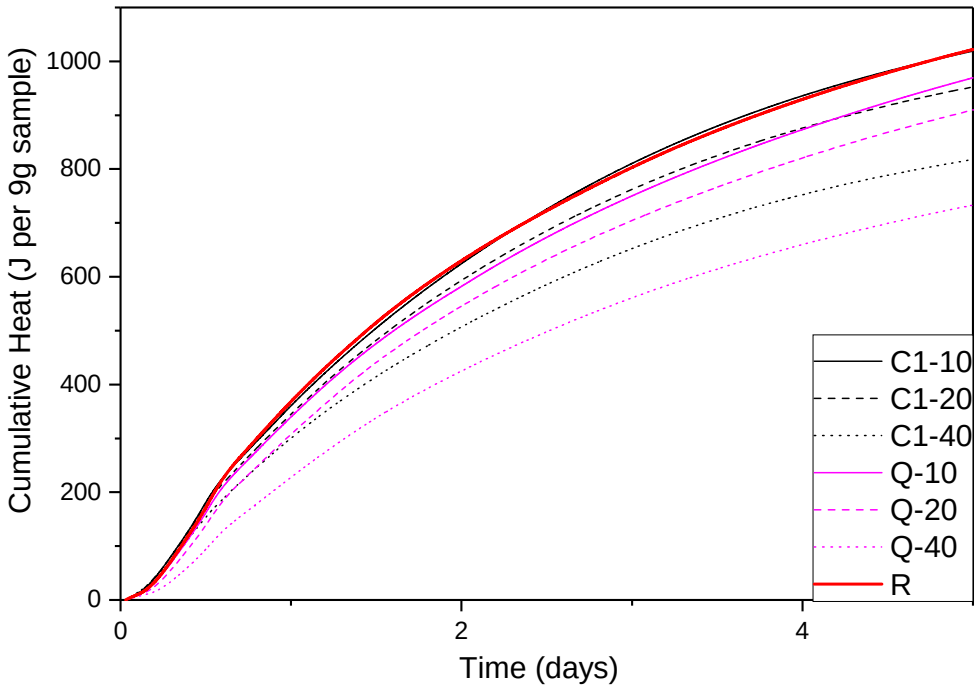

Figure 5.2.3: Cumulative heat from isothermal calorimetry for Q and C1 mixes, over the first 5 days of hydration

From chapter 4, it has been shown that the degree of hydration (DoH) of the CEM I clinker was 70.7%, and that of the CEM II clinker being 72.4%, with significant quantities of anhydrous material remaining. The increase in hydration of mixes containing scabbled product as opposed to quartz supports the theory that the grinding process has exposed remaining anhydrous material that is contributing to the hydration at early ages, as shown.

The increase in aluminate hydration can also be attributed to remaining CH in the C1 and C2 fractions. With the C1 fraction containing 5.8wt% CH compared to that of 3.2% for that of C2, this would explain the higher aluminate hydration peaks observed in the C1 compared to the C2 mix, shown in fig. 5.2.1, with CH activating the slag hydration[33].

By comparing the strength of grout cubes at different ages, it is possible to gain further insight into the hydration of the grout. Figure 5.2.5 shows the strength profile, using characteristic failure load, of R, C1 and C2 grouts for the first 7 days of testing.

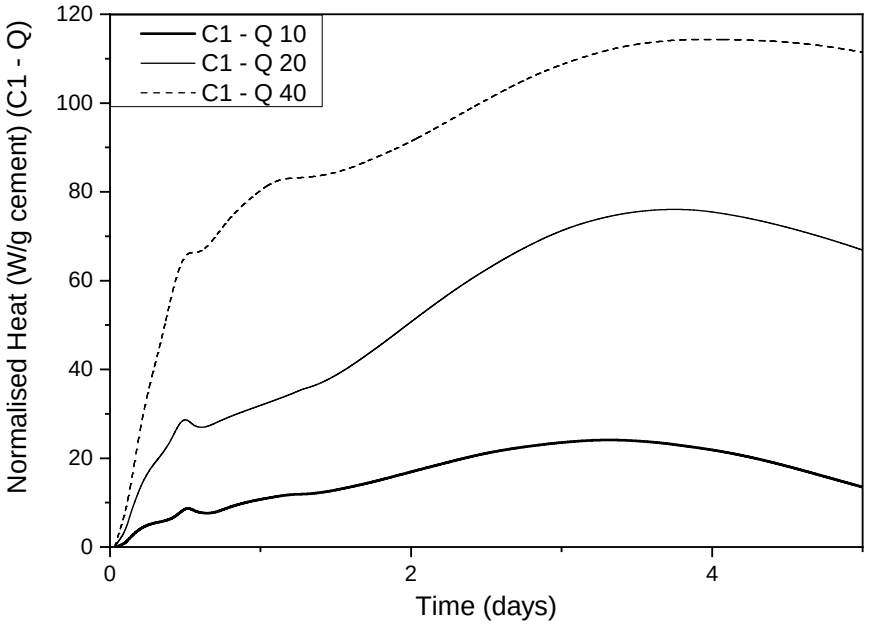

Figure 5.2.4: Heat of hydration of C1 samples, minus the filler effect (from quartz samples), normalised per gram of cement

Within the first 7 days, the C1-10 mix has comparable or greater strength to that of the reference mix, with the C1-20 mix also falling within the standard deviation of the reference mix. The C2-10 and C2-20 mixes both show reduced compressive strength compared to the C1 and reference mixes, while the C2-40 is also below that of the C1-40 at early ages, although with a smaller difference between the two mixes. The increase in CH content and thus increased and accelerated aluminate hydration can explain these differences. From this strength testing, it is shown that through either the filler effect or through contributions to early age hydration, the C1 mix, and possibly C2 mix, are producing grouts of comparable, or greater strengths, to that of the reference mix. Within the CEM I concrete, compared to the CEM II, there is a higher initial clinker content, and thus despite having very similar DoH, the increased clinker content may explain the slight increase in early age reactivity and strength of the C1 mixes compared to that of the C2 mixes.

Within the strength and calorimetry results, at early ages, it has been shown that the use of the synthesised scabblings has altered the hydration process, compared to the use of quartz as an inert filler. As there is remaining anhydrous material in the ground concrete, it is likely that this is contributing to the early age hydration of the grout.

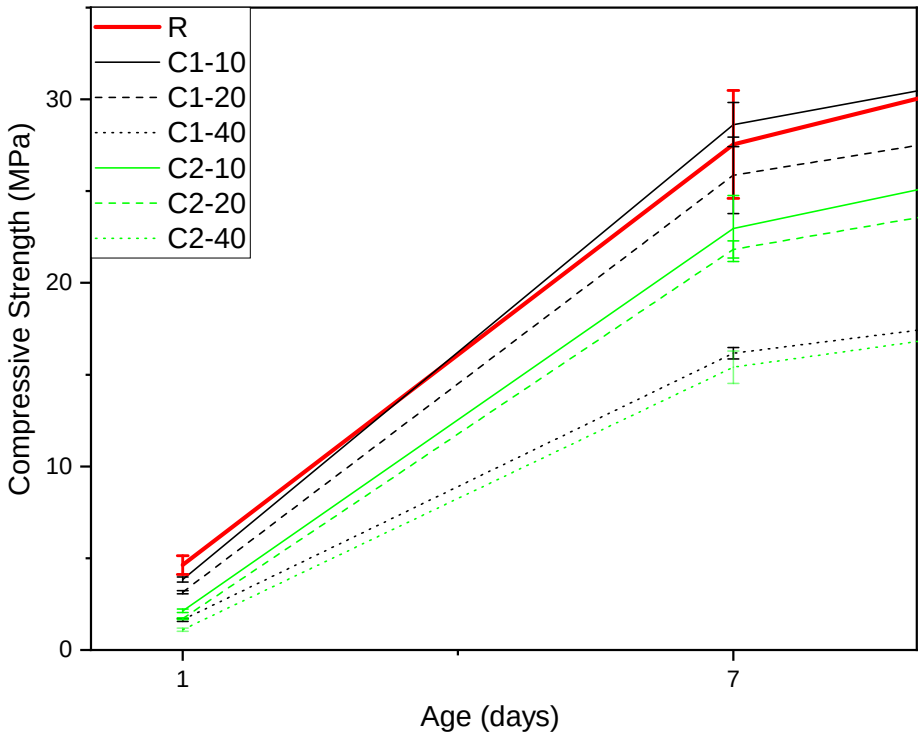

Figure 5.2.5: Mean compressive strength, with standard deviation shown, for the first 7 days, for R, C1 and C2 mixes

5.2.0.2 Long Term Hydration

Nuclear encapsulation grouts, in order to limit the heat of hydration at early ages, and to hold the pore solution pH in a range that limits the solubility of radionuclides, contain large quantities of GGBS, and so hydration reactions continue for many months and years after initial mixing, particularly compared to a standard OPC. Thus understanding the full extent of the recycled material on these reactions is vital.

When using heat flow during isothermal calorimetry, beyond the early stage reactions, the heat generation from reactions is generally so low that it is very difficult to determine on-going reactions. When cumulative heat is used however, it becomes possible to determine longer term hydration. Figure 5.2.6 shows the cumulative heat of hydration for the C1 and C2 mixes, over 14 days. Initially, as discussed in section 5.2.0.1 and shown in fig. 5.2.1 it is seen that the C1 mixes hydrate at a higher, or equal rate to that of the C2 mixes, within the first day of hydration. Over 14 days however, the C2 mixes show comparable overall heat of hydration compared to the C1 mixes, with the C2-10 mix showing very slightly higher overall hydration.

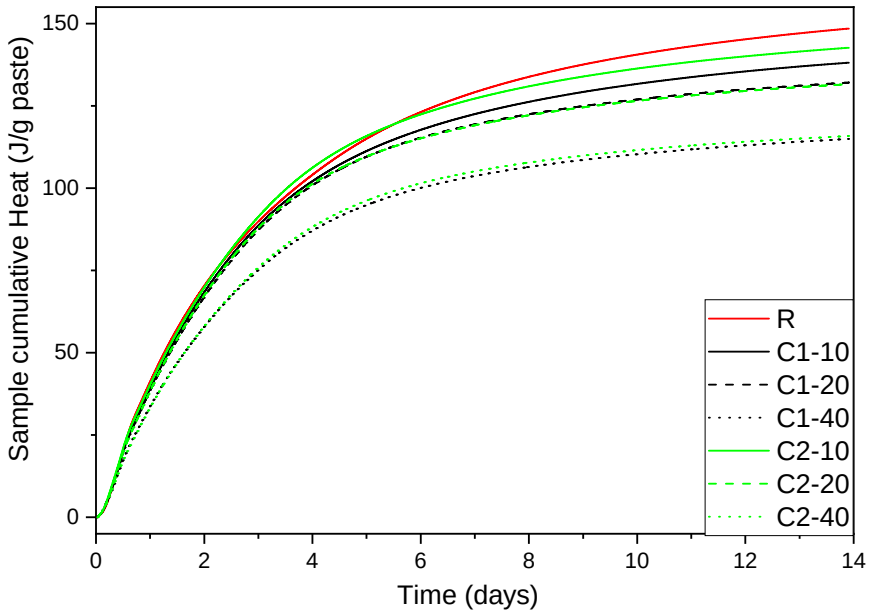

Figure 5.2.6: Cumulative heat, for C1 and C2 mixes, over the first 14 days of hydration, normalised per gram of paste

The original CEM II concrete contained 20% PFA, and through EDX mapping, it has been shown that unreacted PFA remains in the CEM II concrete, in line with the work of Liu et al., finding significant unreacted PFA remaining in a number of blends and w/b ratios[159]. As there is no other source of PFA within the project, any PFA within the ground C2 powder, or in the C2 replacement mixes originates from the original concrete. As a high performance concrete, with a low w/c ratio, the water content may have been a limiting factor in their hydration. With some unreacted fly ash remaining in the ground material, it is likely that this is contributing to the slightly higher heat of hydration observed in the C2 mixes.

In fig. 5.2.7, the failure stresses are shown for C1 and C2 mixes for 1, 7, 28 and 90 day tests. While there is a difference in the early age strength, shown in fig. 5.2.5, with the C1 mixes outperforming the C2, beyond 14-28 days there is little overall difference in compressive strength of the grouts produced with the C1 and C2 filler, with the C2 mixes falling within the standard deviation, and therefore error, of the C1 mixes.

The bound water content, calculated from thermal analysis, as the difference in mass between 550 °C and following removal of free water by solvent exchange, is shown with

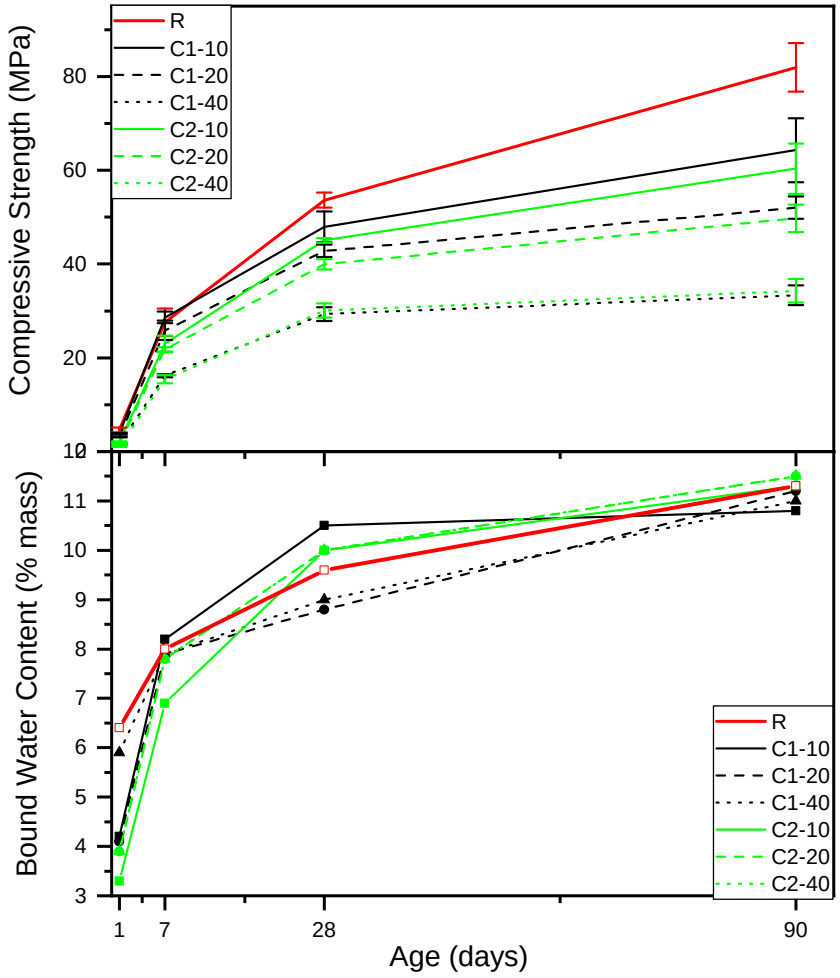

Figure 5.2.7: Mean failure stress, with standard deviation shown, for C1 and C2 mixes up to 90 days, with bound water content, from thermal analysis, for the same mixes

compressive strength in fig. 5.2.7. Bound water content can be used to assess the degree of hydration of portland cements[141]. After 1 day of curing, as discussed previously, the C1 mixes show a slight increase in hydration, determined via isothermal calorimetry, and an increased compressive strength, compared to the C2 mixes. This is linked to the increased portlandite content in the C1 ground concrete, activating the slag. Although the results show scatter, at 1 day the C1 mixes all show increased bound water content compared to the C2 mixes, corroborating with the compressive strength and calorimetry results, although the effect isn't large. At later ages, the scatter within the bound water content is large, and as with compressive strength data, there is no discernible difference between the two mixes, particularly at 28 days. At 90 days, the C2 mixes all show slightly higher bound water content than the C1 mixes, which could be evidence for the pozzolanic effect of the unreacted PFA in the C2 ground concrete (from the original CEM II concrete). Ev-

idence from compressive strength data doesn't support this, and the scatter in the bound water content is such that the reliability of solely these results is low.

When quartz is used as an inert filler, instead of the C1 and C2 powders, initial hydration has been shown to be occurring at a slower rate, or to a lesser extent, compared to the other mixes, with remaining anhydrous material in the C1 and C2 mixes contributing to the early hydration reactions. When quartz is ground and fractured, as seen in fig. 5.2.8, in general, the surfaces are smoother and flatter than those of ground concrete powders, like the C1 and C2 powders, which are shown previously in section 4.2.2.

As the C1 and C2 powders are ground and fractured, the quartz within them from sand and quartzite aggregate will fracture, but the cement paste will also fracture, and so some quartz frament will be left with much rougher edges where cement paste remains intact.

The filler effect is created by providing nucleation sites for the growth of hydration products, particularly C-S-H and CH[65]. In terms of providing nucleation sites for the formation of hydration products at early ages, the increased roughness and surface area provided by the cement paste may help to significantly contribute to the filler effect of the C1 and C2 powders compared to the quartz at early ages.

In terms of later age hydration however, isothermal calorimetry shows the quartz mixes, after ages of between 5-10 days, begin to have a higher rate of hydration, with the Q-10 mix having a higher total heat that the C1-10 and C2-10 mixes after 8 and 5 days respectively, shown in fig. 5.2.9. While increasing early age hydration in most cementitious systems is wholly beneficial, in systems such as nuclear encapsulation grouts where an uncharacteristically high percentage of the binder is much slower reacting blast furnace slag, the early formation of hydration products may inhibit the hydration of the slag at later ages, by limiting the available pore space in which hydration products can form, and limiting the amount of free water available for further hydration.

Through isothermal calorimetry, and thermal analysis, it has been shown that in longer term hydration, there is little difference between the C1 and C2 mixes, with bound wa-

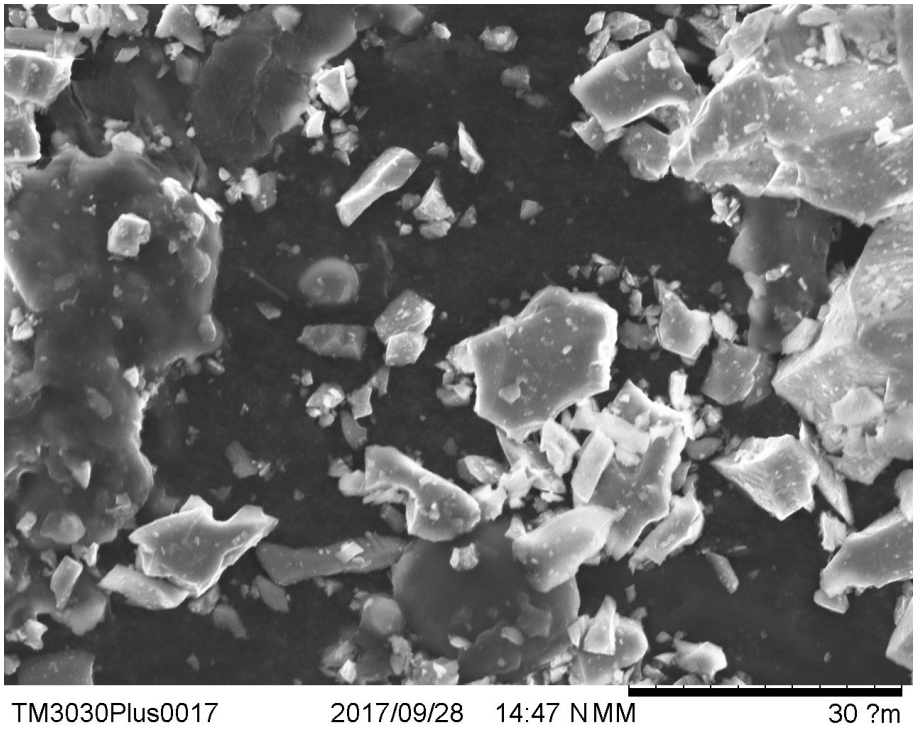

Figure 5.2.8: Scanning electron image, at 2500x magnification, of the ground quartz (Q) fraction

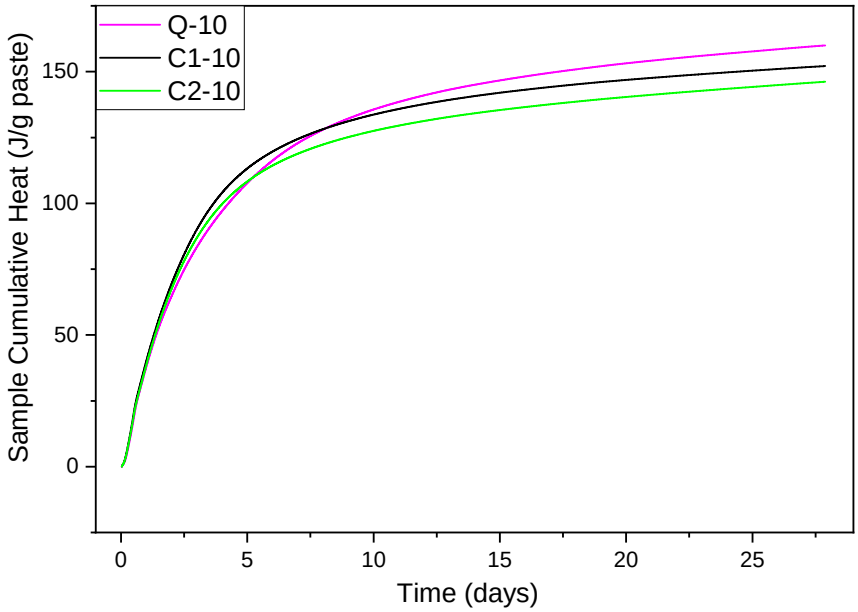

Figure 5.2.9: Isothermal calorimetry 28 day run, of sample cumulative heat, for Q, C1 and C2 mixes at 10 % replacement, normalised per gram of paste

ter content showing possible slight increased hydration of the C2 mixes, linked to the pozzolanic reaction of the PFA from the original CEM II concrete, but the difference is within the scatter of the data, and can't be linked to solid conclusions. Overall, compared to quartz used as an inert filler, both the C1 and C2 fractions affect the hydration of the grout above and beyond that of the filler effect. This is shown through differences in hydration compared to mixes where quartz is used at the same percentage replacement. Although this increase in early age hydration has been observed, over longer age hydration, the quartz mixes showed increased hydration at a greater rate than the C1 and C2 mixes, possibly due to the increased early age hydration from the replacement mixes preventing the slag content of the encapsulation grout having sufficient pore space in which additional hydration products can occur[126].

5.3 Effect on Microstructure and Engineering Properties

While strength and hydration are an important requirement for encapsulation grouts, the microstructure and engineering properties are vital for appropriate encapsulation of nuclear waste, and so an understanding of how a filler material affects these properties is vital. Of primary importance for the microstructure and engineering performance is the ability for groundwater to penetrate into the grout during deep geological disposal conditions, and leach radionuclides out of their protective environment and into the wider geo- and eco-sphere.

Through gas permeability and water sorptivity testing, as described in section 3.2, the porosity and permeability, and the ease with which water can flow through the grout, can be investigated.

5.3.1 Permeability

Through measuring the time taken for a known volume of gas to pass through a sample of known dimensions, under known pressure, the intrinsic permeability can be calculated. Within permeability testing, the values are highly dependent on the sample, the prepara-

tion, and equipment. Cracking within a sample is known to have a large impact on the values obtained using this method[143], and so individual values for samples need to be used carefully, but the overall trends within the data can be used with confidence.

Figure 5.3.1 shows the intrinsic permeability, at 1.5 bar, for R, C1 and C2 mixes at 28 days. At 10% replacement, the permeability is greater than that of the reference mix, at around 8.0 x10^{-14}m^2, compared to around 5.7x10^{-14}m^2 for the R mix. At 20% replacement, the increase in permeability is more noticeable, and roughly double the increase in permeability found from the 10% mix compared to the reference. At 40% inclusion however, the increase in permeability is much more marked, with both mixes having a very similar value at 1.38x10^{-14}m^2. The 40% permeability values are substantially greater than the 10 and 20% replacement values.

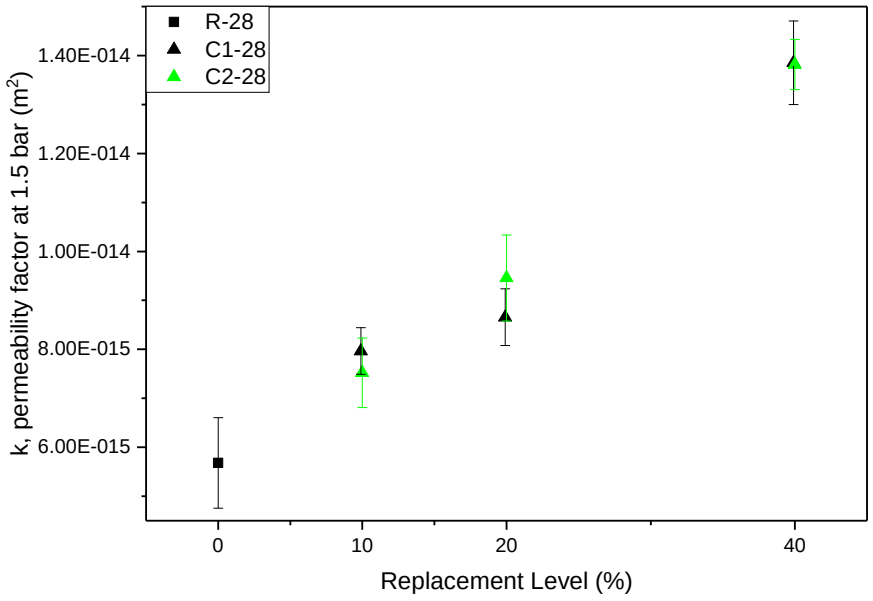

Figure 5.3.1: Intrinsic permeability values for R, C1 and C2 mixes 28 day samples

By 90 days, the permeability of all mixes has dropped significantly, from a maximum of 1.38x10^{-14}m^2 at 40% inclusion, to 9.9x10^{-15}m^2, and a minimum, from the reference mix of 5.7x10^{-15}m^2, dropping to 5.0x10^{-15}m^2, shown in fig. 5.3.2. In their original investigation, Cabrera and Lynsdale, using the same apparatus, were calculating intrinsic permeabilities of concrete samples at x10^{-15}m^2 to x10^{-16}m^2. With grout samples containing no aggregate, which is impermeable, there is a significant increase in volume of cement paste, and so

a single order or magnitude difference in permeability between concrete, and the grout samples measured in this investigation, seems appropriate. Hawthorne, in their work on nuclear encapsulation grout samples, were calculating intrinsic permeabilities in the range of $x10^{-12}m^2$ to $x10^{-13}m$[126], significantly higher than the samples measured in this investigation. On investigation, the pressure terms within their work were not properly altered to base SI units, with some areas in cm^2 and some in m^2 and so the order of magnitude is incorrect, but the range of permeability values, over different samples and ages, is similar to the ranges calculated in this investigation.

As would be expected for samples containing such high amount of slag with slow hydration rates, after 28 days there continues to be significant hydration and microstructural development, which is also apparent through strength testing, shown earlier in fig. 5.2.7, where there is still significant strength and degree of hydration increase between 28 and 90 days.

The permeability values for the R and C1 mixes at 28 and 90 days are shown in fig. 5.3.3, where the decrease in intrinsic permeability values is shown clearly. For 0, 10 and 20% replacement, the drop in permeability is doubled, whereas the drop at 40% is much greater. At this high level of replacement, with the resultant dilution of cementitious material, the initial hydration reactions will be insufficient to fill the pore volume, providing sufficient volume for hydration products from further slag hydration to fill the pore voids and have a more significant impact on the lowering of the permeability between 28 and 90 days.

5.3.2 Sorptivity

While air permeability is measured using a pressure head to drive gas through the sample, water sorptivity takes into account the capillary action of the sample itself, and the ability for waster to be absorbed into the sample over time. As the overriding mechanism for damage to waste packages and leaching of radionuclides is through groundwater intrusion, understanding the water transport properties through a grout is important.

Figure 5.3.4 shows the sorptivity data for C1 and C2 mixes at 90 days. Table 5.4 provides the sorptivity coefficients for the R, C1 and C2 mixes. The C2 mixes all show a

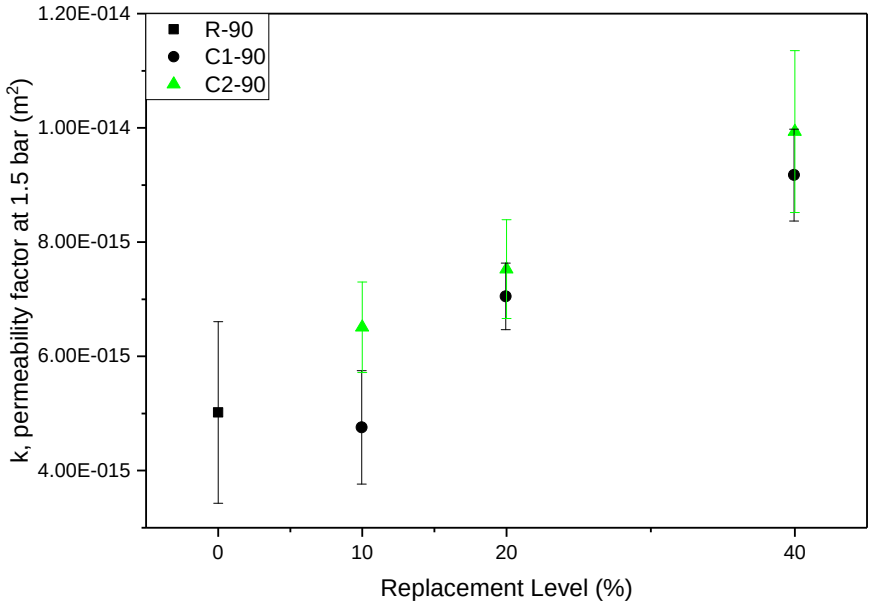

Figure 5.3.2: Intrinsic permeability values for R, C1 and C2 mixes 90 day samples

consistently higher sorptivity compared to the C1 mixes, with C2-10 having a sorptivity coefficient 9% higher than that of C1-10, while C2-20 is 27% higher and C2-40 is 22% higher. While the extent of the differences in permeability isn't as great as sorptivity, the C2 mixes at 90 days also show a slightly increased permeability, showing good agreement between the two methods.

Table 5.4: Sorptivity coefficients for R, C1 and C2 90 day samples

Sample	Sorptivity Coefficient ($m.s^{-0.5}$)x10^{-3}
R	6.97
C1-10-90	6.5
C1-20-90	8.71
C1-40-90	9.03
C2-10-90	7.07
C2-20-90	11.1
C2-40-90	11.03

Sorptivity testing is known to be very sample specific, with the results dependent on local surface features such as carbonation[161]. Carbonation is known to reduce the overall porosity of ordinary cement paste[98], while in blended cements such as those with PFA or BFS, the lower portlandite content, and reduced Ca/Si in the C-(A)-S-H, can result in an increased porosity following carbonation and so differences in the sample carbonation, due to its properties and preparation can easily affect results. .

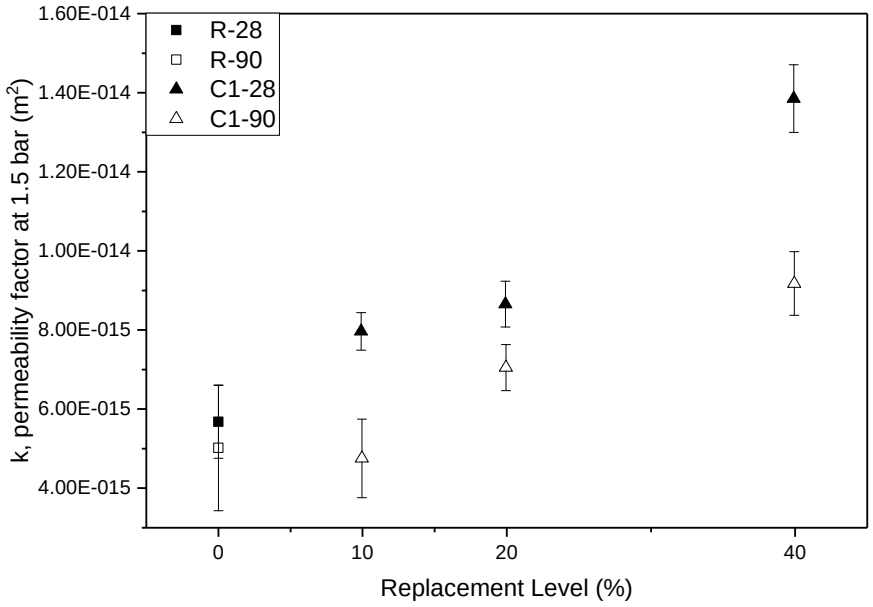

Figure 5.3.3: Intrinsic permeability values for R and C1 28 and 90 days samples

While the C2 samples show a slight increase in sorptivity compared to the C1, at 10% inclusion the samples have very similar permeability to that of the reference mix. The sorptivity data for the reference sample, compared to the C1-10 and C2-10 90 days samples are shown in fig. 5.3.5. The reference sample, at 90 days has a sorptivity coefficient value of 0.00697, while the C2-10 mix has a sorptivity coefficient of 0.00707, or 1.4% difference, which given the error within the method can be regarded as statistically equal. The C1-10 mix has a coefficient of 0.0065, 7.2% lower than the reference mix. Both the C1 and C2 10% mixes show improved, or equal sorptivity characteristics compared to the reference mix, suggesting that at this level of replacement, long term microstructure and engineering performance isn't negatively affected by the inclusion of the recycled concrete.

5.4 Conclusions

Synthesised scabblings were used as a filler in encapsulation grouts, at 10, 20 and 40% replacement levels. Only the finer, reactive fractions, being Ketton OPC and Port Talbot BFS were replaced, with the coarser calumite fraction being maintained, due to having been found in previous studies[126] to be largely unreactive, and being required to maintain appropriate flow characteristics. Part of the finer fraction of the synthesised scabblings,

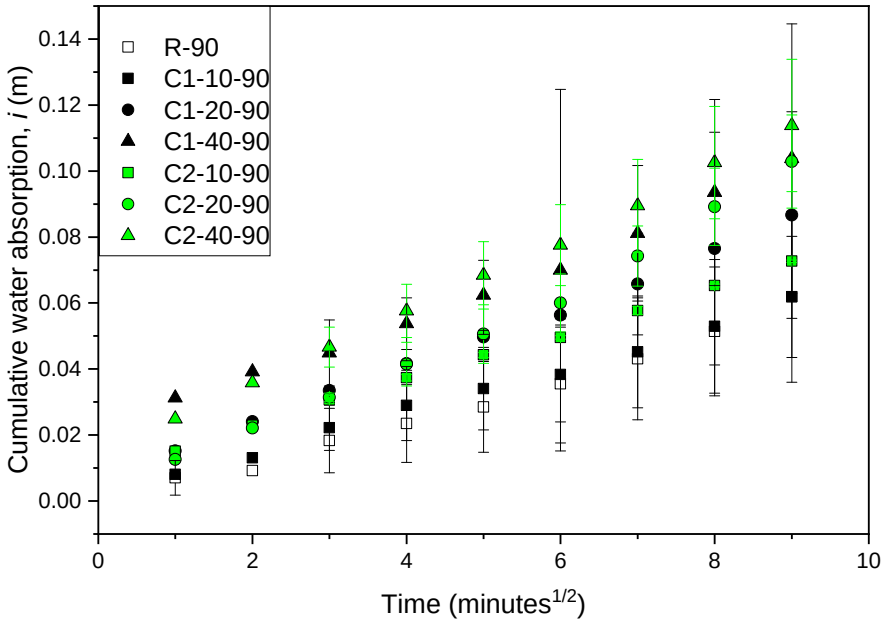

Figure 5.3.4: Sorptivity data for C1 and C2 90 day samples

below 50 µm, was separated for used in calorimetry work to further investigate any affect it had on the hydration process.

Through isothermal calorimetry and strength testing, it was found that both the C1 (ground CEM I concrete) and C2 (ground CEM II concrete), altered the early age hydration of encapsulation grouts when used as a filler, compared to mixes where quartz, as an inert material, was used at the same replacement percentages. The initial alite reaction began at the same time as that of a reference mix, whereas when quartz was used, this initial reaction was delayed. The aluminate peak, from slag hydration, was accelerated compared to a reference mix, while the cumulative heat of hydration reaction showed both C1 and C2 mixes as having a higher total hydration at earl ages. As both the CEM I and CEM II powders had been shown to contain anhydrous clinker, as discussed in section 4.2.2.3, and remaining CH, is is hypothesised that this remaining anhydrous powder is contributing to the early hydration reactions, through activation of the slag content and reaction of remaining anhydrous clinker, and that the synthesised scabblings are not inert material.

At later ages, C2 mixes show increased hydration compared to those of C1, with isothermal calorimetry showing a higher total heat output, while strength testing and and thermal analysis show very little difference between the two mixes, with any differences falling

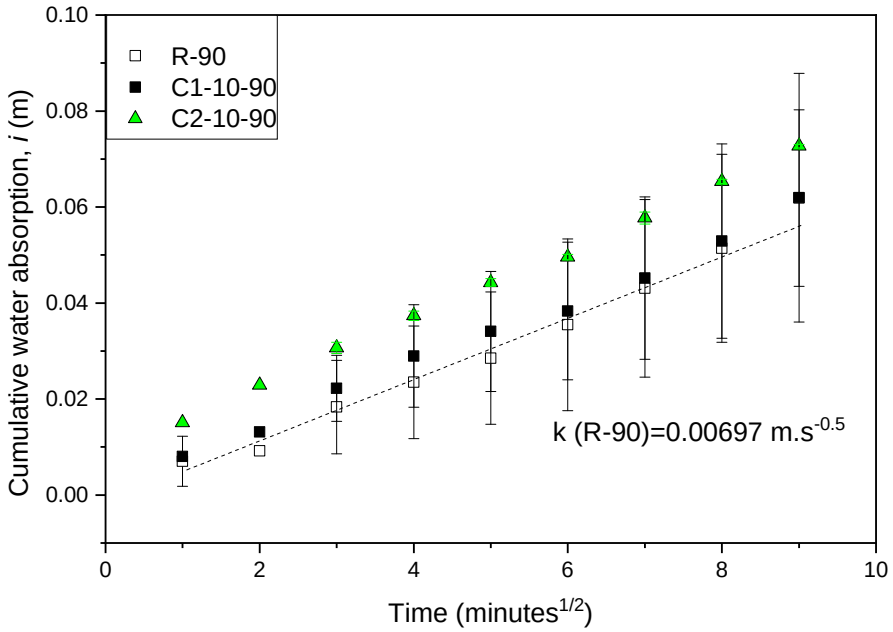

Figure 5.3.5: Sorptivity data for R, C1-10 and C2-10 90 day samples

within the error and scatter of results. As such, there is possible, but inconclusive, evidence of pozzolanic reaction from the unreacted PFA within the ground CEM II material. However, the total amount of PFA within the overall system following replacement is very small, and further SEM work would be the most appropriate way of determining if any additional PFA reaction occured.

Permeability and sorptivity testing have been used to investigate the microstructure and engineering performance of grout samples at 28 and 90 days. At both ages, samples with 20 and 40% inclusion perform significantly worse than a reference mix, with the high level of replacement causing too much dilution of cementitious material, and providing pathways for air and water to permeate through the samples. At 10% inclusion however, the C2 mix had very similar properties to that of the reference mix, while the C1-10 samples outperformed it. At 10% inclusion, the hydration of remaining anhydrous material, as well as the filler effect, is sufficient to counteract the loss of binder.

Overall, it has been found that at replacement levels of 20 and 40%, the hydration and engineering properties of the grout are significantly affected detrimentally, with the reaction of anhydrous material remaining, combined with the filler effect not able to counteract the loss of binder. At 10% inclusion however, for both C1 and C2 mixes, the hydration

process, and resultant strength and engineering properties are equal, or suitably similar, to the reference mix. This suggests that replacement at this level or below is feasible, with the reaction of any remaining anhydrous material, in combination with the filler effect, making up for the loss of binder.

Chapter 6

Ternary Grouts

The depth of radionuclide penetration into concrete, for the more soluble radionuclides such as caesium-137 and iodine-129, can reach several centimetres [16,162]. In aged concrete structures, such as those being decommissioned on nuclear sites, the depth of carbonation front is dependent on a number of factors, such as exposure conditions, mix design of the concrete, and age, as discussed in section 2.4.1. With the ages of many buildings to be decommissioned at Sellafield and the Magnox sites being of 50 years or more, the carbonation front may have penetrated several centimetres into the concrete [89].

With the mechanical scabbling process being used to remove all radioactively contaminated concrete upto a depth of several centimetres, it is likely that a large part of the scabblings will be at least partially, and often fully carbonated.

As discussed in section 2.3.2, the presence of calcium carbonate, primarily from limestone addition, within blended cements affects the hydration process, and has been found to improve the early age performance of blended cement and slag mixes [80], as well as increasing the activity of slag [83].

As the presence of calcium carbonate is likely to affect the hydration process of the grout - with it containing 75% slag content - compared to the non-carbonated scabblings used previously, these effects need to be investigated and understood.

6.1 Methodology and Mix Designs

As with the previously described study looking at the effects of fresh scabblings on encapsulation grout performance, this part of the study was concerned with looking at the effects of replacing defined percentages of slag-cement binder with carbonated scabblings. The carbonated scabblings, T1 and T2, characterised in chapter 4, were used to replace the binder (Ketton OPC and Port Talbot BFS) within an encapsulation grout mix, at 10, 20 and 40% replacement levels. The w/b was kept constant at 0.35. The mix designs, for 6kg mixes, are shown in table 6.2.

Table 6.1 provides a breakdown of the sample naming system, a continuation from chapter 5. The original CEM I and CEM II concretes were ground and carbonated. The carbonated ground CEM I concrete, when used as a filler to create a ternary blend, is designated T1. The T2 mixes are those originating from the carbonated ground CEM II concrete. Using the same sample naming system as in chapter 5, a T2-40-7 mix is that using carbonated CEM II ground concrete, at 40% replacement, and is 7 days old.

Table 6.1: Naming convention for samples

Material	Naming Convention	Colour
CEM I uncarbonated	C1	Black
CEM II uncarbonated	C2	Green
CEM I carbonated	T1	Red
CEM II carbonated	T2	Blue
Quartz	Q	Pink

Table 6.2: Design for 6kg T1 and T2 mixes of all replacement percentages, with all units being mass in kilograms

Material (kg)	**10%**	**20%**	**40%**
Ketton OPC	0.878	0.780	0.585
Port Talbot BFS	1.843	1.638	1.229
Replacement	0.302	0.605	1.209
Calumite	0.878	0.878	0.878
Water	2.10	2.10	2.10

As with the R, C1 and C2 mixes, 12 x 50mm cubes, and 4 x 50mm d x 40mm hcylinders were cast, and following de-moulding, stored under ideal conditions at 20 ± 1 °C and 99 ± 1% relative humidity, until testing. Testing was carried out at 1, 7, 28 and 90 days, to investigate both short and longer term hydration. The number of cubes and cylinders cast

enabled strength testing to be carried out in triplicate, while permeability and sorptivity testing was carried out in duplicate.

For calorimetry and chemical shrinkage testing, the mix designs were altered slightly to further examine the effect of the scabblings on grout hydration. Calumite was omitted from both tests, as it provides very little in the way of reactivity, and is primarily used to maintain the necessary fluidity within the grout. The mix designs for 9g calorimetry samples, at 0.4 w/b to maintain the same specific heat as the reference ampoules, are given in table 6.3.

Table 6.3: Calorimetry mix design for T1 and T2 mixes

Mix	**Ketton OPC** (g)	**Port Talbot BFS** (g)	**Replacement** (g)	**Water** (g)
10%	1.45	4.34	0.64	2.57
20%	1.29	3.86	1.29	2.57
40%	0.96	2.89	2.57	2.57

Hydration stopping of smaller fragments, for thermal analysis, SEM and XRD was carried out using solvent exchange, described fully in section 3.2.10. Samples were quenched in isopropanol for 24 hours, before being placed in a vacuum desiccator to remove any remaining solvent from the sample. The larger samples for sorptivity and permeability testing were hydration stopped using oven drying at 40 °C.

6.2 Effect on Hydration

6.2.1 Early Age Reactions

It is well documented that the presence of calcite, primarly from limestone inclusion, changes the hydration of portland cement at early ages[75,79,82], which when included in blended systems forms a ternary cement. The methods used elsewhere[14,163,164], and within this research to investigate early hydration include XRD, calorimetry and strength testing.

6.2.1.1 Dormant/Induction Period

Following initial mixing, cement systems enter a dormant, or induction, period. Initially, this was though to be brought about by the formation of a protective layer of metastable C-S-H around clinker grains, preventing any hydration of the grains occurring[21]. More recently studies suggest that this protective layer has never, despite advances in imaging techniques, been observed, and that the dormant period is due to an undersaturation of C_3S in the pore solution[27].

Figure 6.2.1 shows the heat flow, from isothermal calorimetry, normalised per gram of OPC, of the C1 and T1 mixes during the first 12 hours of mixing (the 20% replacement mix has been omitted for clarity). As can be seen, the duration of the dormant period within the C1 mixes is largely constant, with very little variation between the reference, 10 and 40% mixes. Within the T1 mixes however, the dormant period is increased, with both the initial slow deceleration in reaction prior to the induction period being increased, as well as the length of the period itself. The trough of the dormant period at 10% is delayed from 1.8 hours to 2.3 hours, at 20% the delay is increased to 2.6 hours, while at 40% inclusion that delay is increased to 3.8 hours.

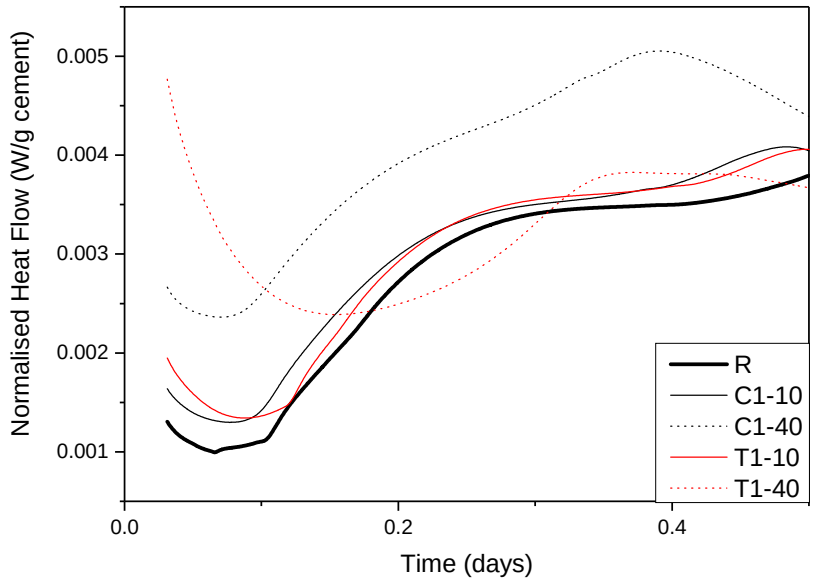

Figure 6.2.1: Heat flow, showing induction period, for C1 and T1 mixes upto 12 hours, normalised per gram of cement

From thermal analysis carried out in chapter 4, the T2 fraction is known to contain less

calcite (calcium carbonate) than the T1 fraction, while the increase in calcite content from the C2 to T2 mix is around half of that from C1 to T1, with a 20.9wt% increase compared to a 11.1wt% increase in the T1 fraction compared to the C1. The increase in calcite content is important, as PFA (present in the ground C2 powder from the original CEM II concrete), can contain carbonates that will cause mass loss over the same range as calcite in thermal analysis, producing a higher than expected value of calcite content.

Figure 6.2.2 shows the heat flow, upto 12 hours, for the C2 and T2 mixes, again with the 20% mixes excluded for clarity. The initial deceleration prior to the dormant period is once again slowed in the T2 mix, and the dormant period is prolonged. Compared to the T1 mix however, the trough of the dormant period isn't as delayed, with the 10% mix having a dormant period occurring at 2h04 compared to 2h15 for T1, 2h21 compared to 2h34 hours at 20% and 3h30 compared to 3h47 at 40% replacement. Although these differences are small, all mixes were made at the same time, and so these small differences can be attributed to the difference in carbonate content.

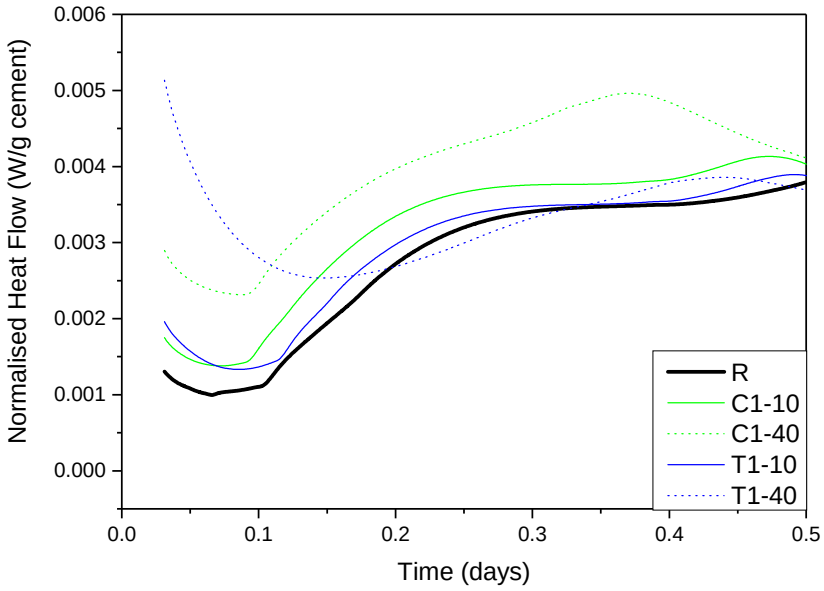

Figure 6.2.2: Heat flow, showing induction period, for C2 and T2 mixes upto 12 hours, normalised per gram of cement

As the T1 and T2 mixes are derived from the same initial ground material as the C1 and C2 mixes respectively, the calcite content is the only difference between the two mixes, and its effect on the dormant period was investigated. Using the calorimetry mix design,

C1-40 and T1-40 mixes were cast, and the pH of the pore solutions monitored over the first day of hydration, in a set up discussed in section 3.2.9. A small head of water was placed above the sample to ensure the probe was surrounded with liquid and the readings were accurate and comparable. While this would dilute any ions in solution, with pH being a log10 scale, any changes would still be readily identified using a probe accurate to two decimal places.

With the pH over time known for the R, C1-40 and T1-40 mixes it was possible to compare the pH with hydration over time. In fig. 6.2.4, the heat flow, from isothermal calorimetry is shown against pH, for the R, C1-40 and T1-40 mixes, within the first 24 hours of hydration. It is immediately clear that the ternary mix, T1-40, shows a substantially reduced pH at early ages compared to the C1-40 and R mixes.

In neat OPC systems, following initial mixing, calcium and hydroxyl ions dissolve into the pore solution, quickly raising the pH to above 12.5[165]. Within blended systems, the pH increase is slower, due to the slower dissolution of alkaline ions out of the glassy phases of PFA or GGBS[166], ending with a reduced, but still high pH, typically in the order of 11-12.5. The pH of the R mix follows this trend, with pH relatively quickly reaching 12.5, and a steady increase, as further alkaline ions dissolve out of the GGBS, upto a pH of 13.0 after 1 day. Within the C1-40 mix, the same fast initial rise in pH is observed, before the pH levels out at above 12.7 after 0.4 days. With significantly lower levels of binder, both cement and slag, the lower eventual pH may be explained. Within the T1-40 mix however, the significantly lower pH can be partially explained by the lack of portlandite in the carbonated CEM I ground concrete (T1 mix) compared to that of the non-carbonated ground CEM I concrete (C1 mix). Table 6.4 shows the pH levels of the mixes at different stages.

With both the C1 and T1 fractions coming from the same original material, the only difference between the two materials is the accelerated carbonation experienced by the T1 fraction, resulting in a significant increase in calcite content, and a reduction in the Ca/Si ratio of the C-(A)-S-H, resulting in a largely decalcified C-(A)-S-H, or an amorphous silica gel. As such, the significant difference in pH level can be being driven the increased

Table 6.4: pH values of mixes at different stages of initial mixing/hydration

System	**pH**
Neat OPC (1 hour)	>12.5
Ref mix (1 hour)	12.4
Ref mix (24 hours)	13.0
C1-40 (1 hour)	12.5
C1-40 (24 hours)	12.7
T1-40 (1 hour)	12.1
T1-40 (24 hours)	12.6

presence of calcium carbonate, and the absorption of alkali metals on the decalcified C-(A)-S-H, buffering the pH low. The C1 fraction, from thermal analysis, was shown to have 23.6% calcite content, compared to the 44.5% of the T1 fraction. With the T1 fraction having been carbonated post grinding however, the calcium carbonate formed is likely to be on the surface of the ground particles, and so readily in contact with the pore solution in which it will slowly diffuse, slightly buffering the pH with the help of the absorption of alkali metals onto the decalcified C-(A)-S-H. As well as the presence of calcium carbonate, from thermal analysis (chapter 4), the T1 fraction has significantly less (4.3wt%) portlandite compared to that of the C1 fraction (5.8wt%), providing less ions to raise the pH, compared to both the reference mix and the C1 mix.

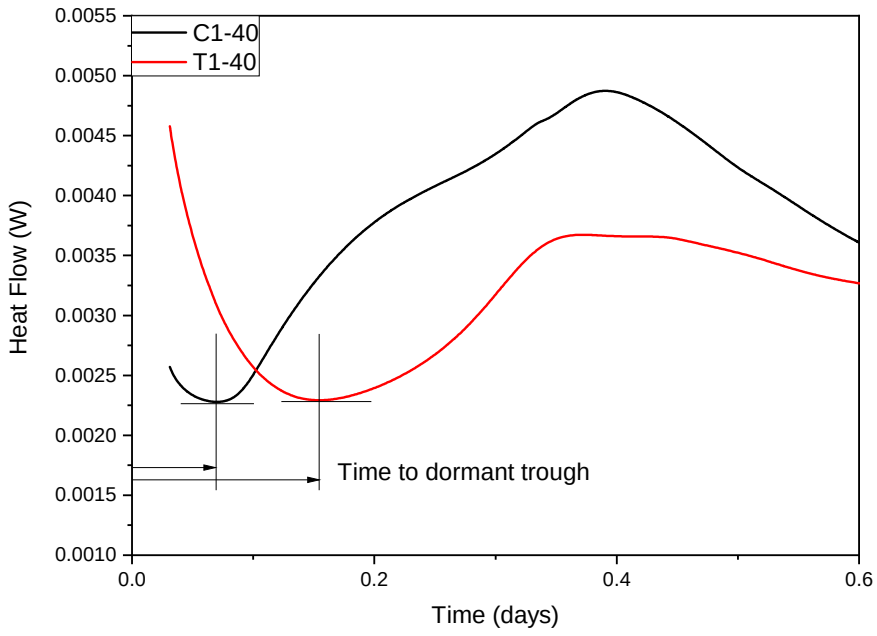

Figure 6.2.3: Heat flow curves for C1 and T1 40% replacement mixes, showing the methodology behind the time of the dormant/induction trough calculations

To investigate the effect of the dilution and pH buffering on the dormant/induction period,

the time of the trough of each dormant period was compared to the calcite content of the ternary blends, as shown in fig. 6.2.5. Figure 6.2.3 shows a sketch of the time taken to the dormant trough for the C1-40 and T1-40 mixes. The R^2 value for the data, of 0.968, shows a strong correlation between the calcite content and delay/extension of the dormant period.

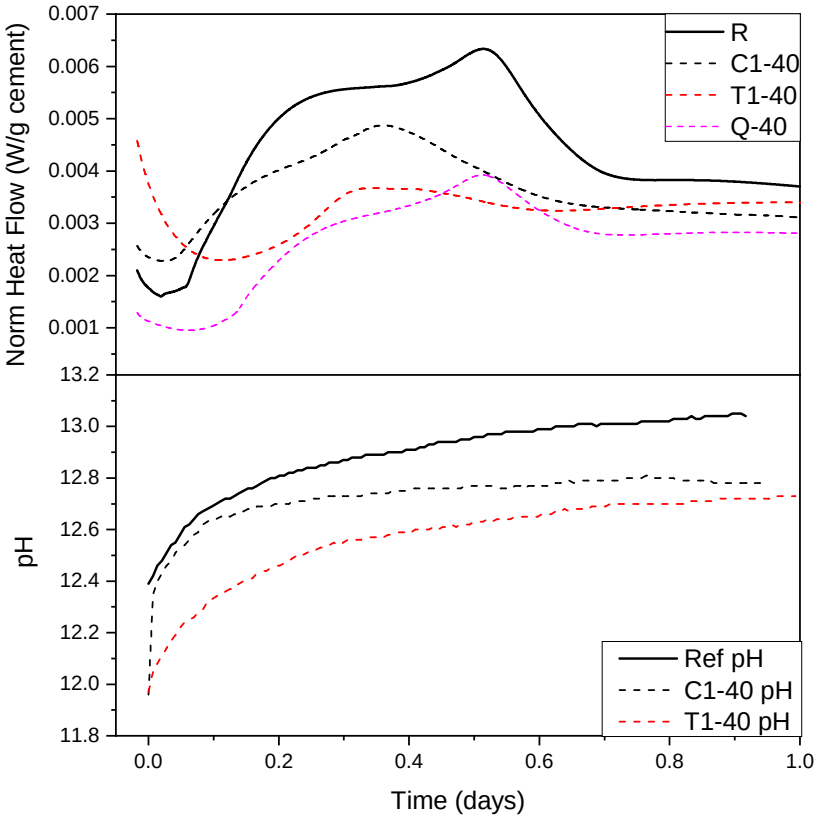

Figure 6.2.4: Heat flow, and pH, for R, C1-40 and T1-40 mixes within the first 24 hours of hydration, with heat flow for the Q-40 mix also shown

Previous studies of ternary systems have found calcite, in the form of limestone, to be either an inert filler [73,74], or to accelerate the early hydration reactions [75,76]. Nuclear encapsulation grouts however, with their unusually high GGBS:OPC ratio, differ from most normal mixes, and with the cement content, particularly at 40% replacement being low, the effect of the dilution and alkali absorption buffering the pH low is even greater, causing this delay and extension of the dormant period.

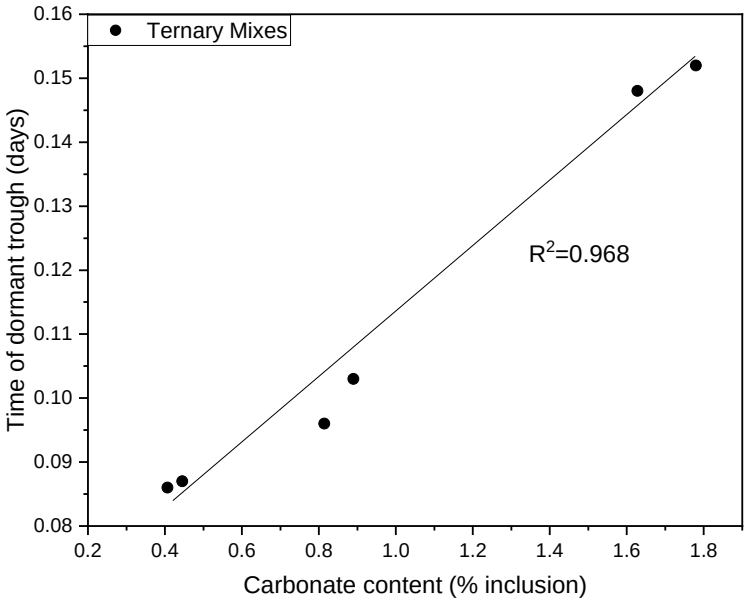

Figure 6.2.5: Time of dormant trough against carbonate content, for ternary mixes

6.2.2 Accelerated Aluminate Hydration

The hydration of the aluminate phase in blended GGBS:OPC mixes is well documented[33,47], and appears as a defined peak in heat flow plots, seen in fig. 6.2.6, where the aluminate peak has been labelled as A. Compared to the slow hydration of neat slag, the hydration of the aluminate peak is greatly accelerated when mixed with cement.

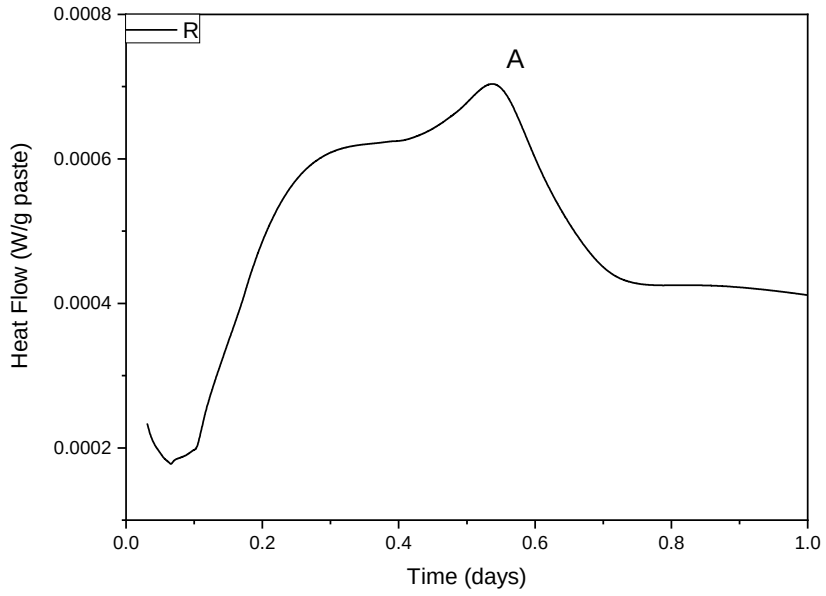

Figure 6.2.6: Heat flow curve for reference mix, with aluminate peak identified with A, normalised per gram of paste

When the heat flow of each sample is examined, and the T mixes compared to the C mixes, it is clear that the ternary mixes display a delayed peak of aluminate hydration. This can be seen in fig. 6.2.7, where the aluminate peak of the C1-20 and T1-20 mixes has been identified and the timing of the peak given, and the small delay in the T1 mix is clear. For all ternary mixes, the aluminate peak was delayed compared to that of the C1 and C2 mixes, initially suggesting that the influence of the calcite was delaying the aluminate hydration, which disagrees with the literature on ternary blended cements.

When compared to both the reference and the quartz mix however, it became clear that the aluminate peak in all the C and T mixes is accelerated. Figure 6.2.8 shows the R and Q mixes, where the aluminate peak can be seen occurring between 12.5 to 13 hours, significantly later than the 10.5 and 11 hours shown in the C1 and T1-20 mixes.

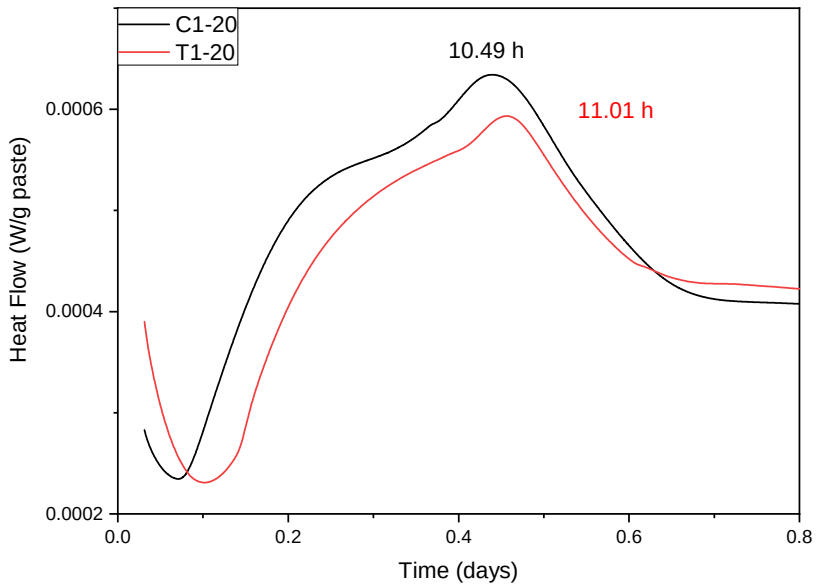

Figure 6.2.7: Heat flow curves for C1-20 and T1-20 mixes within the first day of hydration, with the time of the aluminate peaks shown, normalised per gram of paste

Instead, to further understand the influence of carbonated fines on the rate of hydration, the dormant/induction period must be taken into account. It has already been found, as described in section 6.2.1.1, that the carbonated scabblings have the effect of not only delaying, but also increasing the length of the dormant period. As such, rather than investigating the absolute time of the aluminate hydration, the time of the peak relative to that of the induction period was investigated.

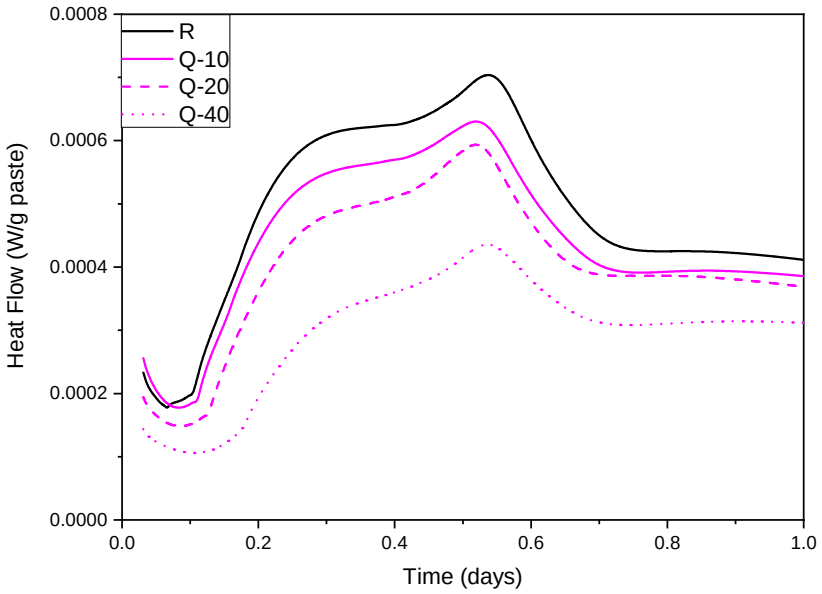

Figure 6.2.8: Heat flow curve for R and Q mixes within the first day of hydration, showing a similar aluminate peak, normalised per gram of paste

When the time between the trough of the dormant/induction period was investigated, for the ternary mixes, at 10% inclusion the C and T mixes show very similar times, with non-carbonated material having a slightly shorter time between the dormant trough and aluminate peak than that of the carbonated mixes. As seen in table 6.5, at 20 and 40% inclusion the carbonated mixes are showing significantly shorter times between the dormant trough and aluminate peak, suggesting accelerated hydration, in line with the literature. In fig. 6.2.9, the time between the dormant trough and the aluminate peak has been plotted against the carbonate content, as % replacement, with the linear fit and correlation also shown. With an R^2 value of 0.90, there exists a strong correlation between the carbonate content and accelerated hydration. The values for the quartz mixes are also plotted, in order to examine the difference between any filler and dilution effect caused by an inert filler. While the initial increased dormant/induction period of the ternary mixes is likely to be a dilution effect and absorption of alkali metals by the decalcified C-(A)-S-H, the accelerated aluminate hydration is clearly different from that of the quartz mix, suggesting further reactions taking place, in line with the literature.

In fig. 6.2.10, the time between the dormant trough and aluminate peak has been plotted against carbonate content for all samples. The correlation between samples isn't as strong

(R^2 of 0.80) as with solely the ternary samples, as the mass carbonate content calculated by thermal analysis, particularly for the C2 mix containing PFA (present from the grinding of the original CEM II concrete), may not be solely related to the de-carbonation of calcium carbonate, skewing the data and producing a poorer correlation, but it is sufficient to further suggest that the presence of calcite is accelerating early age hydration, when compared to the filler effect of an inert powder as with the quartz samples. Added to this is the variation in calcite content, with the non-carbonated samples having significantly higher calcite contents, with an inverse correlation between calcite and carbonate content. As both these processes will affect the aluminate activation, a single trend isn't likely to encompass both these processes.

Table 6.5: Times of dormant trough and aluminate peak for all samples

Sample	Carbonate Content (% inclusion)	Dormant Trough (hours)	Aluminate Peak (hours)	Difference (hours)
C1-10	2.36	1.85	11.57	9.72
C2-10	2.96	1.68	11.38	9.70
T1-10	4.45	2.09	11.98	9.89
T2-10	4.07	2.06	11.83	9.77
C1-20	4.72	1.70	10.66	8.95
C2-20	5.92	1.68	10.13	8.45
T1-20	8.9	2.47	10.99	8.52
T2-20	8.14	2.30	10.44	8.14
C1-40	9.44	1.70	9.31	7.61
C2-40	11.84	2.04	8.90	6.86
T1-40	17.8	3.65	10.56	6.91
T2-40	16.28	3.55	10.54	6.98
Q-10	0	2.06	12.40	10.34
Q-20	0	2.20	12.70	10.50
Q-40	0	2.61	12.72	10.12

6.2.3 Degree of Hydration

Through a number of techniques, the total hydration at early ages can be examined. Cumulative heat of hydration from isothermal calorimetry, bound water content from thermal analysis, and strength testing can be used to determine the degree of hydration over time. As shown previously, the ternary blended systems, containing carbonated scabblings, show different hydration rates and characteristics compared to systems containing non-carbonated scabblings. Figure 6.2.1 and fig. 6.2.2, shown previously, showed

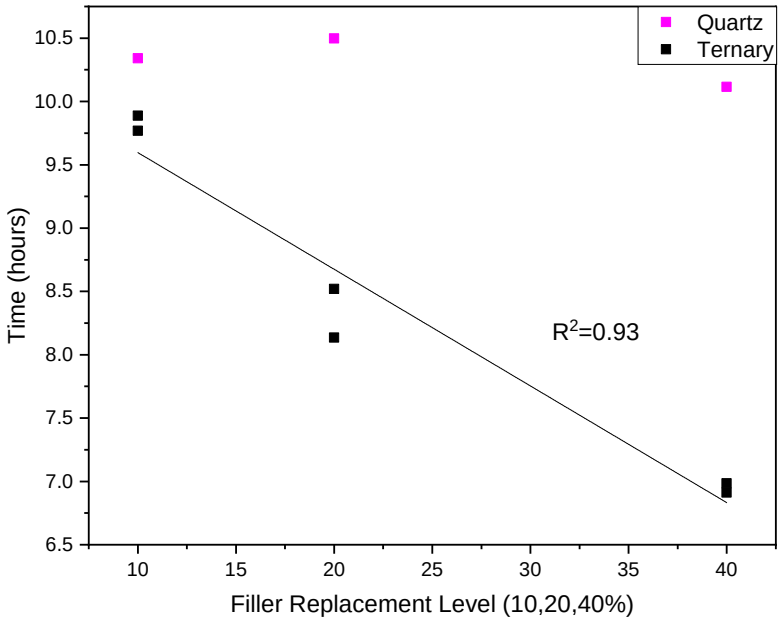

Figure 6.2.9: Time between dormant trough and aluminate peak (showing onset of the acceleration period), vs carbonate content, for ternary and quartz mixes at 10, 20 and 40% replacement, with ternary correlation shown

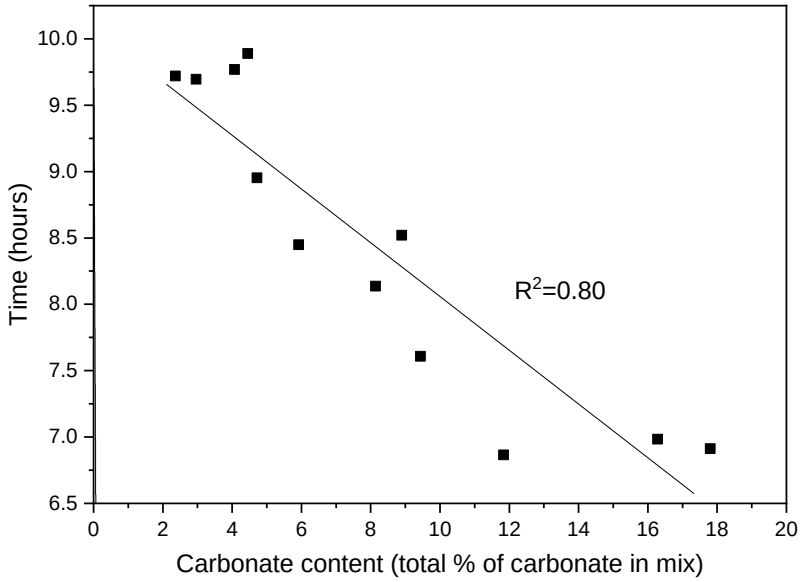

Figure 6.2.10: Time between dormant trough and aluminate peak (showing onset of the acceleration period), vs carbonate content, for all mixes at 10, 20 and 40% replacement, with correlation shown

an increased dormant period and a change in the timing of the aluminate hydration peak in the T1 and T2 mixes compared to C1 and C2. Also, while the overall profiles of the hydration curves remained similar, it was noticeable that within the ternary blended systems, the total heat of hydration wasn't as high as that in the C1 and C2 systems. This was most obvious within the 40% replacement mixes, where the maximum heights

of the alite and aluminate peaks were significantly different. The significantly lower heat flow values suggest that the dilution was affecting the overall total hydration at early ages.

In fig. 6.2.11, the cumulative heat of hydration for the C1 and T1 mixes is shown within the first 3 days of hydration. In all T1 mixes, the cumulative heat is below that of the C1 mixes for at least the first 24 hours, before the curves cross, and by 3 days of hydration, the T1 mixes are all showing greater total heat of hydration than the C1 mixes. In fig. 6.2.12, the same curves are shown for the C2 and T2 mixes, with a similar trend showing, although the difference isn't as pronounced, particularly in the 10 and 20% mixes.

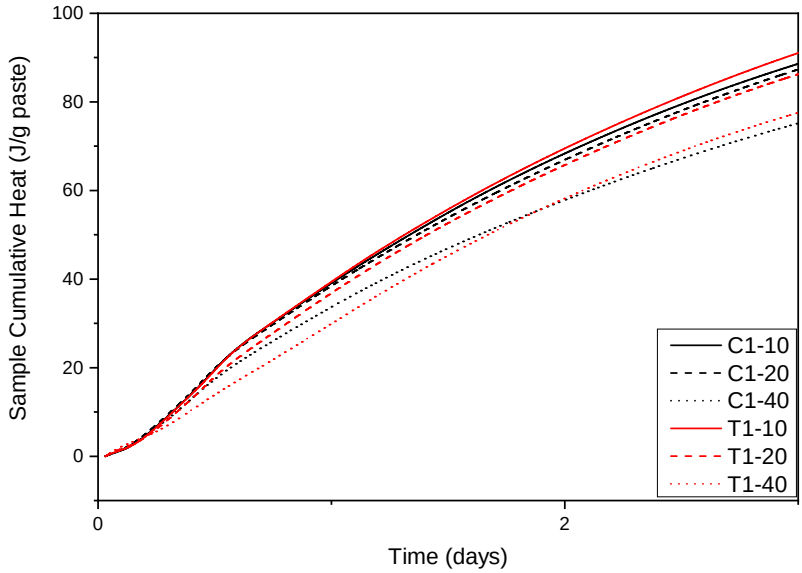

Figure 6.2.11: Heat of hydration, during first 3 days of hydration, for C1 and T1 mixes, normalised per gram of paste

With the 40% mixes showing the largest difference in total hydration, and the T1 showing a larger difference than the T2 mixes, it is clear that calcite content is affecting the early age hydration, producing lower total hydration within the first 24 or 48 hours of hydration, but showing increased hydration after this period.

6.3 Long Term Hydration

Strength testing provided information on the ongoing hydration of the grouts. In fig. 6.3.1, the 1, 7, 28 and 90 day mean failure stresses, and standard deviation, are shown for the

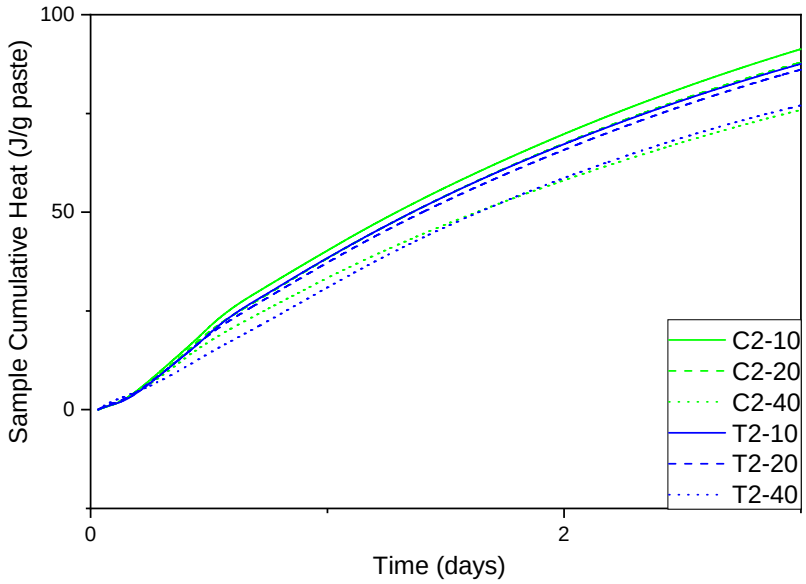

Figure 6.2.12: Heat of hydration, during first 3 days, for C2 and T2 mixes, normalised per gram of paste

C1 and T1 mixes, as well as bound water content from thermal analysis. For the T1 20 and 40% mixes, there is a significant difference in failure stress at 7 and 28 days, while at 90 days, the failure stresses are within the standard deviation of the C1 mixes. The T1-10 and C1-10 mixes both show comparable strength and bound water content, suggesting little difference in overall long term hydration.

When the C2 and T2 mixes were compared, a similar trend was observed, with the T2 mixes having higher 1 and 7 days strength than the C2 mix, before achieving a similar failure stress to the C2 mixes at 90 days, with only the 40% replacement mixes not falling within the standard deviation of the opposite mix. Figure 6.3.2 shows the failure stress and bound water plots for the C2 and T2 systems.

In both the ternary T1 and T2 mixes, when bound water content is used to investigate degree of hydration, the bound water content is comparable, or grater than that of the non-carbonated C1 and C2 mixes. At 90 days however, although the differences are small, and there is scatter within the data, the ternary mixes show consistently lower bound water content than the C1 and C2 mixes, yet comparable strength and engineering properties. This can be related to the formation of carboaluminates, discussed in section 6.4.3.

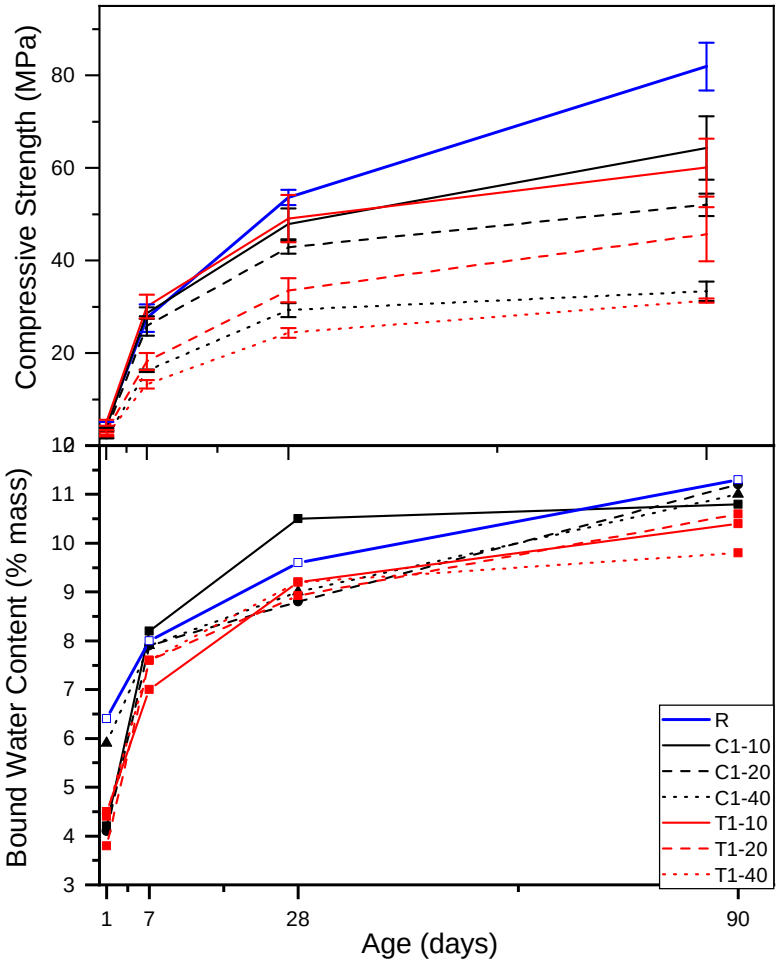

Figure 6.3.1: Mean failure stress, with standard deviation shown, at 1, 7, 28 and 90 days, for the C1 and T1 mixes

6.4 Microstructure and Engineering properties

With the hydration of the ternary mixes found to be different than that of the binary mixes, the effect this change in hydration has on the microstructure of the samples was investigated. As with the C1 and C2 samples, permeability and sorptivity testing was used, with samples cast and tested in duplicate.

6.4.1 Permeability

Figure 6.4.1 shows the calculated intrinsic permeability, at 1.5 bar, for the T1 and C1 mixes at 28 days, with the T1 mixes having significantly lower intrinsic permeability than the C1 samples. Although the 20% mix shows much closer values than the 10 or 40% mix,

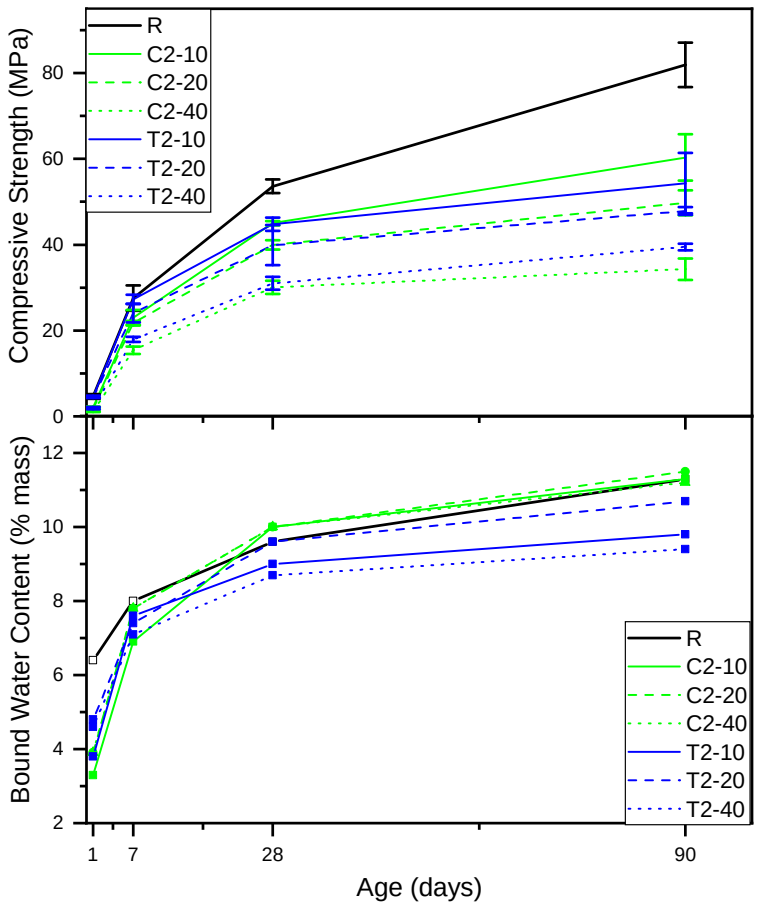

Figure 6.3.2: Mean failure stress, with standard deviation shown, at 1, 7, 28 and 90 days, for the C2 and T2 mixes

the overall trend of lower permeability values compared to the C1 mix is clear, and with the 10 and 40% mixes showing distinctly lower permeability than the C1 mix, there is a clear improvement in permeability performance when T1 is used over C1.

In fig. 6.4.2 the calculated intrinsic permeability, at 1.5bar, for the T2 and C2 mixes at 28 days is shown. Once again, as with the T1 mix, the T2 mix shows significantly improved permeability compared to the C2 mix, with a similar largely linear relationship between replacement level and permeability.

Of particular interest, is that in both ternary mixes, the 10% inclusion mix shows a reduced permeability, not just compared to the C1 and C2 mixes, but also to the reference mix with no inclusion.

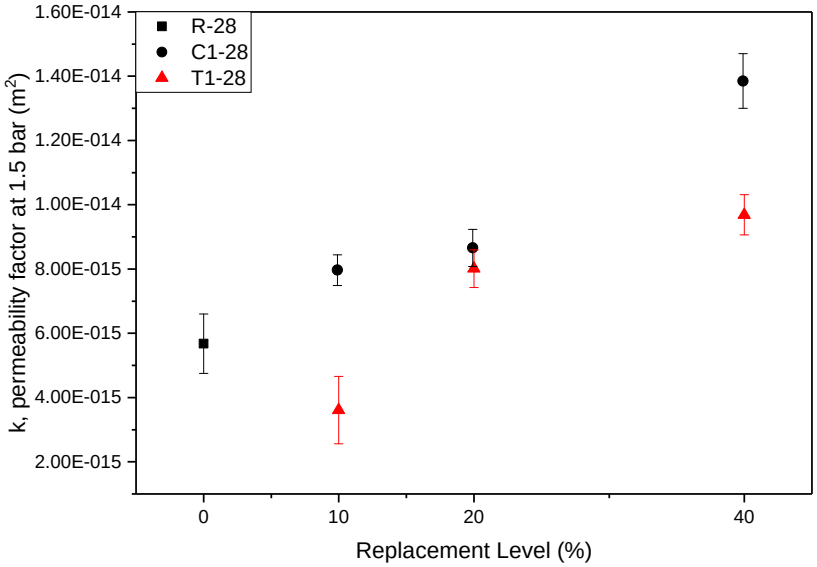

Figure 6.4.1: Intrinsic permeability, calculated at 1.5bar, for C1 and T1 mixes 28 day samples

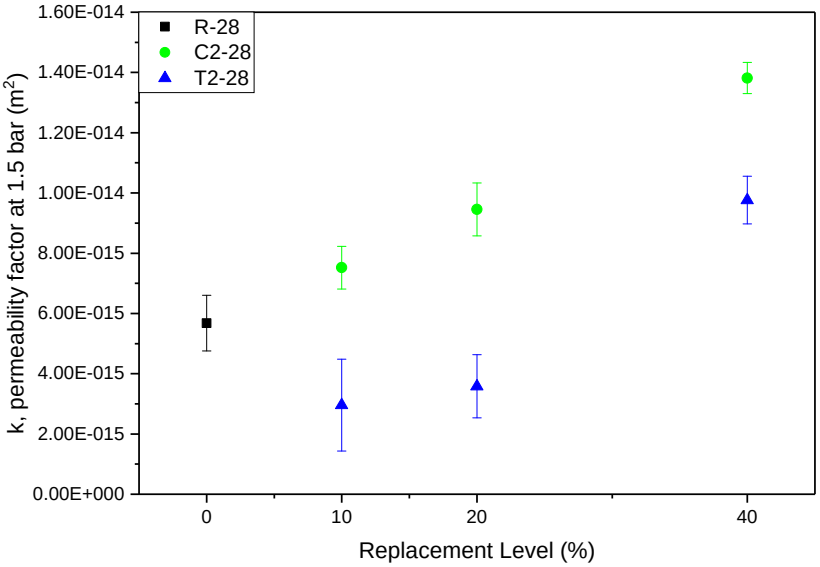

Figure 6.4.2: Intrinsic permeability, calculated at 1.5bar, for C2 and T2 mixes 28 day samples

By 90 days, the non-carbonated samples were found to have intrinsic permeability values closer to that of the ternary mixes, with the 40% inclusion mixes for T1 and T2 now both showing a higher permeability than that of the C1 and C2 mixes. As seen in fig. 6.4.3, and fig. 6.4.4, the permeability of the mixes at 20% show very similar values, but again at 10% inclusion, the ternary mixes show lower permeability than their non-carbonated counterparts. As well as being below their C1 and C2 counterpart mixes, the ternary samples once again show a lower permeability than the reference mix at 90 days.

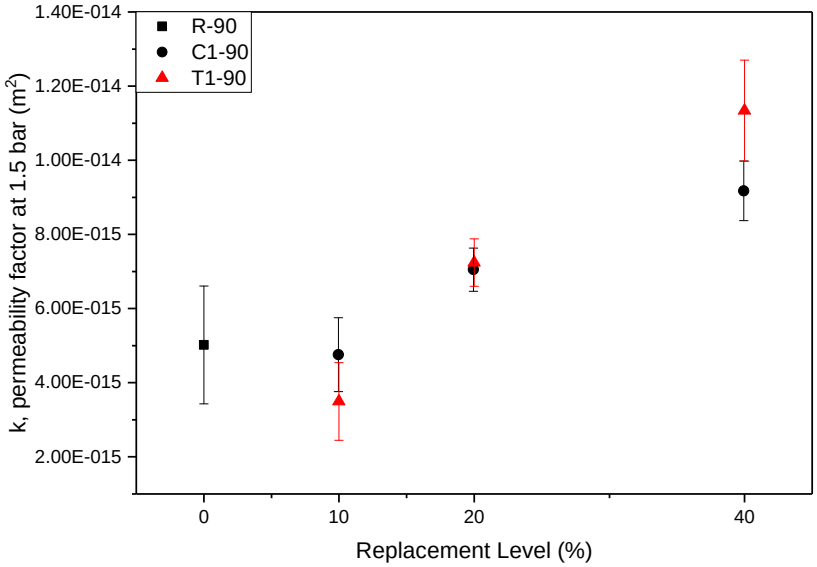

Figure 6.4.3: Intrinsic permeability, calculated at 1.5bar, for C1 and T1 mixes 90 day samples

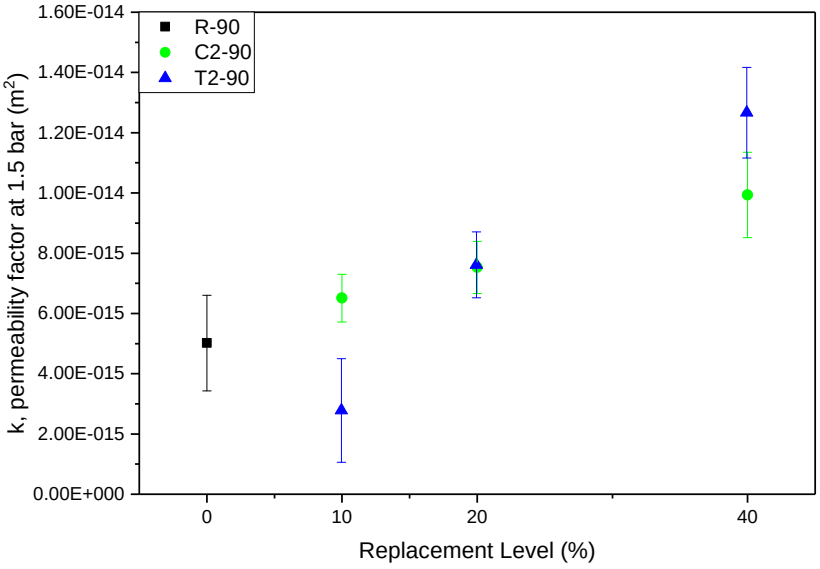

Figure 6.4.4: Intrinsic permeability, calculated at 1.5bar, for C2 and T2 mixes 90 day samples

A reduction in grout permeability through the inclusion of calcite in the ternary blend is a significant finding. As discussed in section 2.5, favourable properties for encapsulation grouts include low permeability, as this reduces the pathways for groundwater ingress into the conditioned waste packages and subsequent leaching of radionuclides.

6.4.2 Sorptivity

Once samples had been used for permeability testing, they were then tested for sorptivity, to investigate the degree to which water was absorbed into the samples through capillary action. In fig. 6.4.5, the sorptivity plots for T1-10 and T2-10 samples are compared to the reference at 90 days. At this replacement level, the ternary mixes, with sorptivity coefficients of 0.00536 for the T1-10 mix and 0.00581 for the T2-10 mix, are below that of the reference mix, which has a sorptivity coefficient of 0.00697.

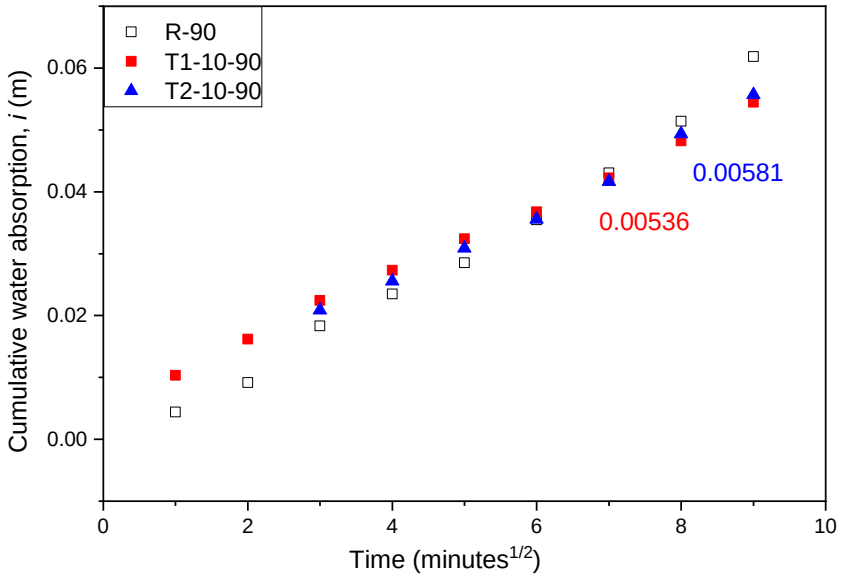

Figure 6.4.5: Sorptivity data for R, T1-10 and T2-10 samples at 90 days

Within permeability testing, at 90 days the 10% replacement mixes for the ternary samples were also below that of the reference mix, agreeing with the sorptivity data. Figure 6.4.6 shows the ternary samples compared to the C1 and C2 samples, also at 10% replacement and 90 day samples. While the overall values are close, it is clear that the ternary samples show lower sorptivity than the non-carbonated samples.

At replacement levels higher than 10%, the ternary mixes start to show a larger increase in sorptivity compared to the C1 and C2 mixes, and with a significant increase compared to the 10% inclusion mixes, as with the permeability results. Figure 6.4.7 shows the sorptivity data for the C1 and T1 mixes at 90 days, where the T1-20 and T1-40 mixes are showing sorptivity values two to three times that of the equivalent C1 mixes. The same

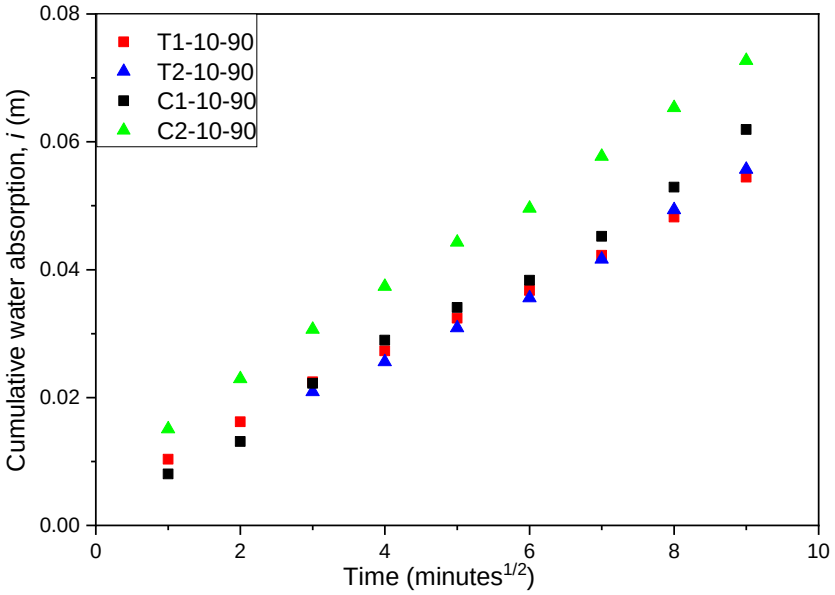

Figure 6.4.6: Sorptivity data for all 10% replacement samples at 90 days

trend is seen in the T2 and C2 mixes, with the ternary mixes at 20 and 40% replacement showing significantly higher sorptivity that that of the C2 mix.

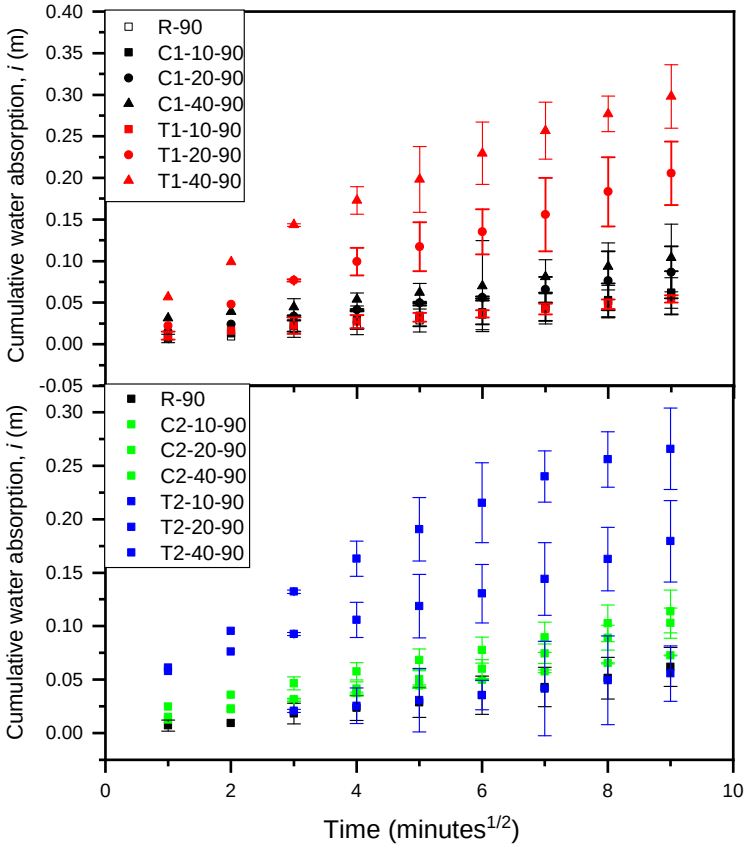

Figure 6.4.7: Sorptivity data for all 10% replacement samples at 90 days

Overall, it has been shown that at 10% replacement levels, the T1 and T2 ternary mixes outperform not only the equivalent C1 and C2 mixes, but also the reference mix, suggesting that at 10% replacement, the use of carbonated scabblings, or the presence of calcium carbonate, can improve the longer term engineering properties.

6.4.3 Formation of Carboaluminates

X-ray Diffraction has been used to examine the phases present in the samples over the course of hydration, in order to further investigate changes to the hydration and engineering properties. Figure 6.4.8 shows the XRD patterns, for the C1 and T1 mixes, over the 8-30 2θ degree range. Quartz, portlandite, ettringite, calcium monosulphate, calcium hemi-carboaluminate and calcium mono-carboalumite phases are identified.

Through examining the changes in intensity for the phases, the hydration mechanism can be determined. The quartz peaks in all samples remain relatively constant, as a result of the aggregate inclusion in the ground material. Portlandite content was maximum at 28 days, while at 90 days the level had dropped due to continued consumption for slag hydration.

After 1 day of hydration, the ettringite content in both mixes was similar, while the peaks for monosulphate (Ms), hemi-carboaluminate (Hc) and mono-carboaluminate (Mc) were hardly discernible. As hydration continued however, the C1-10, binary, mix showed increasing amounts of monosulphate, known to form from ettringite[168]. Some hemi- and mono-carboaluminates were also formed from the C1 mix - the presence of carbonate in the synthesised material means this was expected - as well as monosulphate. In the ternary, T1, blend, there was no monosulphate present, while the ettringite, and both carboaluminate phases had higher intensity peaks that the C1 mix.

De Weerdt et al. investigated the synergy between fly ash and limestone powder in a ternary blend with OPC, and found that the presence of calcium carbonate, from the limestone, caused the formation of hemi- and mono-carboaluminates as opposed to monosulphate, stabilising the ettringite and leading to increased volume of hydration products,

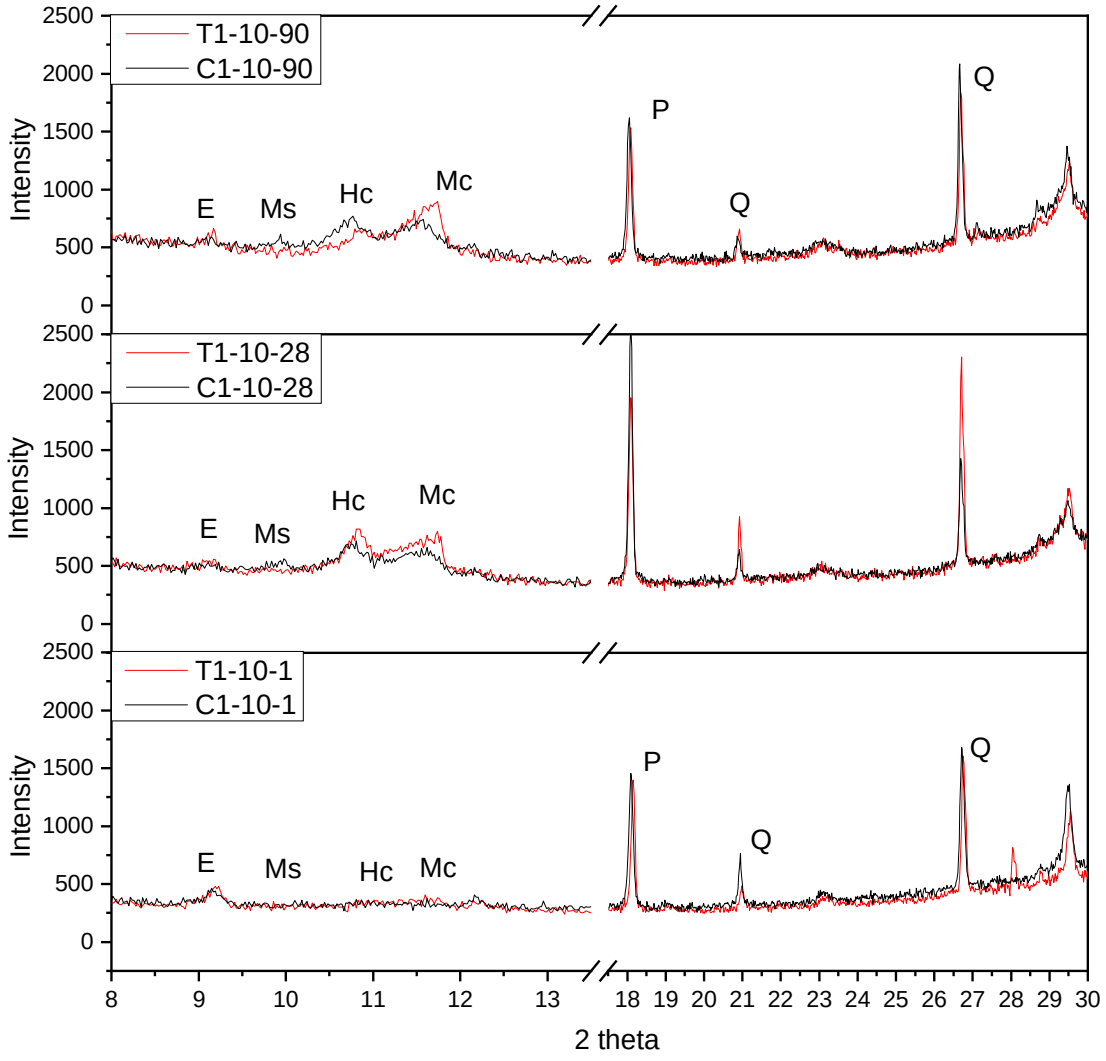

Figure 6.4.8: XRD patterns, over 8-30 2θ degrees, at 1, 28 and 90 days, for C1-10 and T1-10 mixes. Where Q=quartz (COD 1011097), P=portlandite (COD 1001787) , E=ettringite (trace, COD 9011103), Ms=calcium monosulphate (trace), Hc=calcium hemi-carboaluminate, Mc=calcium mono-carboaluminate. Carbonate positions taken from Ipavec at al.[167] (using PDF 000-41-0221 for hemi-carboaluminate peak fitting)

and thus reduced porosity and permeability[164]. Ghrici et al. also found improved durability at later ages in ternary limestone-fly ash mortars[86]. Adu-Amankwah et al. investigated the formation of carboaluminates in ternary slag-limestone cements, and found that while the effect of carboaluminate formation and ettringite stabilisation wasn't as prevalent as limestone-PFA ternary mixes, the same process was observed.

The formation of carboaluminates, and subsequent stabilisation of ettringite in the ternary blends therefore helps to explain the reduction in permeability and sorptivity in the T1-10 mix, particularly at later ages, compared to both the C1-10 mix and reference sample.

Overall, the inclusion of calcium carbonate from carbonated scabblings can have a beneficial impact on the engineering performance of encapsulation grouts, at lower levels of replacement.

6.5 Conclusions

The effect of carbonated scabblings on the performance of encapsulation grouts has been examined, and their performance compared to that of a reference mix containing no scabblings, and also to mixes where non-carbonated scabblings have been used at the same replacement level. The investigation has been split into two main sections, investigating the effect of the scabblings on the hydration process, and on the microstructure and engineering properties.

During early ages of hydration, the influence of the carbonated scabblings leads to a delayed, and extended, dormant/induction period. When the pH of the T1-40% mix was compared to that of the C1-40 and R mix, it was found to be diluted lower than the other mixes for a significant period of time, with both the R and C1-40 mix reaching a pH >12.5 within the first hour after mixing. The T1-40 mix however, doesn't reach a pH of 12.5 until over 5.5 hours after mixing. With calcium carbonate having a pH of ∼9.9 in solution, it is likely the presence of this diluting the pH low, while the decalcified C-(A)-S-H is absorbing sme of the alkali metals that would otherwise raise the pH. With the cement content in these systems being low, particularly at 40% replacement, the remaining active material at early ages isn't sufficient to raise the pH higher and activate hydration, thus the dormant period last significantly longer in the ternary mixes. The correlation between the time of the dormant trough and carbonate content is strong, and supports this conclusion.

The timing of the aluminate peak from hydration has been investigated. Initially, a delayed aluminate peak was found, with a strong correlation to calcite content. This runs contrary to other findings in literature. When the time between the dormant trough and aluminate peak was investigated, it was found that the presence of calcite accelerated the aluminate hydration. While the aluminate hydration is accelerated, the total hydra-

tion of the ternary mixes, within the first days of hydration, is below that of the mixes with non-carbonated scabblings. Failure stresses show slightly reduced strength of ternary blends at 28 days compared to the binary mixes, but at 90 days there failure loads of the ternary mixes were comparable to that of the binary mixes, while bound water content, from thermal analysis, shows similar degrees of hydration.

When the effect of carbonated scabblings on the engineering performance and properties of the grouts was investigated, it was found that at 10% replacement levels, the ternary mixes showed improved permeability and sorptivity characteristics, not only compared to that of the non-carbonated equivalent mixes, but also compared to the reference mix, suggesting that the presence of carbonated scabblings, or calcium carbonate, can help improve the overall long term engineering properties, reducing permeability and sorptivity. At 20 and 40% replacement however, there is a significant increase in permeability and sorptivity, above that of the samples with non-carbonated scabblings and the reference mix.

XRD was used to investigate the phase assemblage over the hydration period. In the ternary mixes, the formation of hemi- and mono-carboaluminates, and subsequent stabilisation of ettringite, lead to an increased volume of hydration products compared to both the non-carbonated mixes. The increased volume of hydration products explains the increase in engineering performance of the ternary 10% inclusion mixes, compared to their binary equivalent mixes and also the reference mix, through the reduction in pore volume and thus permeability.

At replacement levels of 10%, the hydration of the grout is not negatively affected, with a slight delay and extension of the dormant period, which may even improve the setting time of the mix, providing a longer period before initial setting. The engineering properties of the grouts have shown to be improved with the inclusion of 10% of carbonated scabblings, while above 10% replacement, the properties begin to be significantly detrimentally affected. Overall, it has been shown that using scabblings at upto 10% inclusion will improve the waste to volume container ratio, and not detrimentally affect the properties of an encapsulation grout.

Part III

Laser-Induced Breakdown Spectroscopy for Radiological Contamination in Concrete

Chapter 7

Laser-Induced Breakdown Spectroscopy for Radiological Contamination in Concrete

7.1 Laser-Induced Breakdown Spectroscopy

7.1.1 History

While the production of sparks in air by a pulse ruby-laser beam was observed in 1963[169], it wasn't until the spectroscopic investigations of Cremer and Radziemski at Los Alamos National Laboratory in 1983[170] that the use of spark emission for elemental analysis was possible, and the term Laser-Induced Breakdown Spectroscopy was formed. In the following decades as both laser and detection technologies developed and improved, the use of LIBS became more widespread and in a number of different fields. Compared to techniques such as X-ray diffraction and electron microscopy however, it is still a relatively new and developing analytical technique.

7.1.2 Theory

Upon contact between a high-power laser pulse and the surface of a material, the irradiation at the small focal point of the laser results in material removal (*ablation phenomenon*[171]). Rapid material removal results in a number of phenomena including rapid

local heating, melting and evaporation. The evaporated material, and the high temperatures involved, lead to the creation of a plasma above the sample surface[172]. Light spectroscopy can then be carried out on the resultant plasma, and an elemental breakdown of the material can be gathered[173].

7.1.3 Application

The real-time data production and analysis ability of LIBS makes it an attractive analysis technique when an elemental breakdown of a material is required, but other aspects such as phase composition and microstructure are not. One such case is in contamination detection in concrete, particularly in terms of nuclear decommissioning, where the presence of radionuclides determines the waste classification of the material.

7.2 Contamination Detection

7.2.1 Research Basis

As described in section 2.4.2.2, laser scabbling as a method for removal of contaminated concrete has been researched, with promising results[117]. Within this method, high powered, remotely operated lasers would be in use, and so the possibility of using LIBS in conjunction with this method is to be explored. Through the use of LIBS to monitor the contamination levels, during laser - or any other physical removal technique - scabbling, the contamination levels could be monitored with depth of material removed. Through this monitoring, the overall volume of contaminated scabbled material could be reduced by minimising the amount uncontaminated material that is removed along with contaminated material.

7.2.2 Equipment

The hardware used in this investigation is an Applied Photonics LIBS 6 machine, with a Quantel Q-Smart 450 Nd:YAG laser, and the spectrometer used for this work covered 312-417nm, with 2 other spectrometers available, with the 250-500nm range being covered. Samples were placed and moved within a SC-2L modular sample chamber, capable of

movement along x, y and z axes. The software used to control both the laser and sample chamber was LIBSoft V16. Automated sample movement and multiple point testing can be used.

7.2.3 Experimental Details

7.2.3.1 Materials

Simulant radionuclide salts were cast into ordinary portland cement (OPC) paste samples at 0.1 weight %. The simulants used and the resultant weight percentage of radionuclide were nickel chloride ($NiCl_2$, 0.045 wt% Ni) and cobalt sulphate ($CoSO_4.7H_2O$, 0.021 wt% Co). Cement paste was used as opposed to mortar or concrete, as there has been found to be orders of magnitude difference in the concentration of radionuclides within cement paste as opposed to aggregates[114].

The solid contaminant salts were weighed out and dissolved within the required amount of deionised water for each mix, with an ultrasonic bath used to ensure full dissolution. CEM I 52.5 N ordinary Portland cement powder was added to a 9g mix design with a water to cement ratio (w/c) of 0.5, and the samples were mixed using hand shaking for 1 minute, followed by 2 minutes on a vibrating machine to ensure full mixing. Following curing for longer than 28 days (values vary, as phase composition will have no effect on elemental breakdown results), the samples were analysed, together with an uncontaminated reference mix against which peaks could be compared.

7.2.3.2 Methodology

Following curing, silicon carbide paper was used to remove the outer layer of each sample, to ensure the bulk material was being examined. Spectra were obtained in triplicate in order to obtain a representative analysis for each sample. 100 conditioning shots were used for each point, in order to remove any surface contamination due to sample storage or handling. Laser energy was the maximum of 395mJ, with 100 accumulations per spot at 20Hz.

7.2.3.3 Analytical Technique

Following data accumulation, mean intensities were calculated for each sample, from the three spots analysed. The intensities were then normalised; Spectra were normalised against a peak found to be present in both the reference and doped samples. The most intense peaks for the key elements present in cement (Ca, Si, Al, Fe) were excluded because they swamped the detector. However, the Cu peak at 334.893 nm was found to be suitable, being sufficiently discernible above the baseline and being present in all samples.

Normalised peaks for each contaminated sample were then compared with the reference cement sample, and a ratio of peak heights, r, was calculated, by dividing the normalised sample peak height by that of the reference. In an ideal situation the r value for two identical samples would be 1 at all wavelengths. If an additional element (contaminant) is present in the contaminated sample, or an element is found at greater concentrations the value of r would be greater than one at that wavelength. To accentuate differences in peak ratios, this was then multiplied to the fourth power (r^4), and so differences between peak ratios will be visible when plotted, and can be compared to the NIST spectral database[174].

7.2.4 Results and Discussion

By using the maximum laser intensity of 395 mJ, saturation of some peaks occurred, which shows where the major peaks all have a maximum at around 6.5 x10^6. This is shown in fig. 7.2.1, as is the Cu peak at 334.893nm against which other peaks were normalised.

Following normalisation, and the calculation of r and subsequent r^4 values, a comparison of this data with the sample and reference spectra was carried out, as shown in fig. 7.2.2 and fig. 7.2.3. The intensity of the peaks being compared can be seen at around 100,000 counts for both, compared to the 6.5 x10^6 counts of those for the main in the sample, showing why using maximum laser intensity was required to maximise the minor peaks.

Identification of the largest r^4 peaks was carried out, and as in fig. 7.2.2 and fig. 7.2.3, can be compared to the spectral data from the sample and reference specimens. In both

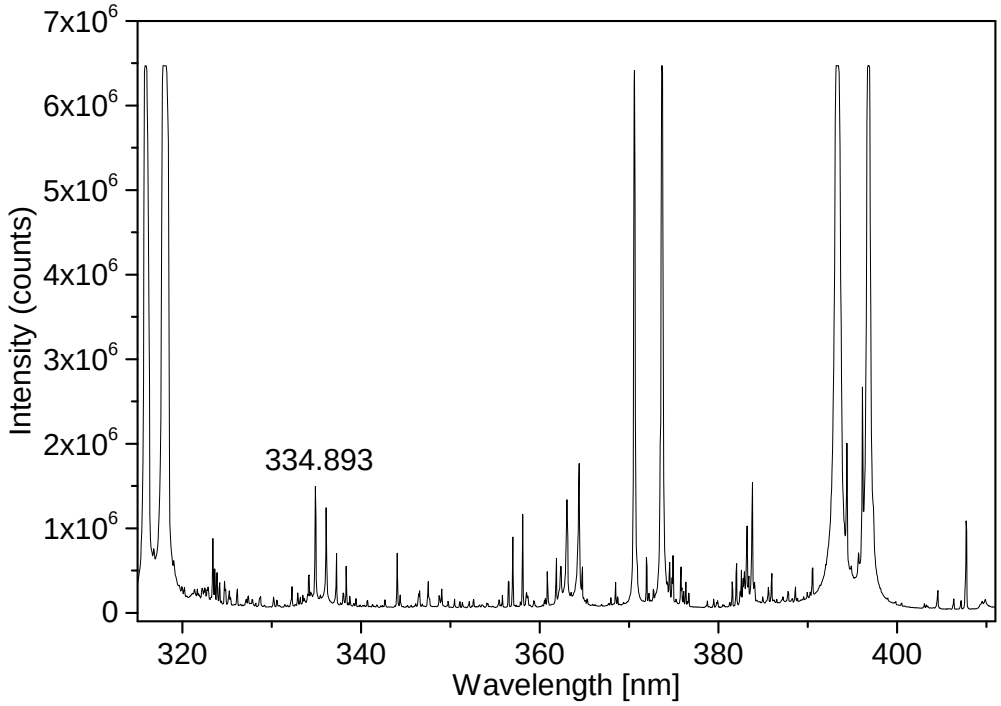

Figure 7.2.1: intensity vs wavelength plot for cement reference, showing 334.893 Cu peak for normalisation

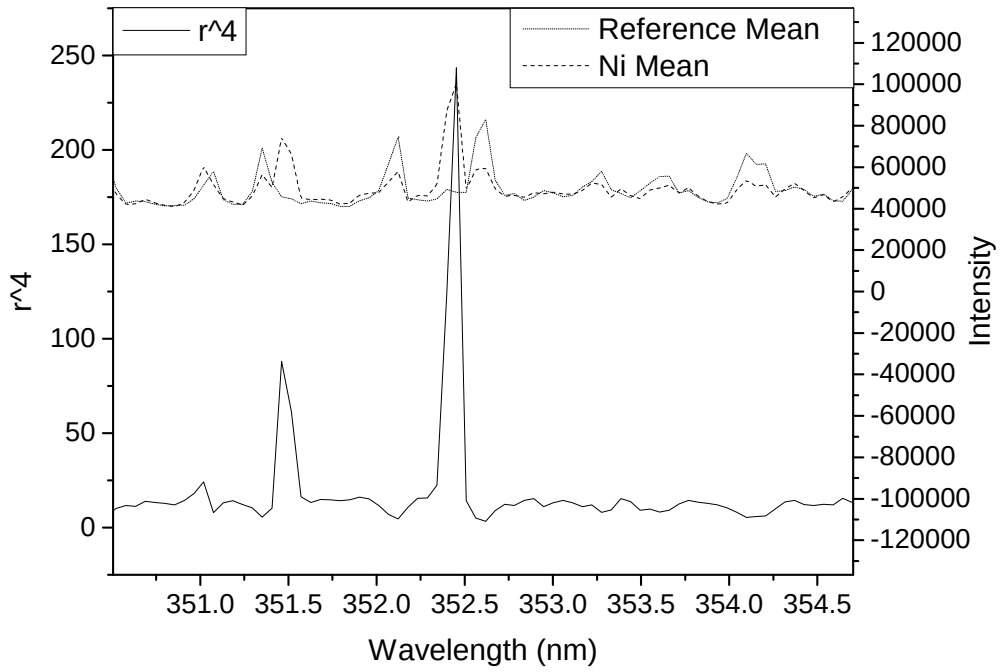

Figure 7.2.2: r^4 with sample and reference intensity plots for Ni

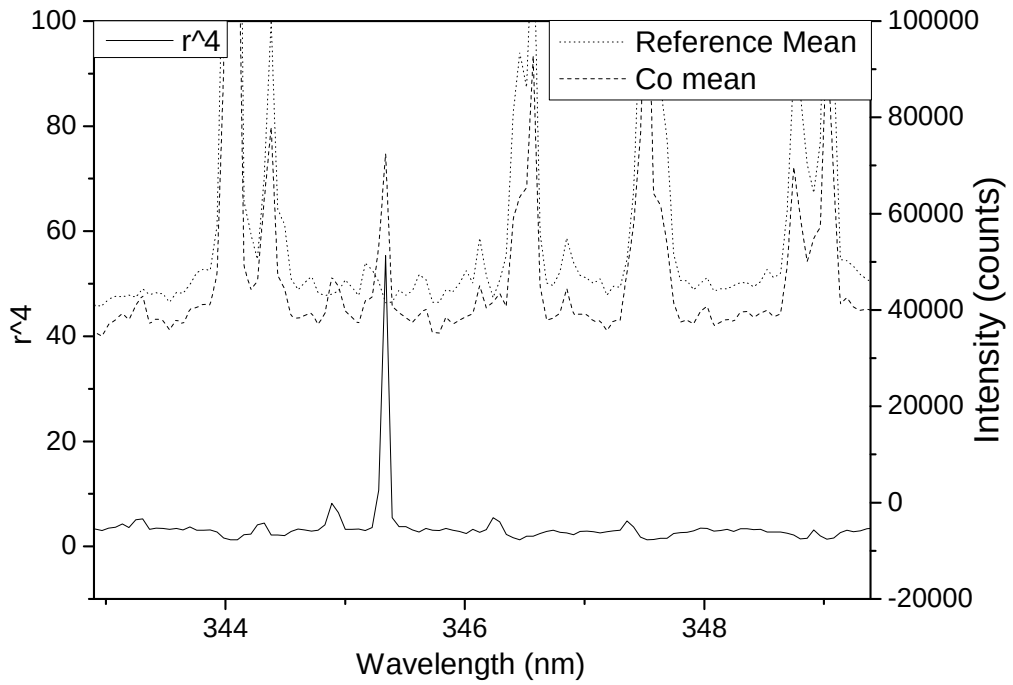

Figure 7.2.3: r^4 with sample and reference intensity plots for Co

figures, it can be seen that the r^4 peak matches with a difference in peak heights between the sample and reference, confirming that the process of normalisation and peak difference ratio calculation has been successful.

Following identification of the most intense peaks, they were compared to the NIST spectral database for the contaminant element concerned[174]. Figure 7.2.4 shows the r^4 plot for Ni and Co over the whole spectrometer range, with most intense peaks labelled. Comparing the two plots, noise could be seen around 325-335 and 375 nm to 385 nm. Small peaks were also visible at 318 nm, 393 nm and 396 nm. The presence of these peaks in both r^4 plots, and their relatively low height compared to others in the range, suggests that these peaks were noise. The major r^4 peaks in both plots centre around the 340 nm to 360 nm range and so it is these areas that analysis was focussed on.

When r^4 values are compared with those of the NIST literature in the 340 nm to 360 nm range, there is a very close match between the experimental and database values, for both Ni and Co, as shown in fig. 7.2.5 and fig. 7.2.6. Further evidence of the positive match between experimental and literature values lie in the similar peak heights of both data sets, where highest Co r^4 peak at 345.337 nm matches the highest peak from the NIST data at

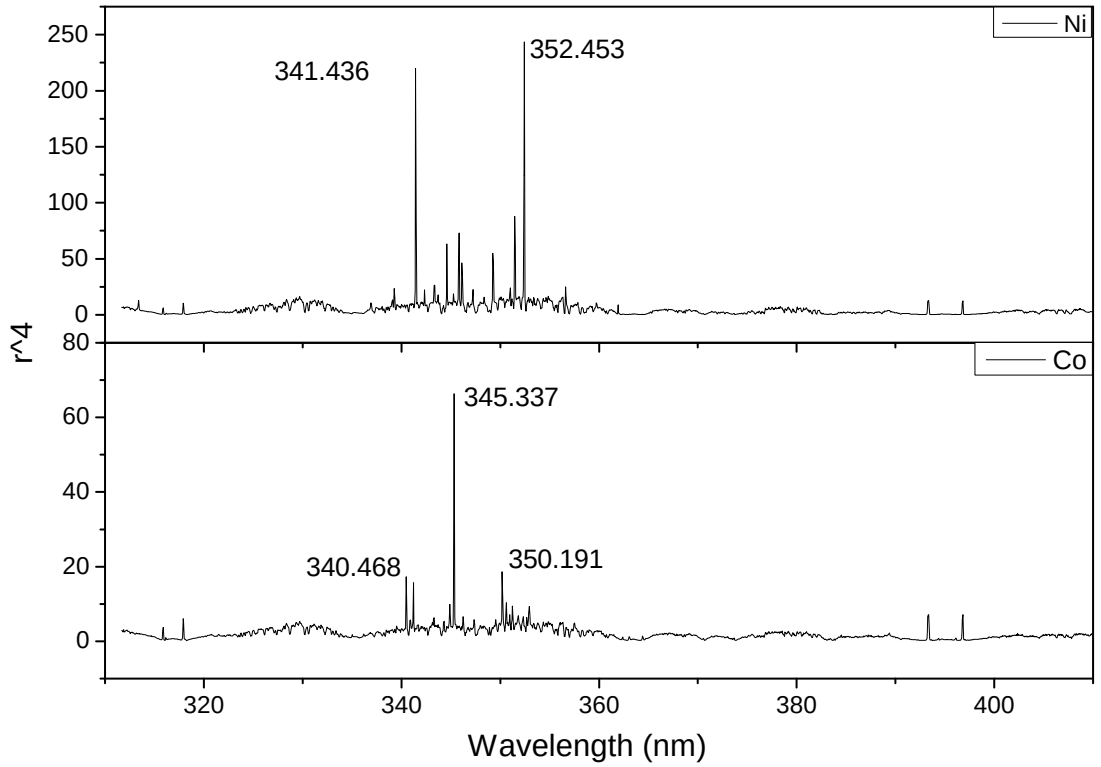

Figure 7.2.4: r^4 value for Ni and Co over whole spectrometer range

345.350 nm. The slight discrepancies in r^4 and NIST values is related to the precision of the detectors used.

7.3 Conclusions

Simulant radionuclides were cast in to cement paste samples. LIBS was then used to detect the contamination, with the ratio between peak intensities used to spot radionuclides at low inclusion levels. This method successfully detected Ni and Co at 0.045 and 0.021wt% respectively. The ability of LIBS to successfully detect at low inclusion levels provides the possibility for remotely operated, real time detection of radionuclides in concrete.

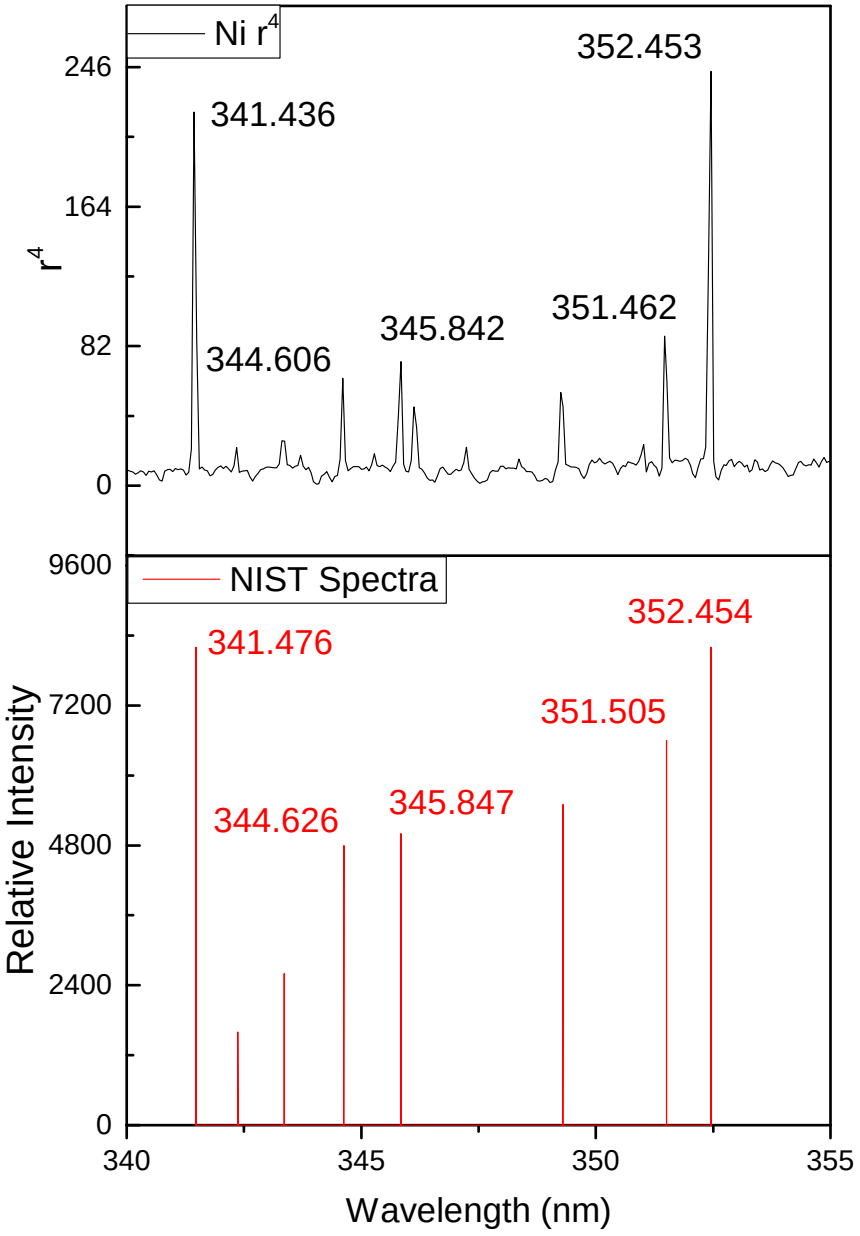

Figure 7.2.5: Comparison of r^4 to NIST data for Ni

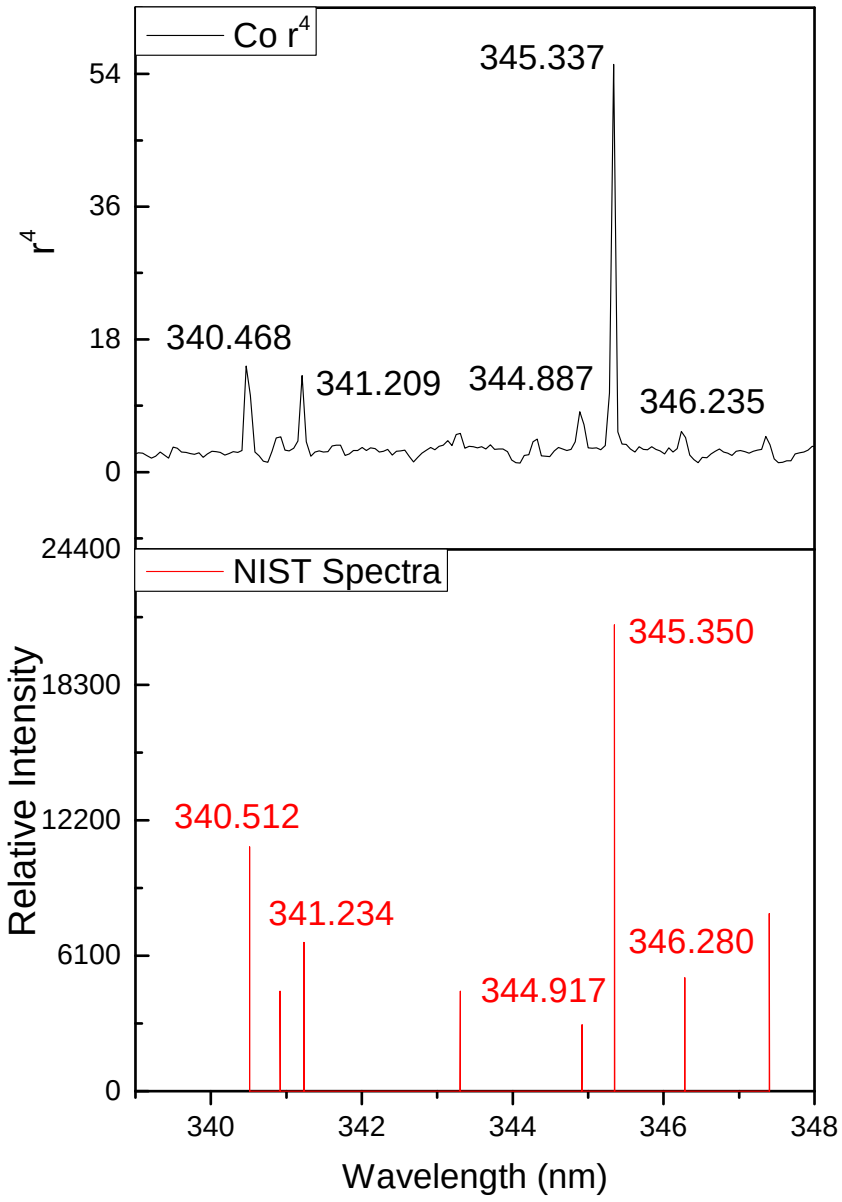

Figure 7.2.6: Comparison of r^4 to NIST data for Co

Part IV

Conclusions and Further Work

Chapter 8

Conclusions

8.1 Synthesis

Two concretes were cast, a CEM I 50MPa and a CEM II 50MPa with 20% PFA inclusion. The two concretes were ground into fine powders to mimic the resultant material found when concrete is scabbled. As the depth of radionuclide contamination has been found to be upto several centimetres[16], this is similar to the possible depth of carbonation in aged concrete structures, depending on concrete type, its mix design, and the exposure conditions. As such, accelerated carbonation was carried out on half of each ground material, such that there were four resultant fractions, C1, C2, T1 and T2. A further fine fraction, below 50 µm of each, was separated for further analytical work, as this was where the cement paste was found to be concentrated post grinding.

Backscattered electron analysis from scanning electron microscopy was used to determine the degree of hydration of each concrete, with the CEM I found to be 70.7% hydrated, and the CEM II found to be 72.4% hydrated, after over 6 months of hydration. Using thermal analysis, the degree of carbonation of each fraction was calculated, with the C1 and C2 fractions found to be 8.5 and 10.0% carbonated, although the C2 fraction will also include carbonated material in the PFA, and so the calcium carbonate content will be lower than 10.0%. The T1 and T2 fractions were found to be 16.3% and 14.3% carbonated respectively.

8.2 Waste Replacement in Encapsulation Grout

The C1 and C2 fractions were used as filler in encapsulation grouts at 10, 20 and 40% replacement, with only the finer binder fractions (Ketton OPC and Port Talbot BFS, d50's 20.5 and 15.0 micron) being replaced (with full particle size distribution of the filler, d5 2 micron, d50 13.5 micron, d90 160 micron), with the coarser blast furnace slag fraction, calumite (d50 470 micron), being maintained. Following casting of cubes and cylinders for investigating changes to engineering properties using the full PSD of the filler, a finer fraction of filler was separated for analytical work, using a 50 micron sieve, resulting in a d5 of 2 micron, d50 of 8-10 micron, and d90 of 34 micron. For analytical work, the calumite content was also omitted from investigations.

A number of techniques, including strength testing and isothermal calorimetry, were used to investigate the effect of the scabblings on the hydration and engineering performance of encapsulation grout. It was found that both the C1 (ground CEM I concrete) and C2 (ground CEM II concrete), altered the early age hydration of encapsulation grouts when used as a filler, compared to mixes where quartz, as an inert material, was used at the same replacement percentages. The initial alite reaction began at the same time as that of a reference mix, whereas when quartz was used, this initial reaction was delayed. The aluminate peak, from slag hydration, was accelerated compared to a reference mix, while the cumulative heat of hydration reaction showed both C1 and C2 mixes as having a higher total hydration at early ages. As both the C1 and C2 powders had been shown to contain anhydrous clinker, as discussed in section 4.2.2.3, it is hypothesised that this remaining anhydrous powder is contributing to the early hydration reactions, and that the synthesised scabblings are not inert material. The presence of portlandite in the C1 and C2 powders, once mixed with water, acted to accelerate the slag hydration, creating the increase in early age hydration compared to an inert filler, shown when quartz was used.

Overall, it has been found that at replacement levels of 20 and 40%, the hydration and engineering properties of the grout are significantly affected detrimentally, with the reaction of anhydrous material remaining, combined with the filler effect not able to counteract the loss of binder. At 10% inclusion however, for both C1 and C2 mixes, the hydration

process, and resultant strength and engineering properties are equal, or suitably similar, to the reference mix. This suggests that replacement at this level or below is feasible, with the reaction of any remaining anhydrous material, in combination with the filler effect, making up for the loss of binder.

8.3 Ternary Replacement

Using many of the same experimental methods, the carbonated scabblings, T1 and T2, were used as a replacement material in encapsulation grout, with a particular focus on any changes to the hydration mechanism, as the presence of calcium carbonate is known to alter the hydration mechanism of binary systems, when added as a ternary addition [75,76].

During early ages of hydration, the influence of the carbonated scabblings leads to a delayed, and extended, dormant/induction period, as well as a slight acceleration in the aluminate hydration. These phenomena correlate well with the calcite content. When pH was investigated, it was found that the T1-40 mix had a significantly lower pH in the early stages of hydration compared to the C1-40 and reference mix. With the pH of calcium carbonate in solution being lower than that of pore water in Portland cement, the presence of calcium carbonate, rather than the portlandite found in the C1 and C2 mixes, the presence of declacified C-S-H which absorbs alkali metals, and the replacement diluting the cement content, the pH increase is much slower than in the reference and C1 and C2 mixes, delaying the onset of hydration.

When engineering performance of the ternary mixes was investigated, and compared against that of the non-carbonated C1 and C2 mixes, it was found that at 10% inclusion, the ternary mixes both had reduced permeability and porosity, compared to their comparative non-carbonated mix, and also a reference mix with no replacement. At 20 and 40% replacement however, the impact of the scabblings was strongly detrimental to the engineering properties of the grout, compared to both the reference mix and the equivalent replacement mixes for the non-carbonated mixes. Through XRD analysis, the formation of carboaluminates and stabilisation of ettringite was found. This lead to a larger volume

of hydration products , and explained the improvement in engineering performance of the ternary mixtures at low replacement percentages.

Overall, at high replacement percentages, the inclusion of carbonated scabblings has a detrimental affect on the hydration and engineering performance of encapsulation grouts, significantly increasing the permeability and sorptivity. At a replacement percentage of 10% however, the hydration isn't noticeably altered, beyond a slightly delayed and increased dormant period, which may prolong the setting time of the grout, which can be regarded as beneficial. At 10% replacement, the engineering performance of the grout is improved compared to the reference mix, suggesting that the presence of a small amount of calcium carbonate is beneficial to the grouts performance, and that carrying out accelerated carbonation on scabblings prior to use as a replacement, can improve the waste to container volume ratio, as well as improving the overall properties of the grout for waste encapsulation.

8.4 Laser-Induced Breakdown Spectroscopy for Contamination Detection

The suitability of the LIBS technique for real-time detection of radionuclide contamination in concrete has been investigated. As laser scabbling is a method proposed for remotely operation removal of contaminated concrete from the bulk, the suitability of using the same laser to determine the contamination level and ascertain whether further scabbling is required, is promising. By detecting contamination in real time, it is possible to reduce the overall volume of scabbled contaminated concrete requiring disposal, by preventing non-contaminated concrete being scabbled unnecessarily.

Cement paste samples were cast containing simulant radionuclides Ni and Co at 0.045 and 0.021 weight % respectively. Triple spot analysis, using maximum laser intensity, was used to collect spectra. By using a non-contaminated reference sample against which to compare spectra and to normalise peak heights, a ratio of peak heights, r^4, was used to detect differences in spectra, even in very minor peaks. By comparing the ratio of peak

heights to the National Institute of Standards and Technology (NIST) spectral database, it was possible to spot with very high confidence, contamination at levels as low as 0.021wt%.

LIBS has been proven to be a suitable technique for remotely operated, with real time analysis, detection of contamination in concrete at very low levels.

Chapter 9

Further Work

This project has focussed on the re-use of synthesised waste within an encapsulation grout, replacing the fine binder content as a whole. Determining the interactions between waste, radionuclides and the encapsulation grout matrix over the long time frame of grout encapsulation is a complex issue. It is proposed that by utilising scabbled concrete as a replacement material, rather than a waste-form itself, the waste to container volume ratio can be increased, thus making economic savings through reducing the overall total volume of waste drums for storage and disposal. To fully investigate the feasibility, and to optimise the process, of using waste as part of an encapsulation grout mix, a number of areas of further work are proposed.

9.1 Further Investigations Within this Project

While much of the work carried out within this project has lead to a conclusion regarding the influence of recycled fines on the performance of encapsulation grouts, there is the opportunity for further work to either further confirm these findings, or to extend the scope of the investigation. Permeability and sorptivity testing was carried out to investigate the engineering performance of the grouts, yet there were no micro-scale techniques carried out to further confirm these findings. Of particular relevance, mercury intrusion porosimetry (MIP) could be carried out to investigate changes to the porosity of the grout, both gel and capillary. Scanning electron microscopy (SEM) and x-ray Computed Tomography (XCT) could also be used to investigate changes to the capillary porosity, evidenced by

improvements in permeability and sortptivity of the T1 and T2 mixes compared to the C1 and C2 mixes at 10% inclusion.

Nuclear grouts are designed to provide encapsulation of radioactive waste on timescales up to tens of thousands of years, with radionuclide immobilisation of particular importance. Within encapsulation grouts, this is achieved largely through the maintaining of a high pH to maintain conditions that limit the solubility of waste species, or through the sorption of radionuclides onto phases within the cementitious matrix. While this project focussed on the hydration and engineering properties, there is another side to the issue of recycling contaminated concrete within encapsulation matrices, and that is the mobility and encapsulation of radioactive species, and whether the increased presence of radionuclides inhibits the ability of the grout to encapsulate and absorb radioactive species.

9.2 Coarse Fraction Replacement

Due to the nature of mechanical scabbling, the resultant material will have a wide range of particle sizes. This project focussed on the finer fraction, examining any reactivity in the finer fraction of the scabblings. In nuclear encapsulation grouts, calumite, a coarse blast furnace slag, is used to maintain the required particle size distribution and flow characteristics, while not affecting the overall pH of the grout. Despite being a blast furnace slag, the large particle size has been found to make it a largely inert material[126].

In order to avoid the need to further process the scabbled material, it is proposed that replacement of some of the calumite content within the encapsulation grout mix with the coarse fraction of the scabbled material be investigated, as this would provide a further opportunity to increase the re-use rate of scabbled material and further reduce the overall waste volume. In this investigation, less focus would be placed on the effect of the scabblings on the hydration process, and more on the engineering properties such as workability and fluidity, and any increased water demand due to the use of recycled aggregate.

9.3 Mineral Additions to Grout Composition

The present cement in use in UK encapsulation grout mixes, as described in section 3.1.1, uses no grinding aids or mineral additions, including limestone, in order to reduce the risk of unwanted and unexpected interactions with waste forms.

The use of limestone as an addition in ternary blended cements, to improve the early age strength and mechanical properties is well documented, and this research has shown the addition of calcium carbonate in the form of carbonated scabblings improves the longer term engineering properties such as sorptivity and permeability. Therefore, it is proposed that the addition of limestone or other calcium carbonate sources be investigated, in order to improve the long term properties of the encapsulation grout, reducing permeability and sorptivity and thus reducing the risk of radionuclide leaching out of the conditioned waste packages.

Bibliography

[1] Pöyry Energy Limited, A. plc, and Nuclear Decomissioning Authority, "The 2013 UK Radioactive Waste Inventory," tech. rep., Moor Row, Cumbria, 2014.

[2] Department of Energy & Climate Change, "Implementing Geological Disposal," tech. rep., London, 2014.

[3] Office of Nuclear Regulation, "Basic principles of radioactive waste management An introduction to the management of higher activity radioactive waste on nuclear licensed sites," no. February, pp. 1–22, 2015.

[4] IAEA, "Protocol Additional to the Agreement between the United Kingdom of Great Britain and Northern Ireland, the European Atomic Energy Community and the International Atomic Energy Agency for the Application of Safeguards in the United Kingdom of Great Britain," no. April 2004, 2005.

[5] Nuclear Decommissioning Authority, "Radioactive Wastes in the UK: Executive Summary of the 2016 Inventory," pp. 1–20, 2017.

[6] Nuclear Decommissioning Authority, "Radioactive Wastes in the UK: A Summary of the 2016 Inventory," tech. rep., 2017.

[7] Environment Agency, "Low Level Waste Repository," Tech. Rep. August, 2014.

[8] BNFL Commercial, "Product Quality Assessment of High Colflow Matrix Grouts Produced in MEP," tech. rep., 2002.

[9] B. Mcluckie, "Colcrete Flow Channel Test," pp. 18–21, 2014.

[10] Radioactive Waste Management, "A safer future by managing radioactive waste effectively, to protect people and the environment," tech. rep., 2015.

[11] Department of Energy & Climate Change, "Waste Transfer Pricing Methodology for the Disposal of Higher Activity Waste from Nuclear Power Stations," tech. rep., London, 2011.

[12] LLW Repository Ltd, "Service Price List - 1 April 2018 to 31 st March 2019," Tech. Rep. March, 2018.

[13] Nuclear Decomissioning Authority: NDA, "Radioactive Wastes in the UK : A Summary of the 2013 Inventory," *Department of Energy & Climate Change*, pp. 1–15, 2013.

[14] K. L. Scrivener, T. Fullmann, E. Gallucci, G. Walenta, and E. Bermejo, "Quantitative Study of Portland Cement Hydration by X-Ray Diffraction/Rietveld Analysis and Independent Methods," *Cement and Concrete Research*, vol. 34, pp. 1541–1547, 2004.

[15] S. Adu-Amankwah, M. Zajac, C. Stabler, B. Lothenbach, and L. Black, "Influence of limestone on the hydration of ternary slag cements," *Cement and Concrete Research*, vol. 100, no. June, pp. 96–109, 2017.

[16] A. Bath, G. Deissmann, and S. Jefferis, "Radioactive Contamination of Concrete: Uptake and Release of Radionuclides," 2003.

[17] B. Šavija and M. Luković, "Carbonation of cement paste: Understanding, challenges, and opportunities," *Construction and Building Materials*, vol. 117, pp. 285–301, 2016.

[18] G. Villain, M. Thiery, and G. Platret, "Measurement methods of carbonation profiles in concrete: Thermogravimetry, chemical analysis and gammadensimetry," *Cement and Concrete Research*, vol. 37, no. 8, pp. 1182–1192, 2007.

[19] T. Ishikura, H. Ueki, K. Ohnishi, and D. Oguri, "Utilization of Crushed Radioactive Concrete for Mortar to Fill Waste Container Void Space," *Journal of Nuclear Science and Technology*, vol. 41, no. 7, pp. 741–750, 2004.

[20] A. M. Neville, *Properties of Concrete*, vol. Fourth. 7 ed., 2011.

[21] H. F. W. Taylor, *Cement Chemistry*. London: Thomas Telford, 2 ed., 1997.

[22] F. Geoffrey, "Calculation of Compounds in Portland Cements," *A Century of Excellence in Measurements, Standards, and Technology: A Chronicle of Selected NBS/NIST Publications, 1901-2000 (SP958)*, pp. 33–37, 2001.

[23] R. H. Bogue, "Calculation of the compounds in Portland Cement," *Industrial Engineering Chemistry Analytical Edition*, vol. 1, no. 4, pp. 192–197, 1929.

[24] European Centre for Standardization, "BS EN 197-1," 2010.

[25] WHD Microanalysis Consultants Ltd, "Cement Hydration," 2019.

[26] K. L. Scrivener and A. Nonat, "Hydration of cementitious materials, present and future," *Cement and Concrete Research*, vol. 41, no. 7, pp. 651–665, 2011.

[27] P. Juilland, E. Gallucci, R. Flatt, and K. Scrivener, "Dissolution theory applied to the induction period in alite hydration," *Cement and Concrete Research*, vol. 40, no. 6, pp. 831–844, 2010.

[28] D. P. Bentz, E. J. Garboczi, C. J. Haecker, and O. M. Jensen, "Effects of cement particle size distribution on performance properties of Portland cement-based materials," *Cement and Concrete Research*, vol. 29, no. 10, pp. 1663–1671, 1999.

[29] E. ichi Tazawa, S. Miyazawa, and T. Kasai, "Chemical shrinkage and autogenous shrinkage of hydrating cement paste," *Cement and Concrete Research*, vol. 25, no. 2, pp. 288–292, 1995.

[30] T. Zhang, P. Gao, R. Luo, Y. Guo, J. Wei, and Q. Yu, "Measurement of chemical shrinkage of cement paste: Comparison study of ASTM C 1608 and an improved method," *Construction and Building Materials*, vol. 48, pp. 662–669, 2013.

[31] I. G. Richardson, "Nature of C-S-H in hardened cements," *Cement and Concrete Research*, vol. 29, no. 8, pp. 1131–1147, 1999.

[32] I. G. Richardson, "Tobermorite/jennite- and tobermorite/calcium hydroxide-based models for the structure of C-S-H: Applicability to hardened pastes of tricalcium silicate, β-dicalcium silicate, Portland cement, and blends of Portland cement with blast-furnace slag, metakaol," *Cement and Concrete Research*, vol. 34, no. 9, pp. 1733–1777, 2004.

[33] I. G. Richardson, C. R. Wilding, and M. Dickson, "The hydration of blastfurnace slag cements," *Advances in Cement Research*, vol. 2, no. 8, pp. 147–157, 1989.

[34] I. G. Richardson and G. W. Groves, "Microstructure and microanalysis of hardened cement pastes involving ground granulated blast-furnace slag," *Journal of Materials Science*, vol. 27, no. 22, pp. 6204–6212, 1992.

[35] D. L. Rayment and A. J. Majumdar, "The composition of the C-S-H phases in portland cement pastes," *Cement and Concrete Research*, vol. 12, no. 6, pp. 753–764, 1982.

[36] S. Diamond, "Aspects of concrete porosity revisited," *Cement and Concrete Research*, vol. 29, no. 8, pp. 1181–1188, 1999.

[37] I. G. Richardson, "Nature of the hydration products in hardened cement pastes," *Cement and Concrete Composites*, vol. 22, no. 2, pp. 97–113, 2000.

[38] P. C. Carman, "Permeability of saturated sands, soils and clays," *The Journal of Agricultural Science*, vol. 29, p. 262, 1939.

[39] R. Mark and P. Hutchinson, "On the Structure of the Roman Pantheon," *The Art Bulletin*, vol. 68, pp. 24–34, mar 1986.

[40] G. C. Cordeiro, R. D. Toledo Filho, L. M. Tavares, and E. M. R. Fairbairn, "Pozzolanic activity and filler effect of sugar cane bagasse ash in Portland cement and lime mortars," *Cement and Concrete Composites*, vol. 30, no. 5, pp. 410–418, 2008.

[41] B. Lothenbach, K. Scrivener, and R. D. Hooton, "Supplementary cementitious materials," *Cement and Concrete Research*, vol. 41, no. 12, pp. 1244–1256, 2011.

[42] Cement Sustainability Institute, "Recycling concrete," p. 8, 2009.

[43] R. Siddique, "Ground Granulated Blast Furnace Slag," in *Waste Materials and By-Products in Concrete*, vol. 000, pp. 1–39, 2008.

[44] I. G. Richardson and G. W. Groves, "The incorporation of minor and trace elements into calcium silicate hydrate (CSH) gel in hardened cement pastes," *Cement and Concrete Research*, vol. 23, no. 1, pp. 131–138, 1993.

[45] J. Duchesne and M. Berube, "Effect of supplementary cementing materials on the composition of cement hydration products," *Advanced Cement Based Materials*, vol. 2, no. 2, pp. 43–52, 1995.

[46] A. Oner and S. Akyuz, "An experimental study on optimum usage of GGBS for the compressive strength of concrete," *Cement and Concrete Composites*, vol. 29, no. 6, pp. 505–514, 2007.

[47] M. Whittaker, M. Zajac, M. Ben Haha, F. Bullerjahn, and L. Black, "The role of the alumina content of slag, plus the presence of additional sulfate on the hydration and microstructure of Portland cement-slag blends," *Cement and Concrete Research*, vol. 66, pp. 91–101, 2014.

[48] H. Zhou, G. Ye, and K. van Breuge, "Hydration process and pore structure of portland cement paste blended with blastfurnace slag," *Proceedings of the 6th International Symposium on Cement & Concrete and Canmet/Aci International Symposium on Concrete Technology for Sustainable Development, Vols 1 and 2*, no. January, pp. 417–424, 2006.

[49] V. G. Papadakis, "Effect of fly ash on Portland cement systems: Part I. Low-calcium fly ash," *Cement and Concrete Research*, vol. 29, no. 11, pp. 1727–1736, 1999.

[50] M. Narmluk and T. Nawa, "Effect of Curing Temperature on Pozzolanic Reaction of Fly Ash in Blended Cement Paste," *International Journal of Chemical Engineering and Applications*, vol. 5, no. 1, pp. 31–35, 2014.

[51] V. Corinaldesi and G. Moriconi, "Behaviour of cementitious mortars containing different kinds of recycled aggregate," *Construction and Building Materials*, vol. 23, no. 1, pp. 289–294, 2009.

[52] G. C. Gifford, *National Structural Concrete Specification for Building Construction.* 2009.

[53] H. J. Chen, T. Yen, and K. H. Chen, "Use of building rubbles as recycled aggregates," *Cement and Concrete Research*, vol. 33, no. 1, pp. 125–132, 2003.

[54] J. S. Ryu, "An experimental study on the effect of recycled aggregate on concrete properties," *Magazine of Concrete Research*, vol. 54, no. 1, pp. 7–12, 2002.

[55] l. B. Topcu and N. F. Guncan, "Using waste concrete as aggregate," *Cement and Concrete Research*, vol. 25, no. 7, pp. 1385–1390, 1995.

[56] N. Yong Ho, Y. P. K. Lee, W. F. Lim, T. Zayed, K. C. Chew, G. L. Low, and K. T. Seng, "Efficient Utilization of Recycled Concrete Aggregate in Structural Concrete," *Journal of Materials in Civil Engineering*, vol. 25, no. March, pp. 318–327, 2013.

[57] K.-h. Ng, C.-m. Tam, and V. W.-y. Tam, "Deformation and Sorptivity of Recycled Aggregate Concrete Produced by Two Stage Mixing Approach," *Surveying and Built Environment*, vol. 17, no. 1, pp. 7–14, 2006.

[58] R. Sri Ravindrarajah, "Utilization of waste concrete for new construction," *Conservation and Recycling*, vol. 10, no. 2-3, pp. 69–74, 1987.

[59] A. K. Padmini, K. Ramamurthy, and M. S. Mathews, "Influence of parent concrete on the properties of recycled aggregate concrete," *Construction and Building Materials*, vol. 23, no. 2, pp. 829–836, 2009.

[60] W.-y. V. Tam, X.-f. Gao, and C.-m. Tam, "Comparing Performance of Modified Two-Stage Mixing Approach for Producing Recycled Aggregate Concrete," *Magazine of Concrete Research*, vol. 58, no. 7, pp. 477–484, 2006.

[61] V. W. Tam, X. Gao, and C. Tam, "Microstructural analysis of recycled aggregate concrete produced from two-stage mixing approach," *Cement and Concrete Research*, vol. 35, pp. 1195–1203, 2005.

[62] Standards Council of Canada, "CAN3-A5-M83 Portland Cement," 1983.

[63] European Standards, "Eurocode 2: Design of concrete structures," 2004.

[64] CEMBUREAU, *Cement Standards of the World.* Brussels: CEMBUREAU, the European Cement Association, 1991.

[65] W. A. Gutteridge and J. A. Dalziel, "Filler Cement: The Effect of the Secondary Component on the Hydration of Portland Cement," *Cement and Concrete Research*, vol. 20, pp. 778–782, 1990.

[66] E. M. J. Berodier, *Impact of the Supplementary Cementitious Materials on the kinetics and microstructural development of cement hydration.* PhD thesis, 2015.

[67] T. Oey, A. Kumar, J. W. Bullard, N. Neithalath, and G. Sant, "The filler effect: The influence of filler content and surface area on cementitious reaction rates," *Journal of the American Ceramic Society*, 2013.

[68] E. Berodier and K. Scrivener, "Understanding the filler effect on the nucleation and growth of C-S-H," *Journal of the American Ceramic Society*, 2014.

[69] B. Schiller and H.-G. Ellerbrock, "The Grinding and Properties of Cement with Several Main Constituents," *Zement-Kalk-Gips*, vol. 45, no. 7, pp. 325–334, 1992.

[70] M. Scmidt, "Cement with Interground Additives - Capabilities and Environmental Relief," *Zement-Kalk-Gips*, vol. 45, no. 6, pp. 64–69,296–301, 1992.

[71] P. Hawkins, R. Detwiler, and P. D. Tennis, *The Use of Limestone in Portland Cement : A State-of-the-Art Review*. 2003.

[72] P. Jackson, "Manufacturing Aspects of Limestone-Filled Cements," tech. rep., Building Research Establishment, Watford, 1989.

[73] W. Klemm and L. Adams, "An Investigation of the Formation of Carboaluminates," in *Carbonate Additions to Cement*, pp. 60–72, Philadelphia: American Society for Testing and Materials, 1990.

[74] E. Siebel and S. Sprung, "Influence of Limestone in Portland Limestone Cement on the Durability of Concrete," *Beton*, vol. 41, no. 3, pp. 113–117, 1991.

[75] J. Stark, E. Freyburg, and K. Lohmer, "Investigations into the influence of limestone additions to portland cement clinker phases on the early phase of hydration," *Modern Concrete Materials: Binders; Additions and Admixtures*, pp. 69–77, 1999.

[76] K. D. Ingram and K. E. Daugherty, "A review of limestone additions to Portland cement and concrete," *Cement and Concrete Composites*, vol. 13, no. 3, pp. 165–170, 1991.

[77] B. Lothenbach, G. L. Saout, E. Gallucci, and K. Scrivener, "Influence of limestone on the hydration of Portland cements," vol. 38, pp. 848–860, 2008.

[78] V. S. Ramachandran, "Thermal analyses of cement components hydrated in the presence of calcium carbonate," *Thermochimica Acta*, vol. 127, no. C, pp. 385–394, 1988.

[79] J. Péra, S. Husson, and B. Guilhot, "Influence of finely ground limestone on cement hydration," *Cement and Concrete Composites*, vol. 21, no. 2, pp. 99–105, 1999.

[80] G. Menéndez, V. Bonavetti, and E. F. Irassar, "Strength development of ternary blended cement with limestone filler and blast-furnace slag," vol. 25, pp. 61–67, 2003.

[81] H. J. Kuzel and H. Pöllmann, "Hydration of C_3A in the presence of $Ca(OH)_2$, $CaSO_4.2H_2O$ and $CaCO_3$," *Cement and Concrete Research*, vol. 21, no. 5, pp. 885–895, 1991.

[82] T. Matschei, B. Lothenbach, and F. P. Glasser, "The role of calcium carbonate in cement hydration," *Cement and Concrete Research*, vol. 37, no. 4, pp. 551–558, 2007.

[83] S. Adu-Amankwaha, L. Black, and M. Zajac, "The Microstructure of Composite Slag-Limestone Cements," in *ibausil International Conference on Building Materials*, pp. 16–18, 2015.

[84] M. Bouasker, P. Mounanga, P. Turcry, A. Loukili, and A. Khelidj, "Chemical shrinkage of cement pastes and mortars at very early age: Effect of limestone filler and granular inclusions," *Cement and Concrete Composites*, vol. 30, no. 1, pp. 13–22, 2008.

[85] S. Hoshino, K. Yamada, and H. Hirao, "XRD/Rietveld Analysis of the Hydration and Strength Development of Slag and Limestone Blended Cement," *Journal of Advanced Concrete Technology*, vol. 4, no. 3, pp. 357–367, 2006.

[86] M. Ghrici, S. Kenai, and M. Said-Mansour, "Mechanical properties and durability of mortar and concrete containing natural pozzolana and limestone blended cements," *Cement and Concrete Composites*, vol. 29, no. 7, pp. 542–549, 2007.

[87] P. Purnell and L. Black, "Embodied carbon dioxide in concrete: Variation with common mix design parameters," *Cement and Concrete Research*, vol. 42, no. 6, pp. 874–877, 2012.

[88] V. A. Juverar, M. M. Sharma, and M. Road, "Absorption of CO, in a suspension of lime," *Chemical Engineering Science*, vol. 28, no. 1, pp. 825–837, 1973.

[89] L. J. Parrott, *A Review of Carbonation in Reinforced Concrete*. Camberley: Cement and Concrete Association, 1987.

[90] A. V. Saetta, B. A. Schrefler, and R. V. Vitaliani, "The carbonation of concrete and the mechanism of moisture, heat and carbon dioxide flow through porous materials," *Cement and Concrete Research*, vol. 23, pp. 761–772, 1993.

[91] G. Groves, A. Brough, I. Richardson, and C. Dobson, "Progressive Changes in the Structure of Hardened C_3S Cement Pastes due to Carbonation," *Journal of the American Ceramic Society*, vol. 74, no. 11, pp. 2891–2896, 1991.

[92] M. Castellote, L. Fernandez, C. Andrade, and C. Alonso, "Chemical changes and phase analysis of OPC pastes carbonated at different CO2concentrations," *Materials and Structures/Materiaux et Constructions*, vol. 42, no. 4, pp. 515–525, 2009.

[93] M. Thiery, G. Villain, P. Dangla, and G. Platret, "Investigation of the carbonation front shape on cementitious materials: Effects of the chemical kinetics," *Cement and Concrete Research*, vol. 37, pp. 1047–1058, 2007.

[94] I. Galan, F. P. Glasser, D. Baza, and C. Andrade, "Assessment of the protective effect of carbonation on portlandite crystals," *Cement and Concrete Research*, vol. 74, pp. 68–77, 2015.

[95] A. E. Morandeau and C. E. White, "In situ X-ray pair distribution function analysis of accelerated carbonation of a synthetic calcium-silicate-hydrate gel," *Journal of Materials Chemistry A*, vol. 3, no. 16, pp. 8597–8605, 2015.

[96] L. Black, C. Breen, J. Yarwood, K. Garbev, P. Stemmermann, and B. Gasharova, "Structural features of C-S-H(I) and its carbonation in air-A Raman spectroscopic study. Part II: Carbonated phases," *Journal of the American Ceramic Society*, vol. 90, no. 3, pp. 908–917, 2007.

[97] L. Black, K. Garbev, and I. Gee, "Surface carbonation of synthetic C-S-H samples: A comparison between fresh and aged C-S-H using X-ray photoelectron spectroscopy," *Cement and Concrete Research*, vol. 38, no. 6, pp. 745–750, 2008.

[98] G. W. Groves, D. I. Rodway, and I. G. Richardson, "The carbonation of hardened cement pastes," *Advances in Cement Research*, vol. 3, no. 11, pp. 117–125, 1990.

[99] V. Morales-Florez, N. Findling, and F. Brunet, "Changes on the nanostructure of cementitius calcium silicate hydrates (C-S-H) induced by aqueous carbonation," *Journal of Materials Science*, vol. 47, no. 2, pp. 764–771, 2012.

[100] K. Sisomphon and L. Franke, "Carbonation Rates of Concretes Containing High Volume of Pozzolanic Materials," *Cement and Concrete Research*, vol. 37, pp. 1647–1653, 2007.

[101] T. F. Sevelsted and J. Skibsted, "Carbonation of C-S-H and C-A-S-H samples studied by 13C, 27Al and 29Si MAS NMR spectroscopy," *Cement and Concrete Research*, vol. 71, pp. 56–65, 2015.

[102] National Oceanic and Atmospheric Administration, "Recent Monthly mean CO_2 at Mauna Loa," 2016.

[103] T. A. Harrison, M. R. Jones, M. D. Newlands, S. Kandasami, and G. Khanna, "Experience of using the prTS 12390-12 accelerated carbonation test to assess the relative performance of concrete," *Magazine of Concrete Research*, vol. 64, no. 8, pp. 737–747, 2012.

[104] M. A. Sanjuán, C. Andrade, and M. Cheyrezy, "Concrete carbonation tests in natural and accelerated conditions," *Advances in Cement Research*, vol. 15, no. 4, pp. 171–180, 2003.

[105] A. Leemann and F. Moro, "Carbonation of concrete: the role of CO_2 concentration, relative humidity and CO_2 buffer capacity," *Materials and Structures*, vol. 50, no. 1, p. 30, 2017.

[106] H. Cui, W. Tang, W. Liu, Z. Dong, and F. Xing, "Experimental study on effects of CO_2 concentrations on concrete carbonation and diffusion mechanisms," *Construction and Building Materials*, vol. 93, pp. 522–527, 2015.

[107] Y. F. Houst, "The Role of Moisture in the Carbonation of Cementitious Materials," *Internationale Zeitschrift für Bauinstandsetzen*, pp. 49–66, 1996.

[108] T. Chaussadent, H. Hornain, N. Rafai, A. Ammouche, and V. Baroghel-Bouny, "Effect of Water-Cement Ratio of Cement Pastes on Microstructural Characteristics Related to Carbonation Process," *Special Publication*, vol. 192, pp. 523–538, 2000.

[109] V. G. Papadakis, "Effect of fly ash on Portland cement systems," *Cement and Concrete Research*, vol. 30, no. 10, pp. 1647–1654, 2000.

[110] E. Gruyaert, P. Van Den Heede, and N. De Belie, "Carbonation of slag concrete: Effect of the cement replacement level and curing on the carbonation coefficient - Effect of carbonation on the pore structure," *Cement and Concrete Composites*, vol. 35, no. 1, pp. 39–48, 2013.

[111] A. Morandeau, M. Thiéry, and P. Dangla, "Impact of accelerated carbonation on OPC cement paste blended with fly ash," *Cement and Concrete Research*, vol. 67, pp. 226–236, 2015.

[112] European Centre for Standardization, "BS EN 1992-1-1:2004 - Design of concrete structures. General rules and rules for buildings," 2010.

[113] K. S. Dickerson, M. J. Wilson-Nichols, and M. I. Morris, "Contaminated concrete: occurrence and emerging technologies for DOE decontamination," no. August, p. 377, 1995.

[114] I. Binkhorst and H. Cornellison, "Technology for Reuse of Contaminated Concrete Constituents," pp. 149–160, 1998.

[115] T. Lynch, "Diamond Blade Grinding as a Means for Removing Surface Contamination from Concrete," in *Concrete Decontamination Workshop*, vol. 1, pp. 55–61, 1980.

[116] F. Moggia, A. Benamane, T. Varet, V. Toulemonde, F. Richard, G. Anderson, and F. Damerval, "Nitrojet: A Versatile Tool for Decontamination, Cutting and Concrete Scabbling," 2011.

[117] B. Peach, "Laser scabbling of cementitious materials," no. July, 2015.

[118] J. Halter and R. Sullivam, "Equipment for Removal of Contaminated Concrete Surfaces," in *Concrete Decontamination Workshop*, pp. 27–41, 1980.

[119] C. Wilson and P. C. Demolition, "Windscale chimney decommissioning," 2014.

[120] G. N. Kim, W. K. Choi, and K. W. Lee, "Decontamination of radioactive concrete using electrokinetic technology," *Journal of Applied Electrochemistry*, vol. 40, no. 6, pp. 1209–1216, 2010.

[121] F. P. Glasser, "Progress in the Immobilization of Radioactive Wastes in Cement," *Cement and Concrete Research*, vol. 22, pp. 201–216, 1992.

[122] J. H. Sharp, J. Hill, N. B. Milestone, and E. W. Miller, "Cementitious Systems for Encapsulation of Intermediate Level Waste," *Proceedings of ICEM '03: The 9th International Conference on Radioactive Waste Management and Environmental Remediation*, pp. 1–10, 2003.

[123] F. P. Glasser, "Cements in Radioactive Waste Disposal," Tech. Rep. 49, 2013.

[124] F. P. Glasser, M. Tyrer, K. Quillin, D. Ross, J. Pedersen, K. Goldthorpe, D. Bennett, and M. Atkins, "The chemistry of blended cements and backfills intended for use in radioactive waste disposal: Research and development. Technical Report P98, UK Environment Agency," tech. rep., 1998.

[125] F. P. Glasser, "Mineralogical aspects of cement in radioactive waste disposal," *Mineralogical Magazine*, vol. 65, no. October, pp. 621–633, 2001.

[126] J. D. Hawthorne, *Cementitious Grouts for ILW Encapsulation - Composition, Hydration and Performance.* PhD thesis, University of Leeds, 2017.

[127] R. Deju, D. Gurau, L. Done, C. Mazilu, I. Robu, and N. Engineering, "The Study of Radionuclides Leaching from Mortar," *Romanian Reports in Physics*, pp. 1–17, 2015.

[128] D. E. Hobart, C. J. Bruton, F. J. Millero, I.-M. Chou, K. M. Trauth, and D. R. Anderson, "Estimates of the Solubilities of Waste Element Radionuclides in Waste Isolation Pilot Plant Brines: A Report by the Expert Panel on the Source Term," Tech. Rep. May, 1996.

[129] Tata Steel, "Our Operations," 2017.

[130] K. L. Scrivener, "Backscattered electron imaging of cementitious microstructures: Understanding and quantification," *Cement and Concrete Composites*, vol. 26, no. 8, pp. 935–945, 2004.

[131] M. Balonis and F. P. Glasser, "The density of cement phases," *Cement and Concrete Research*, vol. 39, no. 9, pp. 733–739, 2009.

[132] S. Diamond, "The microstructure of cement paste and concrete - A visual primer," *Cement and Concrete Composites*, vol. 26, no. 8, pp. 919–933, 2004.

[133] E. C. Arvaniti, M. C. G. Juenger, S. A. Bernal, L. Courard, S. Leroy, J. L. Provis, A. Klemm, and N. D. Belie, "Physical characterization methods for supplementary cementitious materials," *Materials and Structures*, vol. 48, pp. 3675–3686, 2015.

[134] P. W. H. Bragg and W. L. Bragg, "The Reflection of X-rays by Crystals," *Proceedings of the Royal Society*, vol. 17, pp. 428–438, 1913.

[135] T. F. Scientific, "Identification and Quantification of Cement Phases by X-Ray Diffraction," *Thermo Fisher Scientific*, pp. 1–4, 2008.

[136] J. Bhatty, "A review of the application of thermal analysis to cement-admixture systems," *Thermochimica Acta*, vol. 189, pp. 313–350, 1991.

[137] N. C. Collier, "Transition and decomposition temperatures of cement phases - a collection of thermal analysis data," *Ceramics - Silikaty*, vol. 60, no. 4, pp. 338–343, 2016.

[138] J. I. Bhatty, "Hydration versus Strength in a Portland Cement Developed from Domestic Mineral Wastes - A Comparative Study," *Therochimica Acta*, vol. 106, pp. 93–103, 1986.

[139] M. J. O'Neill, "Measurement of Specific Heat Functions by Differential Scanning Calorimetry," *Analytical Chemistry*, vol. 38, no. 10, pp. 1331–1336, 1966.

[140] I. Pane and W. Hansen, "Investigation of blended cement hydration by isothermal calorimetry and thermal analysis," *Cement and Concrete Research*, vol. 35, no. 6, pp. 1155–1164, 2005.

[141] B. Lothenbach, P. Durdzinski, and K. De Weerdt, "A Practical Guide to Microstructural Analysis of Cementitious Materials," in *Polymer Synthesis and Characterization*, pp. 177–211, 2016.

[142] J. J. Kollek, "The determination of the permeability of concrete to oxygen by the Cembureau method-a recommendation," *Materials and Structures*, vol. 22, no. 3, pp. 225–230, 1989.

[143] J. G. Cabrera and C. J. Lynsdale, "A new gas permeameter for measuring the permeability of mortar and concrete," *Magazine of Concrete Research*, vol. 40, no. 144, pp. 177–182, 1988.

[144] C. Hall, "Water sorptivity of mortars and concretes: a review," *Magazine of Concrete Research*, vol. 41, no. 147, pp. 51–61, 1989.

[145] D. Lockington, J.-Y. Parlange, and P. Dux, "Sorptivity and the estimation of water penetration into unsaturated concrete," *Materials and Structures*, vol. 32, pp. 342–347, 1999.

[146] C. Tasdemir, "Combined effects of mineral admixtures and curing conditions on the sorptivity coefficient of concrete," *Cement and Concrete Research*, vol. 33, no. 10, pp. 1637–1642, 2003.

[147] O. Idowu and L. Black, *The effect of improper curing on properties that may affect concrete durability.* PhD thesis, 2018.

[148] L. D. Mitchell and J. C. Margeson, "The effects of solvents on C-S-H as determined by thermal analysis," vol. 86, pp. 591–594, 2006.

[149] R. L. Day and B. K. Marsh, "Measurement of porosity in blended cement pastes," *Cement and Concrete Research*, vol. 18, no. 1, pp. 63–73, 1988.

[150] J. Zhang and G. W. Scherer, "Comparison of methods for arresting hydration of cement," *Cement and Concrete Research*, vol. 41, no. 10, pp. 1024–1036, 2011.

[151] N. C. Collier, J. H. Sharp, N. B. Milestone, J. Hill, and I. H. Godfrey, "The influence of water removal techniques on the composition and microstructure of hardened cement pastes," *Cement and Concrete Research*, vol. 38, no. 6, pp. 737–744, 2008.

[152] C. Gallé, "Effect of drying on cement-based materials pore structure as identified by mercury intrusion porosimetry - A comparative study between oven-, vacuum-, and freeze-drying," *Cement and Concrete Research*, vol. 31, no. 10, pp. 1467–1477, 2001.

[153] Royal Academy of Engineering, "Nuclear Construction Lessons Learned," tech. rep., Royal Academy of Engineering, London, 2012.

[154] M. Whittaker, E. Dubina, J. Plank, and L. Black, "The Effects of Cement Prehydration of Engineering Properties," in *Cement and Concrete Science Conference*, vol. 30, (Birmingham), 2010.

[155] J. Stoian, T. Oey, J. W. Bullard, J. Huang, A. Kumar, M. Balonis, J. Terrill, N. Neithalath, and G. Sant, "New insights into the prehydration of cement and its mitigation," *Cement and Concrete Research*, vol. 70, pp. 94–103, 2015.

[156] L. Greenspan, "Humidity Fixed Points of Binary Saturated Aqueous Solutions," *Journal of Research of the National Bureau of Standards - A. Phys ics and Chemistry*, vol. 81A, no. 1, pp. 89–96, 1976.

[157] R. Niry Razafinjato, A. L. Beaucour, R. L. Hebert, B. Ledesert, R. Bodet, and A. Noumowe, "High temperature behaviour of a wide petrographic range of siliceous and calcareous aggregates for concretes," *Construction and Building Materials*, vol. 123, pp. 261–273, 2016.

[158] United Kingdom Quality Ash Association, "COSHH - Safety Data Sheet for PFA / Fly Ash and FBA (including Cenospheres)," tech. rep., 2011.

[159] Z. Liu, D. Xu, and Y. Zhang, "Experimental investigation and quantitative calculation of the degree of hydration and products in fly ash-cement mixtures," *Advances in Materials Science and Engineering*, vol. 2017, 2017.

[160] E. Tajuelo, K. Garbev, D. Merz, L. Black, and I. G. Richardson, "Cement and Concrete Research Thermal stability of C-S-H phases and applicability of Richardson and Groves ' and Richardson C- (A) -S-H (I) models to synthetic C-S-H," *Cement and Concrete Research*, vol. 93, pp. 45–56, 2017.

[161] P. Claisse, H. Elsayad, and I. Shaaban, "Absorption and sorptivity of cover concrete," *Journal of Materials in Civil Engineering*, vol. 9, no. 3, pp. 105–110, 1997.

[162] A. Shippen and M. J. Joyce, "Profiling the depth of caesium-137 contamination in concrete via a relative linear attenuation model," *Applied Radiation and Isotopes*, vol. 68, no. 4-5, pp. 631–634, 2010.

[163] C. Hesse, F. Goetz-Neunhoeffer, and J. Neubauer, "A new approach in quantitative in-situ XRD of cement pastes: Correlation of heat flow curves with early hydration reactions," *Cement and Concrete Research*, vol. 41, no. 1, pp. 123–128, 2011.

[164] K. D. Weerdt, K. O. Kjellsen, E. Sellevold, and H. Justnes, "Synergy between fly ash and limestone powder in ternary cements," *Cement and Concrete Composites*, vol. 33, no. 1, pp. 30–38, 2011.

[165] B. Ersoy, S. Dikmen, T. Uygunoglu, M. G. Içduygu, T. Kavas, and A. Olgun, "Effect of mixing water types on the timedependent zeta potential of portland cement paste," *Science and Engineering of Composite Materials*, vol. 20, no. 3, pp. 285–292, 2013.

[166] A. Vollpracht, B. Lothenbach, R. Snellings, and J. Haufe, "The pore solution of blended cements: a review," *Materials and Structures/Materiaux et Constructions*, vol. 49, no. 8, pp. 3341–3367, 2016.

[167] A. Ipavec, R. Gabrovšek, T. Vuk, V. Kaučič, J. MačEk, and A. Meden, "Carboaluminate phases formation during the hydration of calcite-containing Portland cement," *Journal of the American Ceramic Society*, vol. 94, no. 4, pp. 1238–1242, 2011.

[168] J. Havlica, "Mechanism of Ettringite and Monosulphate Formation," *Cement and Concrete Composites*, vol. 22, no. 2, pp. 671–677, 1992.

[169] J. P. Singh and S. N. Thakur, *Laser-Induced Breakdown Spectroscopy*. 1 ed., 2007.

[170] D. A. Cramers and L. J. Radziemski, *Handbook of Laser-Induced Breakdown Spectroscopy*. Chichester, UK: Wiley, 2 ed., 2013.

[171] N. M. Bulgakova, A. V. Bulgakov, I. M. Bourakov, and N. A. Bulgakova, "Pulsed laser ablation of solids and critical phenomena," *Applied Surface Science*, vol. 198, pp. 96–99, 2002.

[172] F. J. Fortes, J. Moros, P. Lucena, and J. J. Laserna, "Laser-Induced Breakdown Spectroscopy," *Analytical Chemistry*, pp. 640–664, 2013.

[173] H. R. Griem, *Principles of Plasma Spectroscopy*. Cambridge University Press, 2 ed., 2005.

[174] A. Kramida, Y. U. Ralchenko, J. Reader, and NIST ASD Team, "NIST Atomic Spectra Database (ver. 5.3)," 2015.

Appendix A

Appendix A - Thermogravimetric Plots

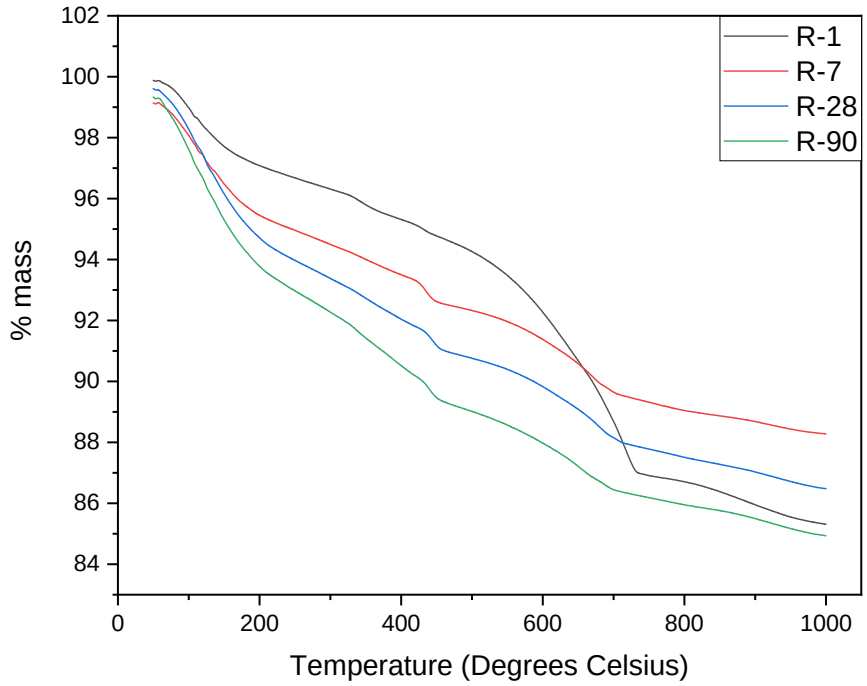

Figure A.0.1: TGA curves for reference (R) mixes, at 1, 7, 28 and 90 days

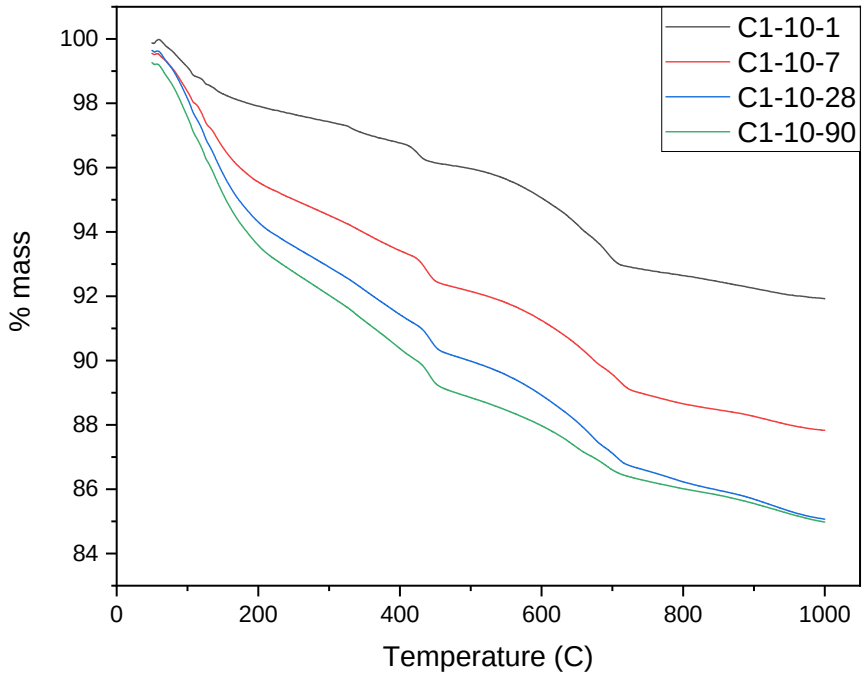

Figure A.0.2: TGA curves for C1-10% replacement mixes, at 1, 7, 28 and 90 days

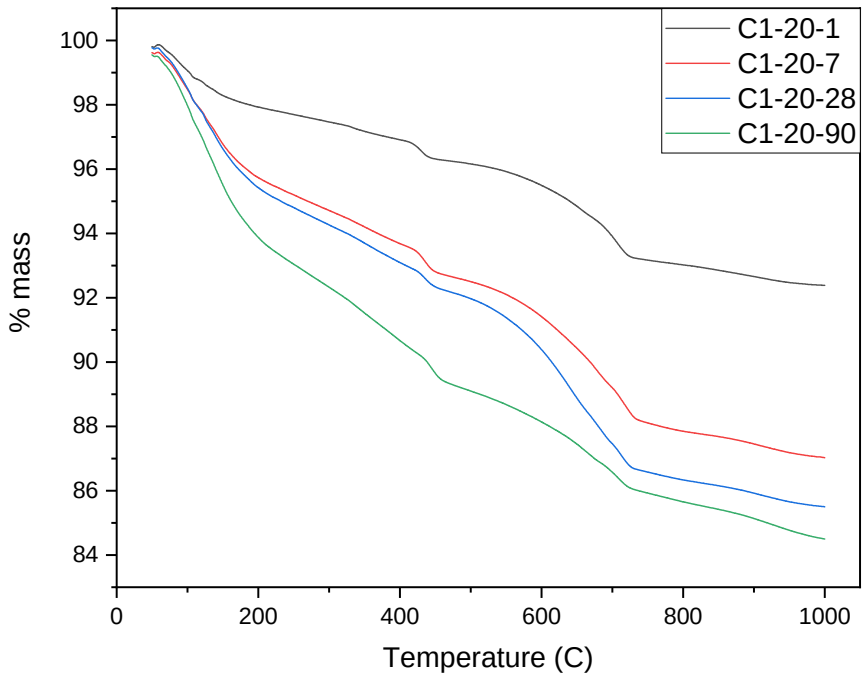

Figure A.0.3: TGA curves for C1-20% replacement mixes, at 1, 7, 28 and 90 days

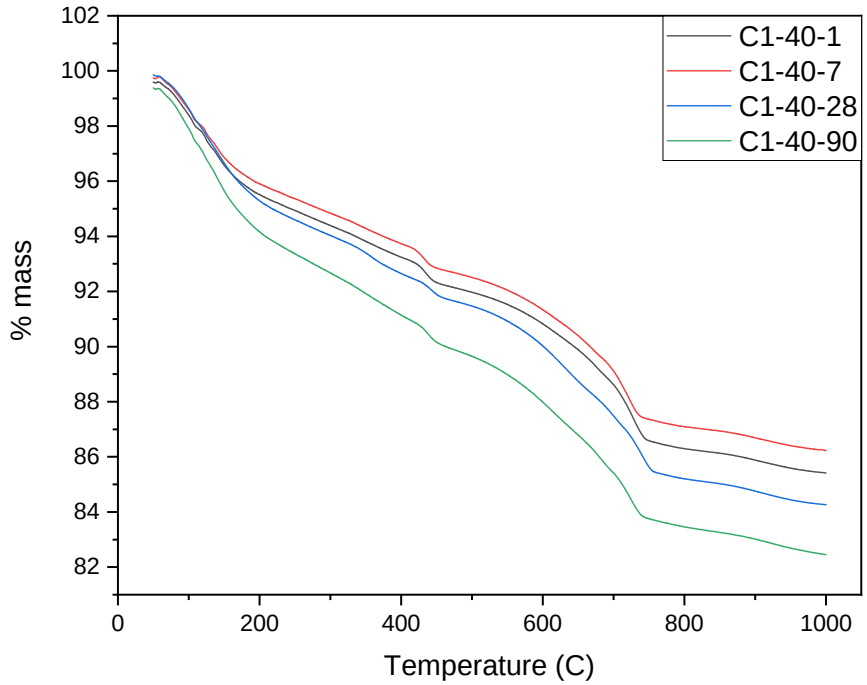

Figure A.0.4: TGA curves for C1-40% replacement mixes, at 1, 7, 28 and 90 days

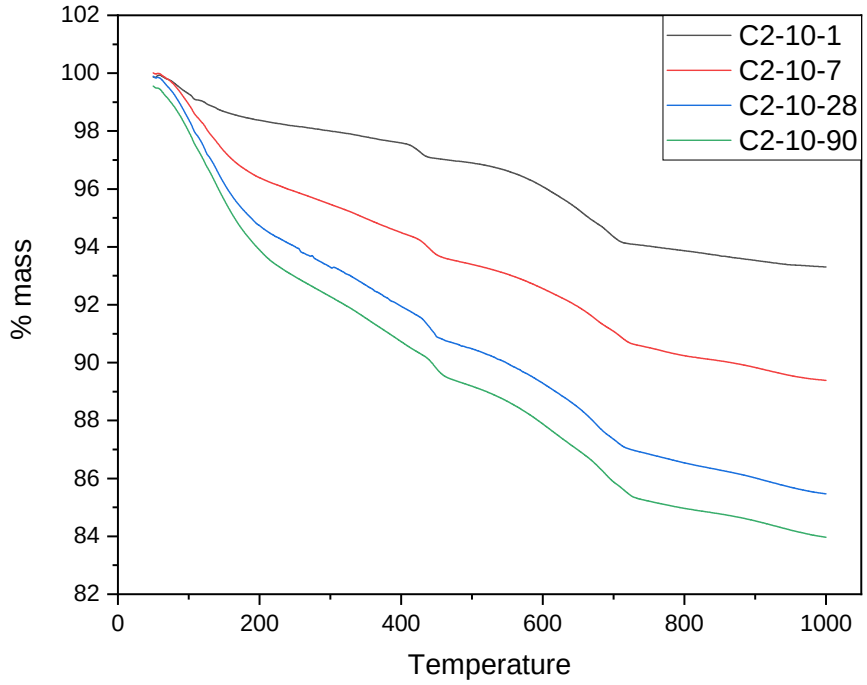

Figure A.0.5: TGA curves for C2-10% replacement mixes, at 1, 7, 28 and 90 days

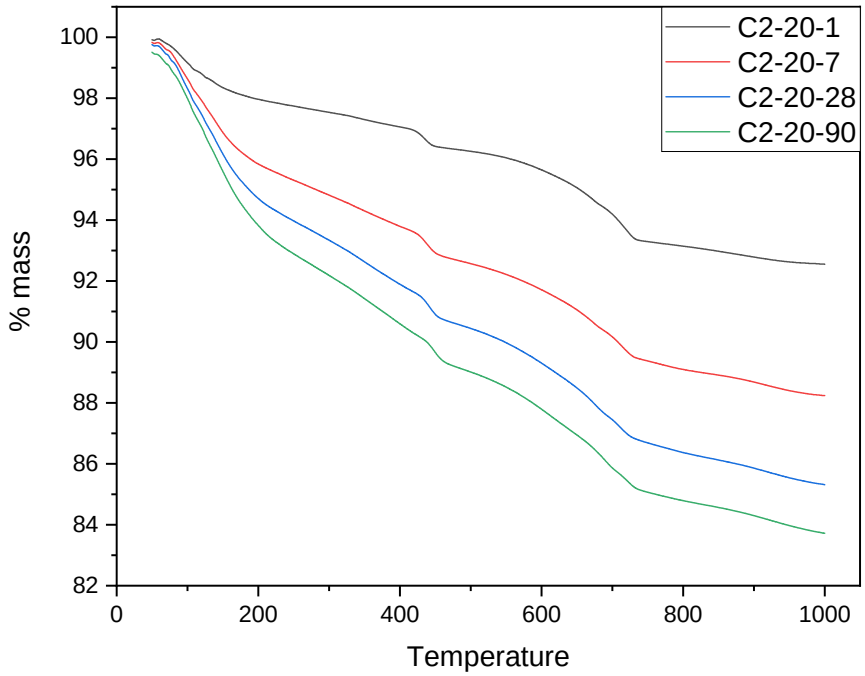

Figure A.0.6: TGA curves for C2-20% replacement mixes, at 1, 7, 28 and 90 days

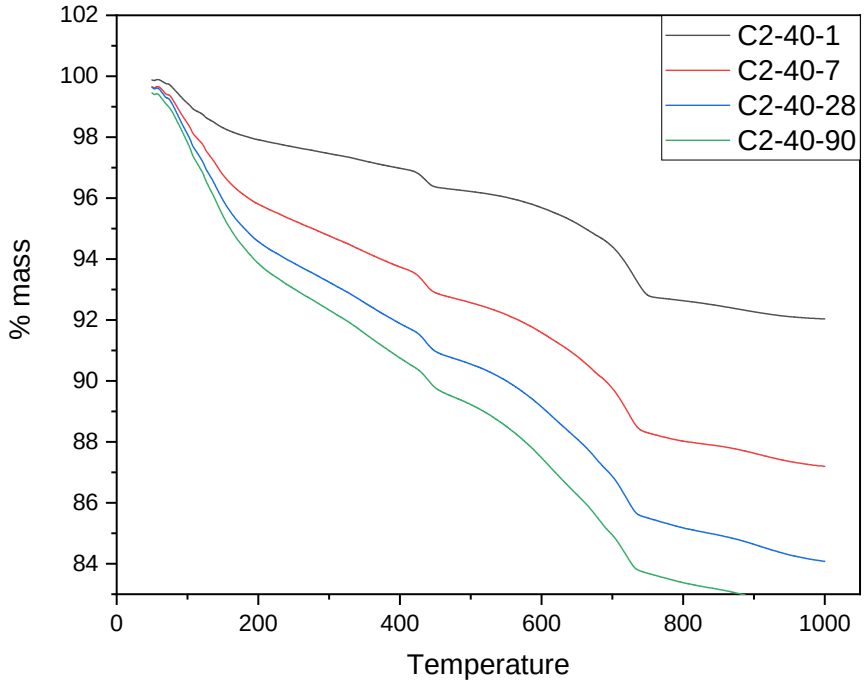

Figure A.0.7: TGA curves for C2-40% replacement mixes, at 1, 7, 28 and 90 days

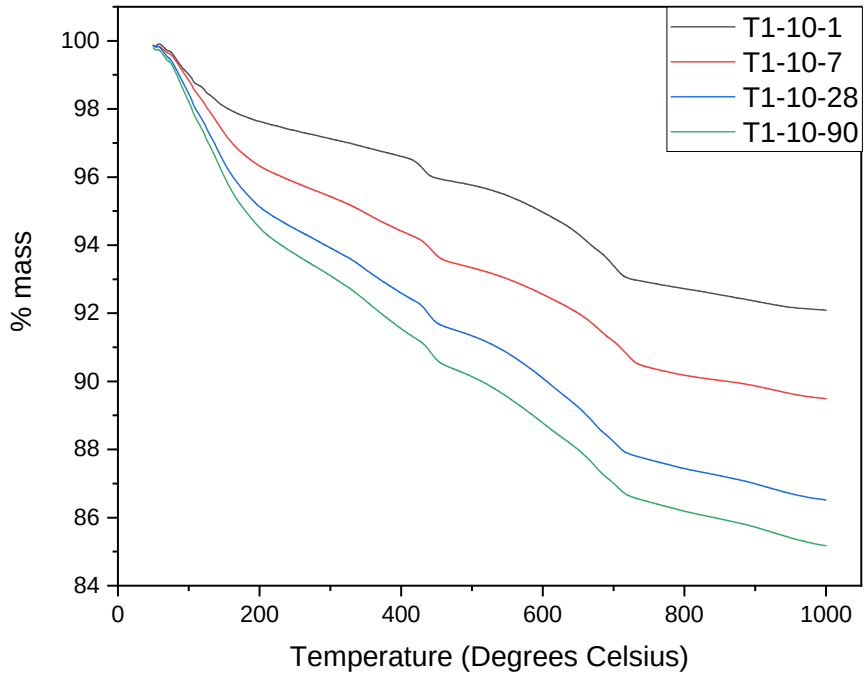

Figure A.0.8: TGA curves for T1-10% replacement mixes, at 1, 7, 28 and 90 days

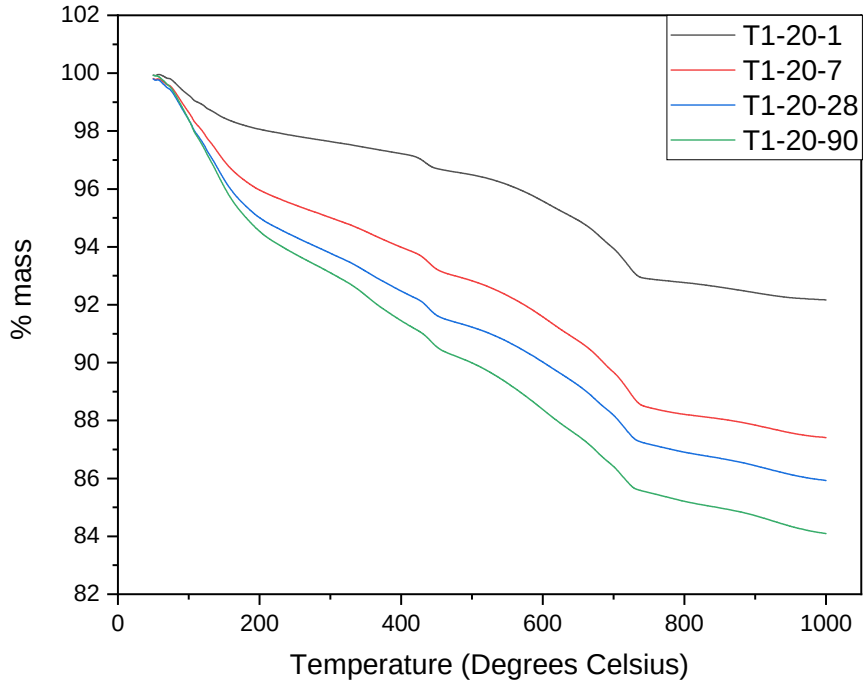

Figure A.0.9: TGA curves for T1-20% replacement mixes, at 1, 7, 28 and 90 days

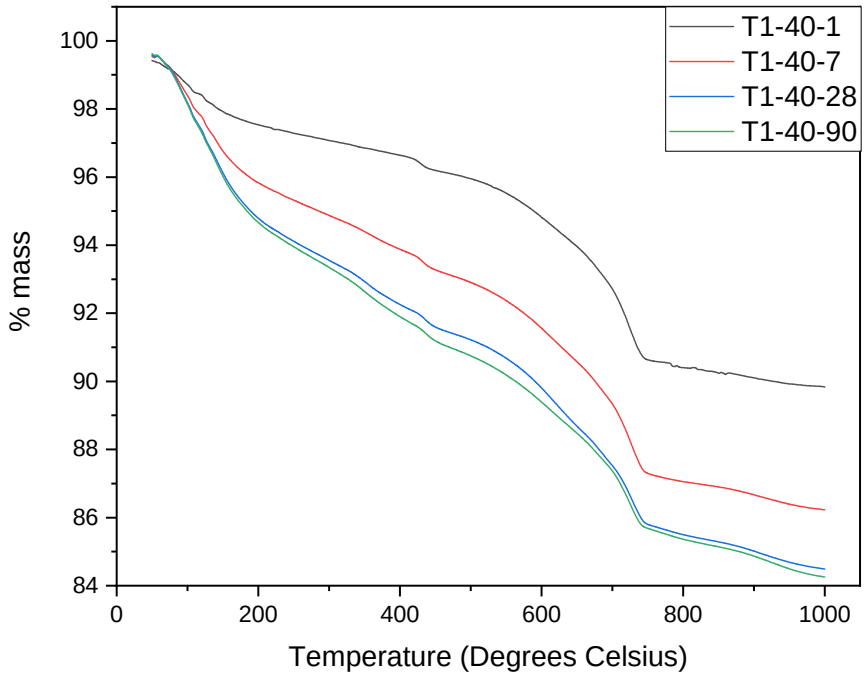

Figure A.0.10: TGA curves for T1-40% replacement mixes, at 1, 7, 28 and 90 days

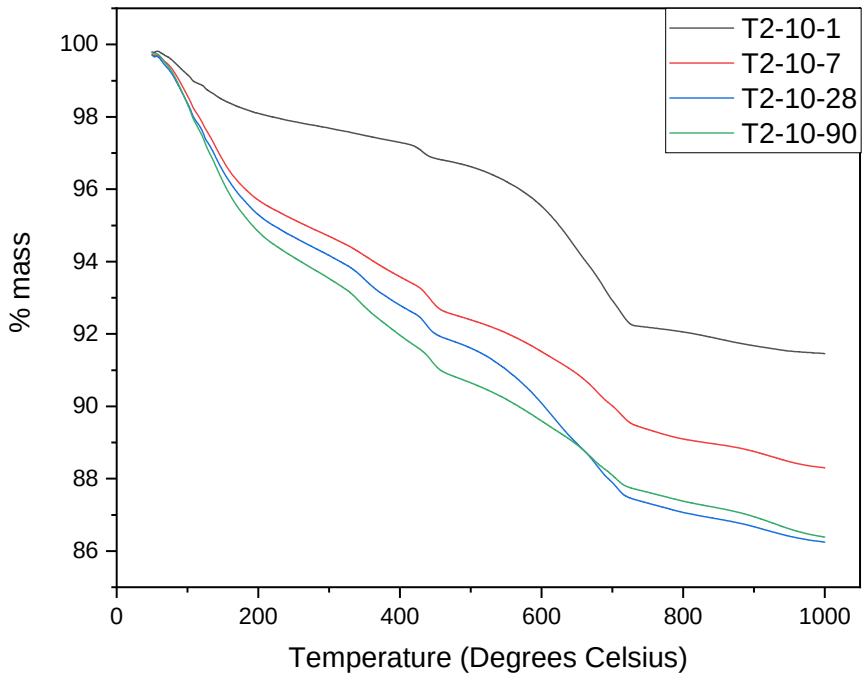

Figure A.0.11: TGA curves for T2-10% replacement mixes, at 1, 7, 28 and 90 days

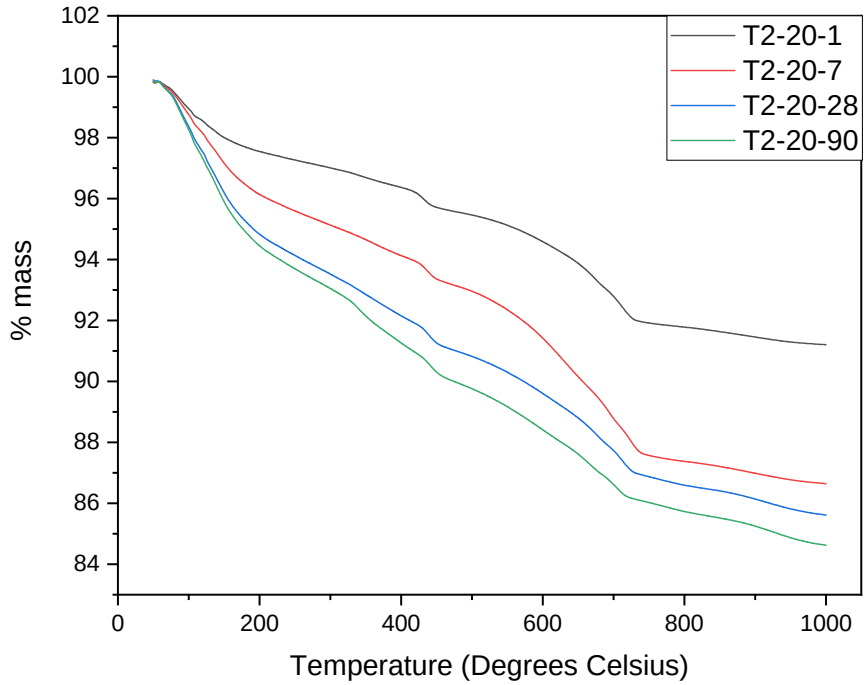

Figure A.0.12: TGA curves for T2-20% replacement mixes, at 1, 7, 28 and 90 days

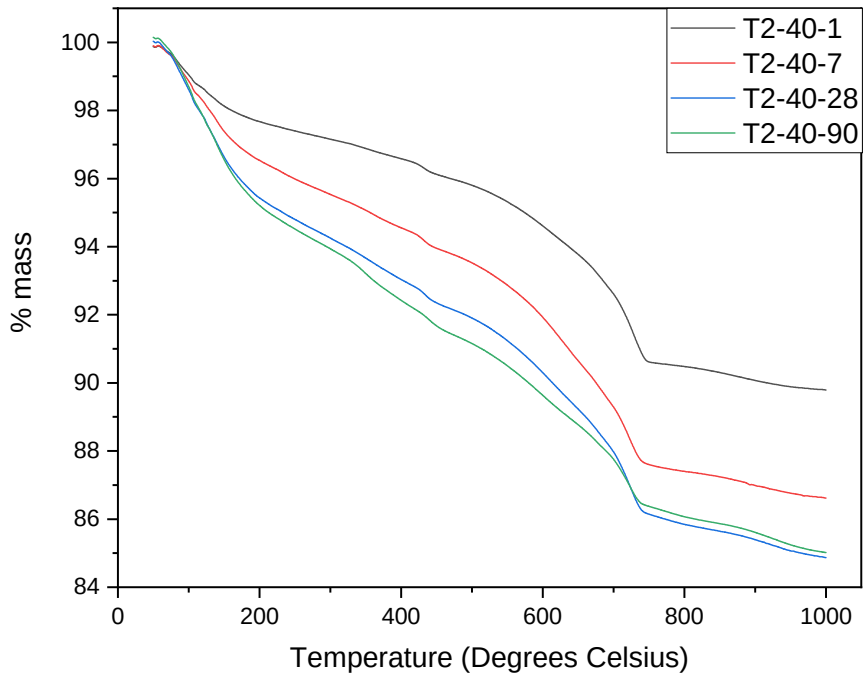

Figure A.0.13: TGA curves for T2-40% replacement mixes, at 1, 7, 28 and 90 days